Regulation of calcium fluxes at endoplasmic reticulum – plasma membrane contact sites

Henry, Christopher

UNIVERSITE DE GENEVE

Département de physiologie cellulaire et métabolisme

Faculté de Médecine
Professeur N. Demaurex

Regulation of calcium fluxes at endoplasmic reticulum – plasma membrane contact sites

THESE

Présentée aux Facultés de médecine et des sciences de l'Université de Genève
Pour obtenir le grade de Docteur ès sciences en sciences de la vie,
Mention Sciences Biomédicales

par

Christopher HENRY
de
France

Thèse n°122

Genève
2021

Table of contents

List of abbreviations

ABD	actin-binding domain
Ag	agonist
CAD	channel activating domain
CaM	calmodulin
CC1	coiled coiled 1
CDI	calcium depending inactivation
CDP-DAG	cytidine diphosphate diacylglycerol
cER	cortical er
CMD	crac modulatory domain
CPA	cyclopiazonic acid
CRAC	ca2+ release activated ca2+
C-term	C-terminal
DAG	diacylglycerol
DGK	diacylglycerol kinase
EM	electron microscopy
ER	endoplasmic reticulum
ESyt	extended synaptotagmin
FCDI	fast cdi
FRET	förster resonance energy transfer
GPCR	G-protein coupled receptors
HEK	human embryonic kidney
I_{CRAC}	crac current
IP_3	inositol trisphosphate
IP_3R	ip3 receptor
KO, DKO	knock-out, double knock-out
LTP	lipid transfer proteins
MAM	mitochondria associated membranes
MCS	membrane contact site
MCU	mitochondrial calcium uniporter
MEF	mouse embryonic fibroblast
NCX	na+/ca2+ exchanger
NFAT	nuclear factor of activated t cell
PA	phosphatidic acid
PB	polybasic
PI	phosphatidylinositol
PIP_2	phosphatidylinositol-4,5-bisphosphate
PIPT	pi transfer protein
PIS	pi synthase
PLC	phospholipase c
PM	plasma membrane
PMCA	plasma membrane calcium atpase
PTH	parathyroid hormone
PTP	permeability transition pore
RCAN1	regulator of calcineurin 1
ROC	receptor operated calcium

ROS	reactive oxygen species
RyR	ryanodine receptor
SAM	sterile alpha motif
SCDI	slow cdi
SERCA	sarco/endoplasmic reticulum ca2+-atpase
SMOC	second messenger operated calcium
SOAR	stim orai-activating region
SOC	store operated calcium
SOCE	store-operated calcium entry
SR	sarcoplasmic reticulum
STIM	stromal interaction protein
Tg	thapsigargin
TIRF	total internal reflection fluorescence
TRPC	transient receptor potential cation
UPR	unfolding protein response
VDAC	voltage-dependent anion channel
VOC	voltage-operated calcium

I) Acknowledgment

I think I could not start this acknowledgment by anyone else than Nicolas. I felt and still feel lucky to have you as professor. Thank you for your support that I saw growing with the years, the trust we built and your incredible optimism when looking at data. I am also thankful for my jury members who accepted to evaluate my manuscript and my thesis defense. Thank you, Pierre, as I know you will have a naïve question to ask. Those are always relevant and sometimes make us rethink our entire project. Thank you, Aurélien, we did not have the chance to interact much yet, but I am looking forward to our discussion that I am sure will be fruitful. Thank you, Barbara, for the early interest you had in my project at my first conferences, for the following up you gave me throughout the years during my TAC meeting and for our non-formal discussions.

So many people entered and left our lab, it feels so hard to imagine I meet so many incredible people during those 5 amazing years. I can't forget the first person that welcomed me in Geneva, Danielle, with his unique laugh but more, for his generous soul. Paula who was always available for me, who was my supporter from day one and who always believed in me. Thank you for all our discussion about results and career development, it helped me to grow in confidence and to know in which direction I wanted to drive my scientific path. A warm thank to Maud, for your kindness and support. We went through a couple things together, specially this FASEB in the California, I will never forget our little walks there, all what we saw and discuss. Thank you for your regular help and advice when it came to science. Monica, always willing to help with experiments and all your advices. Your positive attitude and your curiosity were always inspiring, as well as your patience. I remember when you made me reconsider science to become photographer, you, my first fan ! Stephanie, I will remember when you shown me how to read a paper when we need to find an information, how to critically look at results. The bird crazy lady, the cat crazy lady, Manon ! It always surprised me how you could be so brutally honest and sweet at the same time. Nina, it was such a pleasure to hear you laugh and see you smile during those years, I can't forget when you decided to prepare a little wine tasting accompanied by an amazing cheese plate ! Thank you for our discussion about future and for sharing your precious experience. Mayis, the strongest person I got to know during those 5 years, you are clearly the most inspiring PhD student I meet over the years. I admire how you always found precise and pertinent questions, touching the points I did not think about. Thank you for your never failing support and for all our discussions from science to how politic works in Turkey ! Jen for your investment in the life of the lab, making sure we were never growing apart. Thank you for your good mood and all the interesting experiences you shared with us, hoping your rice allergy is getting better. Amado, your arrival was like heaven sent, you changed the way I saw my project, the way I dealt with challenges. Thank you for your supervision, your advice, and your incredible knowledge regarding science. It might be that without your help, I would have given up more than once. JiHee, you are the unexpected surprise, the joy incarnated, always smiling, and laughing. I learned about kindness through you, and I promise I will not lose the USB stick again ! Camille, thank you for being here, without you no one would have understood so many jokes and references ! I am so glad to have someone who can understand the geek world with me. It is still the beginning of your PhD journey, but I see you are on the right track, good luck ! And my little Cyril, what would I be, what would we all be without you ? Always here to hold us all together, to make sure we were alright. Do you remember when I was sending you a text when I was running late, for you to not worry ? Do you remember every time something was wrong, how you solved all conflicts ? Thank you, Cyril, you are one of the most important persons I meet during these 5 years.

Many people have played a part in my PhD, the different platforms who helped me, the pfmu with Pilar, the FACS with Jean Pierre and Gregory, the READS with Yves and of course the bioimaging

facility. Thank you, Serguei, Olivier, Nicolas, and François. I have to give a special thank to Nicolas for his patience and enthusiasm when I came to him with the plan to learn how to code in Matlab, if I have now successfully developed my own scripts, it is thanks to you. François you always supported me and gave me opportunities, thank you for the time you dedicated on me and for all the precious advice you gave me. Thank you Claes, your knowledge and experience were always welcome, and I am thankful you shared it with us during our lab meeting. I also thank Berni's lab members who we share the office with, Seimia for her craziness, Michael for his good mood, Adama and Aouatef for being so nice. A special shout out to Jeremy, good luck with your PhD. Many thanks to Matthieu Brochet and Dominique Soldati-Favre for their guidance, and support during our meetings.

To all my friends past and present who always stood beside me, some of you have been amazing support, some have even been models and others the reason why I am who I am now and why I did not give up. I feel blessed to have so many close people with so many different, yet amazing qualities. I can't cite you all, but you are all in my heart. I still wish to give a few special thanks. Dobro, can't go around that you always gave more than you expected to receive, I won't forget our open heart talk next to the lake with a bottle of wine. Marta for always making sure I was alright and won't just fall in depression, thank you for all these memes which made me laugh. Ola for your energy that sometimes I can't understand where you take it from, we are kind of PhD siblings as we defend our thesis one day apart, good luck ! Camille because you are always busy and still always find time to talk and make sure I am alright. Burak, you will still be the wisest to me and I won't forget our long Zoom night during the lockdown. Olivier, oh boy when I think about how it started and when I see how it goes now, our friendship has seen crazy moments ! Fabien and Bartosz, you two guys, we arrived together and now look how we all grew up, a pleasure to know you. Jessica, you are the scientist I will forever admire for her determination and dedication, you are also such a nice person, thank you for your support and help to prepare my defense. A big thank to Anna Sinkevich to be beside me since almost a year with all her heart.

I would like to acknowledge my friends back in Montpellier, Maxime P, Maxime T, Kevin, Laureline, Amandine, Claire A, Claire D, Quentin, David, Rémy and probably a few more that I might forget. To all my professors and supervisors that drove me toward this PhD, Monsieur Michel who convinced me to switch from economics to sciences, Yannick Simonin and Sara Salinas for offering me a first lab experience, Bénédicte Delaval for initiating my love of science, Pierre Charnet and Matthieu Rousset for their trust and dedication in making me a better scientist, Laurent Journot and Tristan Bouschet because they helped me to understand what it was to be a scientist and for trusting me. A special thanks to my Master directors who always shown full support and who encouraged me without failing to continue for a PhD, Anne Marie Martinez, and Paul Mangeat.

Et bien sûr, ma famille. Merci Julien, tu n'as jamais abandonné et tu as toujours sus me garder fort et droit. Tu nous as toujours fait passer en premier, maman et moi. Tu auras toujours une place de choix dans mon cœur. Je t'aime comme un père car c'est ce que tu as toujours été pour moi. Et la personne la plus importante au monde à mes yeux, ma mère. Merci de croire en moi, de me motiver, d'être fière de moi et de toujours marcher à mes cotés sans jamais me laisser tomber. Je t'aime de tout mon cœur.

And finally, as surprising as it is and without further transition, I would like to quote Snoop Dogg:

> *"I want to thank me for believing in me, I want to thank me for doing all this hard work. I wanna thank me for having no days off. I wanna thank me for never quitting. I wanna thank me for always been a giver and trying to give more than I receive. I want to thank me for trying to do more right than wrong. I want to thank me for just being me at all times."*

II) Résumé en Français

Les ions calcium jouent un rôle important en biologie cellulaire en tant que messagers secondaires, impliquant que la régulation de leur concentration cellulaire est essentielle pour le maintien de l'homéostasie et l'induction d'évènements de signalisations. Au cours de l'évolution, de nombreuses voies de signalisations ont été développées pour contrôler avec précision les entrées et sorties des ions calcium. Le store-operated calcium entry (SOCE) est une voie de signalisation majeure impliquée dans le développement correct des cellules musculaires et l'activation du système immunitaire. Durant le SOCE, la stimulation par un agoniste génère du inositol trisphosphate (IP_3) à partir de l'hydrolyse du phosphatidylinositol 4,5-biphosphate (PIP_2). Ensuite, IP_3 induit la vidange du calcium stocké dans le réticulum endoplasmique (ER de l'anglais endoplasmic reticulum) via les récepteurs IP_3 (IP_3R). Stromal interaction protein 1 (STIM1), une protéine transmembranaire du ER, détecte la diminution du calcium grâce à ses domaines contenus dans la lumière du ER. Un changement de la conformation de STIM1 est induit et expose des domaines cytoplasmiques essentiels. Le réarrangement de STIM1 favorise son oligomérisation et subséquemment, sa translocation dans le ER cortical (cER) qui est à proximité de la membrane plasmique (PM de l'anglais plasma membrane). Dans ces jonctions ER-PM, STIM1 lie est ouvre le canal calcique ORAI1 situé dans la PM ce qui induit l'entrée de calcium. Le remplissage du ER et les élévations de calcium dans le cytoplasme sont responsable de la terminaison du SOCE à cause de la perte des complexes de STIM et ORAI, notamment par un mécanisme d'inactivation dépendent du calcium.

L'interaction physique de STIM1 et ORAI1 se déroule dans les jonctions ER-PM où la distance est permissive et s'étend de 10 nm à 25 nm. Les jonction ER-PM sont membre de la famille des membrane contact sites (MCS) qui sont des zones où les membranes d'organelles sont en proche apposition avec une distance les séparant de moins de 30 nm. Les contacts ER-PM jouent un rôle important dans la maintenance de la signalisation calcique par le réapprovisionnement de PIP_2 dans la PM. Les MCS sont des structures dynamiques qui utilisent des protéines d'ancrages pour s'adapter aux besoins cellulaires et sont impliqués dans le façonnement des réponses physiologiques. Durant le SOCE, la longueur du cER augmente de façon dépendante de STIM1 et la couverture des jonctions ER-PM augmente de 5 fois. Pendant ce temps, la distance ER-PM est réduite de 21.8 nm à 14.8 nm par le recrutement de ESyt1, une protéine du ER qui est activée par le calcium. La structure et la fonction des MCS ont été démontré comme dépendante l'une de l'autre, cependant, il manque un modèle généralisé.

La première partie de ma thèse se concentre sur la compréhension de la relation entre le SOCE et l'ultrastructure des contacts ER-PM. Pour cet objectif, j'ai modifié les paramètres morphométriques des contacts ER-PM par l'expression de protéines d'ancrage connues (ESyt1 et ESyt2) ou synthétique de la famille MAPPER (MAPPER-Short et MAPPER-Long). En utilisant la microscopie électronique (EM pour l'anglais electron microscopy), j'ai étudié la morphologie des contacts ER-PM lors de l'expression de protéines d'ancrage. La longueur du cER et la distance inter-membrane correspondante ont été systématiquement mesurés et corrélés à différent moment du SOCE. La combinaison des deux paramètres, révèle que lors de la vidange du ER, la longueur du cER augmente de 66 nm à 156 nm sans pour autant modifier significativement la distance entre le ER et la PM. D'un autre côté, l'expression de protéines d'ancrage amplifie l'élongation du cER durant la vidange du ER. C'est particulièrement évident avec ESyt2 et MAPPER-L qui génèrent des contacts plus longs que 1,5 µm. De plus, ces très longs contacts sont stabilisés à une distance entre ER et PM qui est spécifique de chaque famille de protéine d'ancrage. ESyt2 et MAPPER-L ont un comportement similaire concernant la morphologie des jonctions ER-PM mais aussi au niveau de l'entrée de calcium durant le SOCE qui est réduite d'environs 50% dans plusieurs types cellulaires. Ces résultats supportent un rôle

pour l'ultrastructure des contacts ER-PM dans la régulation du SOCE via le recrutement de protéines d'ancrage.

L'imagerie microscopique fait partie des techniques centrales utilisées dans l'étude de la signalisation calcique et des MCS. La génération de nombreuses images présente de nouveaux défis dans la façon dont on traite les informations et des pipelines sont maintenant de plus en plus essentiels pour un traitement des données fluide et fiable. De nouvelles approches sont développés chaque jour pour augmenter le workflow depuis l'acquisition jusqu'à l'extraction des caractéristiques clefs des données. A cause de la masse importante de donnés générées durant cette thèse, j'ai inclus une seconde partie sur le développement de nouveaux outils d'analyse pour créer un puissant et fiable pipeline pour l'analyse des données calcium, TIRF microscopie et jonctions ER-PM. L'objectivité et le gain de temps offert par ce pipeline est significatif et sa fiabilité en fait un outil utilisé par la plupart de mes collègues et également quelques collaborateurs. J'ai aussi généré des stratégies personnalisées pour dépasser les limites que j'ai rencontré dans l'analyse des données provenant de timelapses. J'ai pu extraire des informations qui, sans ces outils analytiques, auraient été hors de portés.

De façon générale, en utilisant la microscopie électronique et l'imagerie calcique avec mon pipeline, je peux conclure que l'expansion du cER durant le SOCE est médié par STIM1 et augmente lorsque des protéines d'ancrage sont recrutées dans les sites de contacts. Ces résultats ont une application potentielle sur la régulation du SOCE durant l'activation immunitaire et ouvre la voie à une meilleure compréhension de comment les cellules régulent leur signalisation à travers l'ultrastructure des MCS.

III) Abstract

Calcium ions play an important role as secondary messenger in cell biology therefore, regulation of its cellular concentration is key to maintain homeostasis and trigger signaling events. A multitude of pathways have been developed during evolution to tightly control the in and out of cellular calcium ions. Store-operated calcium entry (SOCE) is a major signaling pathway involved in proper development of muscle cells and immune system activation. During SOCE, an agonist stimulation generates inositol trisphosphate (IP_3) from phosphatidylinositol 4,5-biphosphate (PIP_2) hydrolysis. Following, IP_3 induces depletion of endoplasmic reticulum (ER) calcium store through IP_3 receptor (IP_3R). Stromal interaction protein 1 (STIM1), an ER transmembrane protein, senses calcium depletion through its luminal domains which induce a conformational change exposing key cytosolic domains. STIM1 new intramolecular arrangement favors its oligomerization and in turn its translocation to cortical ER (cER), which is closely apposed to plasma membrane (PM). Within those ER-PM junctions, STIM1 binds and gate ORAI1 calcium channel on the PM and induce calcium entry. Refilling of the ER store and cytosolic calcium elevations are responsible for SOCE termination due to loss of STIM-ORAI complexes though calcium dependent inactivation processes.

Physical interaction between STIM1 and ORAI1 occurs at ER-PM junctions where the gap distance is permissive and ranges from 10 nm to 25 nm. ER-PM junctions are part of the membrane contact sites (MCS) family which are membranes in close apposition between different organelles or subcellular structures, with an intermembrane distance usually below 30 nm. Interestingly, ER-PM contact sites play an important role in sustaining calcium signaling through replenishment of PIP_2 in the PM. MCS are dynamic structures using tether proteins to adapt to cellular needs and are involved in the shaping of physiological responses. During SOCE, cER length increases in a STIM1 dependent manner and global coverage of ER-PM junctions increases by ~5 fold. Meanwhile, ER-PM gap distance is shortened from 21.8 nm to 14.8 nm by recruitment of ESyt1, an ER resident tether protein activated by calcium entry. MCS structure and function have been dependent one to another, however, a unifying model is missing.

The first part of my thesis focuses on understanding of the relationship between SOCE and ER-PM contact site ultrastructure. To this end, we modified morphometric parameters of ER-PM contact sites by expressing known tether proteins (ESyt1 and ESyt2) or synthetic constructs from MAPPER family (MAPPER-Short and MAPPER-Long). Using electron microscopy (EM), we assessed ER-PM contact morphology upon expression of tether proteins. cER length and its associated ER-PM distance have been systematically measured and correlated at different time points of SOCE. Both parameters combined revealed that ER depletion is increasing cER length from 66 nm to 156 nm without significantly impacting gap distance. On the other hand, expression of tether proteins amplifies cER elongation upon calcium depletion. It is particularly dramatic with ESyt2 and MAPPER-Long which generate contacts longer than 1.5 µm. Additionally, these long contact sites were stabilized to an ER-PM distance specific to each tether family. As ESyt2 and MAPPER-L behave similarly at morphometric level, they were associated with a ~50% reduction of calcium entry in multiple cellular systems. These results support a role for ER-PM ultrastructure in regulation of SOCE through recruitment of tether proteins.

Microscopy imaging is part of the core techniques used in the study of calcium signaling and MCS. Generation of high number of images represents new challenges in the way we deal with information and pipelines are now more and more essential for a smooth and reliable data processing. New approaches are developed every day to increase workflow from acquisition to extraction of key features from data. Due to the high amount of data generated in this thesis I included as a second

part the development of new analytic tools to create a powerful and reliable pipeline for calcium, TIRF and ER-PM junction analysis. The objectivity and time saving opportunities offered by this pipeline are substantial and its reliability makes it used by most of my co-workers and even some collaborators. I additionally generated custom strategies to overcome limitation we were facing in data analysis of our microscopy timelapses. We could extract information that would have been out of reach without help from these analytic methods.

Overall, using electron microscopy and calcium imaging with my pipeline I can conclude that cER expansion during SOCE is mediated by STIM1 and is enhanced by tether proteins recruited to contact sites. This might have potential application for regulation of SOCE during immune cell activation and open the way to a better understanding of how cells regulate their signaling through the MCS ultrastructure.

IV) Introduction

1) Calcium signaling

Calcium was isolated for the first time in 1808 by Sir Humphry Davy using electrolysis {Thomas et al. 2008, Chemphyschem}. It represents the fifth most abundant element in the human body and is mainly acquired by ingestion of dairy products. Human organisms mostly store calcium as crystals within bones where osteoclasts, specialized cells, oversee its storage and release in the bloodstream. Only a small portion is present as a soluble form within the blood, available for uptake by cells. It's concentration within plasma is tightly maintained at around of 2.5 mM (or 9 $mg.dL^{-1}$) {Goldstein, 1990, Serum Calcium}. To keep this concentration steady, the parathyroid glands generate parathyroid hormone (PTH) when calcium concentration decreases. PTH triggers release of calcium from bones by osteoclasts, it increases reabsorption by the kidney and indirectly enhances absorption by small intestine {Khan et al. 2021, StatPearls}.

a. Initiation of calcium signals

Calcium plays an important role as a second messenger regulating cellular functions from muscle contraction to immune response passing by exocytosis and oocyte fertilization. Because of its important role, it needs to be tightly regulated to avoid generation of chaotic cellular responses. To keep calcium under control, cells maintain a low basal calcium concentration within the cytoplasm at around 100 nM. Because of this low cytosolic concentration compared to the extracellular one, the electrochemical gradient favors calcium entry. To prevent an accumulation of calcium within cells, which could lead to undesired stimulation events, the plasma membrane Ca^{2+} ATPase (PMCA), on the plasma membrane (PM) constantly extrudes calcium from cytoplasm to the extracellular medium {Shull and Greeb, 1988, Journal of Biological Chemistry; Carafoli, 1991, Physiological reviews; Cunningham and Fink, 1994, JCB; Strehler and Zacharias, 2001, Physiological Reviews; Prasad and al. 2004, BBRC}. To produce calcium signals and activate calcium-dependent processes, the cells generate cytosolic calcium elevations, characterized by a spatiotemporal component, driving a specific response. For example, local pulsative elevations are involved in vesicle fusion to the PM or in excitation-contraction coupling of muscle cells {Melzer et al. 1995, Biochim Biophys Acta; Burgoyne et Clague, 2003, BBA}. On the other hand, global and sustained calcium elevations are associated with cell death, particularly through a mitochondria-dependent mechanism {Choi, 1988, Neuron; Pend and Greenamyre, 1998, Molecular Pharmacology; Starkov et al, 2004, Cell Calcium}.

Calcium elevation originates either from the extracellular space as an influx through PM or from release of calcium stored within organelles.

Calcium entry via the plasma membrane is regulated by a great variety of cell type specific transporters in order to properly respond to stimulations (Figure 1) {reviewed in Parekh and Putney, 2005, Physiological Review}. Voltage-operated calcium (VOC) channels, for example, are in muscle cells and are opened by depolarization of the PM which is critical for muscle contraction. Extracellular stimulation by agonists activates another family of calcium channels; the receptor operated calcium (ROC) channels, for example, which play a role in the release of pro-inflammatory cytokines by immune cells through P2X receptors. From the inside, second messengers such as the cyclic nucleotides activate second messenger operated calcium (SMOC) channels. Additionally, the Na^+/Ca^{2+} exchanger (NCX) lets 3 Na^+ enter the cell and releases 1 Ca^{2+} to prevent large cytosolic calcium variations in excitable cells but it can also work in reverse. Finally, store operated calcium (SOC) channels are the main calcium entry channels in non-excitable cells and are activated by the depletion of internal calcium stores.

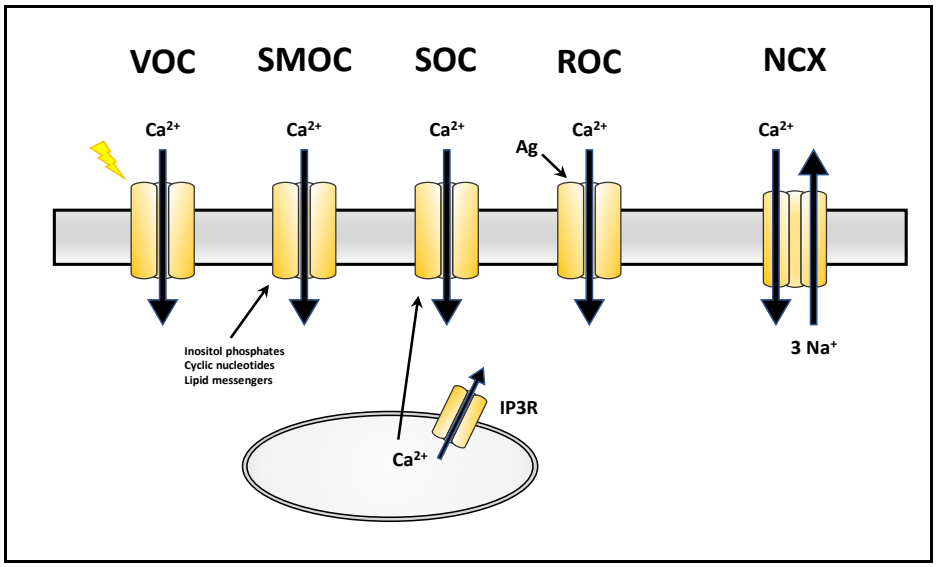

Figure 1: Modes of regulated Ca^{2+} entry across the plasma membrane.

Calcium can enter cells by any of several general classes of channels, including voltage-operated channels (VOC), second messenger-operated channels (SMOC), store-operated channels (SOC), and receptor-operated channels (ROC). VOCs are activated by membrane depolarization, and SMOCs are activated by any of a number of small messenger molecules, the most common being inositol phosphates, cyclic nucleotides, and lipid-derived messengers (diacylglycerol and arachidonic acid and its metabolites). SOCs are activated by depletion of intracellular Ca^{2+} stores, and ROCs are activated by direct binding of a neurotransmitter or hormone agonist (Ag). In addition, under some conditions, Ca^{2+} can enter cells via the Na^+-Ca^{2+} exchanger (NCX) operating in reverse mode. {Redrawn from Parekh and Putney, 2005, Physiological Review}

b. Calcium elevation from the organelles

The endoplasmic reticulum (ER) or sarcoplasmic reticulum (SR) represent the main calcium stores within cells and maintain a resting concentration between 100 µM and 800 µM depending on the cell

type. Maintenance of such stores is regulated by sarco/endoplasmic reticulum Ca^{2+}-ATPase (SERCA) pumps which are localized on the ER/SR membrane specifically dedicated to pumping calcium from the cytosol into the ER/SR {MacLennan, 1970, JBC; Periasamy and Kalyanasundaram, 2007, Muscle Nerve; Boczek et al, 2021, Int J Mol Sci}. SERCA pumps are also compensating for the activity of leak channels on the ER membrane which are continuously depleting ER calcium. The identity of the leak channels is still under debate, but evidence suggests the involvement of multiple proteins, the most probable being the translocon, a protein responsible for the membrane insertion of newly synthetized proteins {Camello et al. 2002, Cell Calcium; Lemos et al, 2021, BBA Mol Cell Res}. Calcium is a key co-signaling factor for ER chaperone proteins, needed for proper folding of newly synthetized proteins to avoid activation of the unfolding protein response (UPR) which could lead to apoptosis {Carreras-Sureda et al. 2017, Front Oncol}.

Mobilization of the ER/SR calcium depends on the ryanodine receptor (RyR) and inositol trisphosphates (IP_3) receptor (IP_3R) which once open, evoke a fast rise of cytosolic calcium. To prevent a calcium leak at rest, the RyR is stabilized in a closed conformation by binding of castalbins {Jayaraman et al. 1992, J Biol Chem}. RyR has evolved to be essential in muscle excitation-contraction coupling (ECC) and was first purified using ryanodine which locks the receptor in its open state subsequently depleting ER calcium and interrupting ECC {Santulli et al. 2017, J Physiol}. Opening of RyR is mediated by cytosolic calcium, up to 10 µM, calcium activates RyR but over this concentration, it becomes inhibitory to the receptor opening {Bezprozvanny et al. 1993, Mol Biol Cell}. On the other hand, IP_3R is present in all cell types and is key in signal transduction of G-protein coupled receptors (GPCR) in response to extracellular stimulation. Upon agonist stimulation of surface receptors, the alpha subunit of GPCR triggers phospholipase C (PLC) activity. PLC induces hydrolysis of plasma membrane phosphatidylinositol 4,5-biphosphate (PIP_2) into diacylglycerol (DAG) and IP_3. Cytosolic IP_3 travels to the ER membrane where it binds and opens its receptor leading to ER calcium depletion {Worley et al. 1987, Nature; Berridge, 1993, Nature}. Functionally, IP_3R activity is the first step for the nuclear factor of activated T cell (NFAT) dependent gene expression and moreover, IP_3R favors ATP production by mitochondria {Rinne and Blatter, 2010, Am J Physiol Heart Circ Physiol}.

Mitochondria can also store calcium to a lesser extent than the ER/SR, settling around 10 µM calcium. The main purpose of mitochondrial calcium is not to be released to trigger signaling but rather to stimulate mitochondrial ATP production. The IP_3R on the ER is coupled to mitochondria to ensure maximal efficiency of calcium transfer from ER to mitochondria {Rizzuto et al. 1998, Science; Jouaville et al. 1999, PNAS}. This transfer occurs via voltage-dependent anion channel (VDAC) on the outer membrane, and mitochondrial calcium uniporter (MCU) on the inner membrane which is the limiting factor of calcium entry into mitochondrial matrix. Interestingly, mitochondria have been shown to recycle calcium to ER during agonist stimulation to prevent depletion of neighboring ER

regions {Arnaudeau et al. 2001, JBC}. By blocking calcium efflux from mitochondria through NCX, agonist-induced depletion of ER calcium was increased. Suggesting that NCX is responsible for recycling of calcium from mitochondria to ER upon agonist stimulation. Additionally, mitochondria have a buffering role to prevent sustained cytosolic elevations. If mitochondria are overloaded with calcium, they can open the permeability transition pore (PTP) which is followed by cell death {Hajnoczky et al. 2006, Cell Calcium}.

2) Store-operated calcium entry (SOCE)

Store-operated calcium entry (SOCE) is a ubiquitous calcium mechanism first hypothesized in 1986 by Putney who tried to explain the two phases of calcium mobilization after receptor stimulation {Putney, 1986, Cell Calcium; Hoth and Penner, 1992, Nature; Mogami et al. 1997, Biochem J; Abdullaev et al. 2008, Circulation Research}. Upon agonist stimulation of surface receptors, such as GPCR, coupled to PLC, PIP_2 hydrolysis generates IP_3 which opens its receptor on the ER membrane inducing ER calcium depletion {Zeng, et al. 2003, Curr Biol}. Calcium release in turn activates calcium release activated calcium (CRAC) channels on the PM which are responsible for SOCE {Prakriya and Lewis, 2015, Physiol Rev}. We had to wait until 2005 for two independent siRNA screenings to reveal stromal interaction protein 1 (STIM1), the first molecular determinant of SOCE which is an ER membrane resident protein responsible for monitoring ER calcium levels {Liou et al. 2005, Current Biology; Roos et al. 2005, Journal of Cell Biology}. A year later, similar screenings led to the discovery of ORAI1, the calcium channel responsible for the CRAC current (I_{CRAC}) and calcium elevation during SOCE {Zhang et al. 2006, PNAS; Vig et al. 2006, Science; Feske et al. 2006, Nature}. Even if SOCE is ubiquitous, it plays a more critical role in muscle cells and immunity. Lately, attention has been put on SOCE in the skeletal muscle field where for a long time it was believed to be secondary. There is now evidence suggesting a role in correct muscle development and more efficient ECC {Ong et al, 2016, Adv Exp Med Biol ; Antigny et al, 2017, BBA Mol Cell Res}. Interestingly, mutations of SOCE molecular determinants are responsible for development of tubular aggregate myopathy (TAM), a disease characterized by muscle weakness and pain with an early childhood onset {Bulla et al, 2019, J Physiol}. On the other hand, SOCE plays an essential role in immunity as other STIM/ORAI mutations lead to severe combined immunodeficiency {Feske et al, 2010, Clin Immunol}. SOCE has been shown to be responsible for activation of T-cells to trigger a proper adaptive immune response {Vaeth et al, 2017, Immunity}.

a. Store depletion and calcium entry

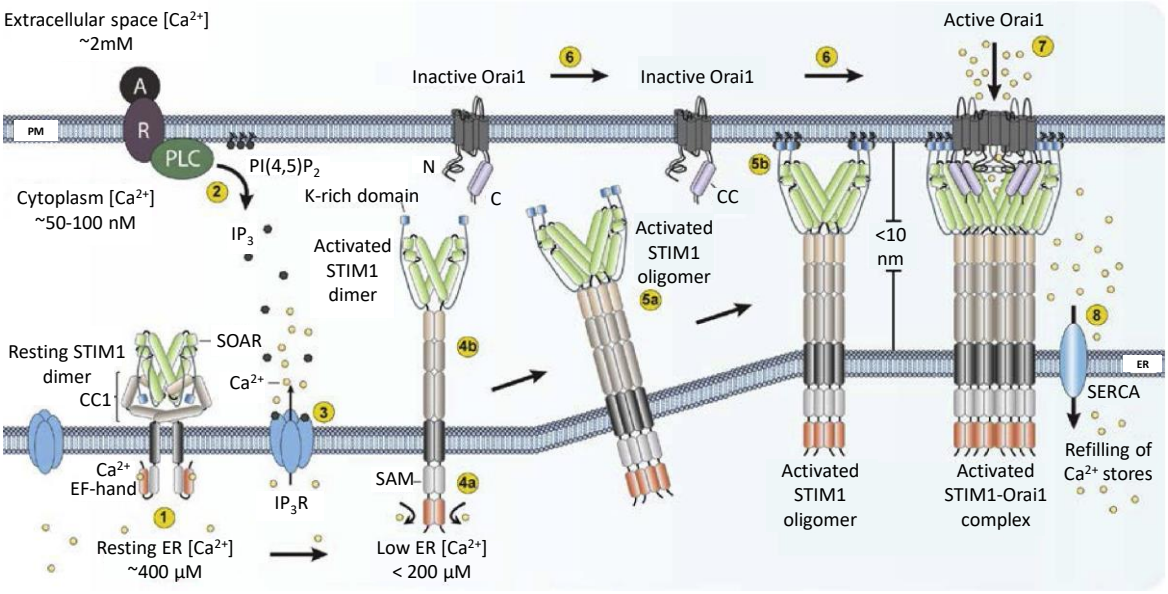

Figure 2: Store-operated calcium entry. Modified from Bhardwaj et al. 2016, Cell Calcium, redrawn from Soboloff et al. 2012, Nat Rev Mol Cell Biol

1) At resting ER Ca^{2+} levels, both STIM1 and ORAI1 have an homogenous localization in the ER membrane and the PM, respectively.
2) The agonist-induced stimulation of G-protein coupled receptors activates phospholipase C, resulting in hydrolysis of phosphatidylinositol 4,5-bisphosphate (PIP_2) on the inner leaflet of PM and release of Inositol 1,4,5-trisphosphate (IP_3).
3) IP_3 diffuses into the cytosol and binds to the IP_3 receptor (IP_3R) on the ER membrane causing release of ER Ca^{2+} from the IP_3R.
4a) STIM1, upon significant drop in ER Ca^{2+} concentration, loses Ca^{2+} bound to its EF-hand domain. Ca^{2+}-dissociation activates the STIM dimer by aggregation and interaction of EF-SAM domains in the ER lumen.
4b) Aggregation and interaction of EF-SAM induces an extended conformation of the cytoplasmic coiled-coil domains, leading to exposure of SOAR and the K-rich domain.
5a) Activated STIM1 dimer further oligomerizes via coiled-coils and translocates to ER-PM contact sites.
5b) Oligomerized STIM1 binds PIP_2 at the inner leaflet of the PM avidly via their PB domains leading to extension and stabilization of ER-PM contact sites.
6) Activated STIM1 oligomers and ORAI1 accumulate at ER-PM junctions.
7) The exposed SOAR domains of activated STIM1 oligomers activate the ORAI1 channel, leading to influx of extracellular Ca^{2+} into the cytosol.
8) Consequently, ER stores are refilled with Ca^{2+} by SERCA, which is co-recruited at these ER-PM contacts.

At rest, STIM1 is localized along the ER in an inactive conformation stabilized by its calcium sensitive EF-hand domain and sterile alpha motif (SAM). EF-SAM domains binds luminal calcium, allowing STIM1 to sense ER calcium levels (Figure 2 - 1). STIM1 is found as a dimer and its diffusion is prevented by the binding of EB1, a protein connecting the microtubule network to the EB1-binding motif of STIM1 {Honnappa et al. 2009, Cell; Chang et al. 2018, J Cell Biol}. In its closed conformation, STIM1 cytosolic domains are locked down by interaction of the coiled-coil 1 (CC1) domain with STIM ORAI-activating region (SOAR) and channel activating domain (CAD) {Muik et al. 2009, JBC; Covington et al. 2010, Molecular Biology of the Cell}. CC1 has been suggested to interact with cytosolic components of STIM1 to slow down its diffusion at rest {Covington et al. 2010, Molecular Biology of the Cell}. Upon agonist stimulation of GPCR, generation of IP_3 opens its receptor on the ER leading to

calcium release (Figure 2 - 2 and 3). Luminal calcium bound to EF-SAM is lost, inducing a conformational change of STIM1 which promotes the EF-SAM dimerization and exposure of cytosolic domains (Figure 2 - 4a). SOAR/CAD is released from CC1, and the K-rich domain gets exposed (Figure 2 - 4b) {Korzeniowski et al. 2010, Calcium Signaling; Zhou et al. 2013, Nat Struct & Mol Biol}. Conformational change of STIM1 allows it to oligomerize within a few seconds. This process is essential for SOCE activation and is mediated by coiled-coil domains and SOAR/CAD (Figure 2 - 5a) {Liou et al. 2007, PNAS; Luik et al. 2008, Nature; Covington et al. 2010, Molecular Biology of the Cell}. In less than a minute, STIM1 oligomers navigate through the ER membrane and translocate to cortical ER (cER), close apposition of ER to PM in ER-PM junctions {Liou et al. 2007, PNAS; Luik et al. 2008, Nature}. STIM1 retains its ability to bind EB1 when ER calcium is depleted, which is suggested to slow down STIM1 translocation and to prevent an excess of SOCE activation {Chang et al. 2018, J Cell Biol}. However, dissociation of EB1 is promoted by phosphorylation of these STIM1 at residues S575, S608, and S621. It has been proposed that ERK1/2 regulate SOCE by phosphorylation of those STIM1 residues and favor the EB1 dissociation {Pozo-Guisado et al. 2013, JCS}. STIM1 phosphorylation is observed 2 to 5 minutes after depletion of the ER stores which suggest that this mechanism takes place after the initial STIM1 translocation. Prior to STIM1 recruitment to ER-PM junctions, ORAI1 is homogenously distributed in the PM {Zhou et al. 2015, Nat Commun}. During STIM1 accumulation in close proximity of ORAI1 channels, SOAR/CAD domains trap ORAI1 into clusters (Figure 2 - 6). Trapped ORAI1 form multimers of higher degree but their exact configuration was under debate until recently. Using concatemers, ORAI1 has been suggested to form either tetramers or hexamers. Tetrameric configuration was first suggested to be the correct one as it displays the highly calcium selective property from I_{CRAC}. Whereas investigation of biophysical properties from concatemers in a hexameric configuration were not consistent {Thompson et al. 2013, Sci Rep; Yen et al, 2016, Biophysical Journal}. Crystallography structure of ORAI1 and chromatography experiments revealed that ORAI1 adopt a hexameric configuration {Hou et la. 2012, Science}. Further investigation revealed that ORAI1 generates hexamers through the formation of "trimer of dimers" {Cai et al. 2016, J Biol Chem; Cai et al. 2018, J Biol Chem}. Opening of ORAI1 is mediated by SOAR/CAD domains binding to the N-terminal and C-terminal tails of ORAI1 channel. Activation of ORAI1 occurs sequentially through cooperative interactions of SOAR and ORAI1 tails {Park et al. 2009, Cell; Kawasaki et al. 2009, Biochem Biophys Res Commun; Zheng et al. 2013, J Biol Chem; Palty et al. 2017, Cell Reports}. This interaction is stabilized by STIM1 polybasic (PB) domain which interacts with phospholipids on the PM (Figure 2 - 5b). The PB domain has been reported to mediate the characteristic inward rectification of I_{CRAC} {Liou et al. 2007, PNAS; Korzeniowski et al. 2009, J Biol Chem; Walsh et al. 2009, Biochem J; Yuan et al. 2009, Nat Cell Biol}. Subsequently,

calcium flow inside the cell through ORAI1 and diffuses into cytosol to generate calcium signals (Figure 2 - 7).

b. SOCE termination

ER refilling is often viewed as the final step to promote termination of SOCE and allow cells to return to resting state (Figure 2 - 8). SERCA pumps transport calcium back into the ER and if this refilling is prevented by treating cells with a SERCA inhibitor, such as thapsigargin (Tg), we observe long lasting cytosolic elevations. However, ER refilling is not sufficient to allow STIM1 de-oligomerization as it also requires a cytosolic calcium elevation {Shen et al. 2011, JBC}.

To slow down and ultimately stop SOCE, the key mechanism is calcium dependent inactivation (CDI) of ORAI1, a process divided in two components, fast and slow. Fast CDI (FCDI) is happening within a milliseconds time scale after channel opening. Calcium influx through ORAI1 itself is believed to be responsible for FCDI by a proposed mechanism of calcium binding to activation sites at the mouth of the channel opening {Zweifach and Lewis, 1995, JBC; Fierro and Parekh, 1999, J Membr Biol}. FCDI is also regulated by the STIM1 protein itself based on the STIM1 to ORAI1 stoichiometry with a stronger FCDI with and increased STIM1:ORAI1 ratio. The effect of STIM1 on FCDI has been narrowed down to its CRAC modulatory domain (CMD), a cytosolic portion of STIM1 enriched in negatively charged amino acids {Scrimgeour et al. 2009, J Physiol; Scrimgeour et al. 2014, BBA}.

Slow CDI (SCDI) is takes seconds to be put in place and accounts for 50% of ORAI1 calcium current inhibition. SCDI is a distinct mechanism from ER refilling, as Tg which blocks SERCA and prevent ER uptake, does not affect SCDI {Zweifach and Lewis, 1995, JBC; Parekh, 1998, J Biol Chem}. Most evidence of SCDI are pointing in the direction of long distance effectors which could explain the longer time needed for its activation. Mitochondria are known for their role as a calcium buffer organelle to prevent excess of calcium during stimulation. They exhibit a matrix calcium elevation during SOCE, forcing mitochondrial respiration to be sustained and abolish SCDI {Glitsch et al. 2002, EMBO J}. Calmodulin (CaM) is the main calcium effector in the cytoplasm, this protein is key in transduction of calcium signaling to many phosphorylation pathways. Recently, CaM has been suggested to play a role in SCDI by binding STIM1 and ORAI1 to help with the dissociation of the STIM1-ORAI1 complex. Both STIM1 and ORAI1 display a CaM binding site and its mutation in STIM1 prevents SCDI {Li et al. 2017, Nat Commun; Bhardwaj et al. 2020, Cell Physiol Biochem}.

Upon translocation to ER-PM junctions, STIM1 recruits another channel family, transient receptor potential cation (TRPC) which are non-specific cation permeant channels localized on the PM. Early on, studies have pointed out that TRPC1 is involved in SOCE as its overexpression increased calcium entry after ER depletion and that its activation was mediated by STIM1 {Zhu et al. 1996, Cell; Antigny

et al. 2013, J Cell Sci; Shi et al. 2017, Channels}. Additional studies have shown that TRPC1 can form a ternary complex with STIM1 and ORAI1 {Ong et al. 2007, J Biol Chem; Jardin et al. 2008, J Biol Chem}. There is no evidence of direct binding between ORAI1 and TRPC1 channels which suggests that the ternary complex is mediated by STIM1 binding through its K-rich domain or by an auxiliary protein. There is a dual role of TRPC1 in regulation of the SOCE, as it is part of the calcium entry channels it mediates part of the calcium influx. On the other hand, more studies are showing that TRPC1 plays a role in the attenuation of calcium entry. Because TRPC1 induces a stronger calcium entry, it could favor CDI by different ways. There is no evidence that associates TRPC1 with FCDI, but some studies are suggesting that SCDI is increased by the additional calcium elevation generated by TRPC1 (Figure 3a) {Lopez et al. 2020, Cells}. TRPC1 is permeant to both calcium and sodium with a 5-fold stronger preference toward calcium {Gees et al. 2010, CSH Perspect Biol}. Sodium entry through TRPC1 favors the sodium uptake and calcium release from mitochondria which adds up to the global cytosolic calcium elevation during SOCE {Villalobos et al. 2018, Pharmacol Res}. Cation entry during TRPC1 activity induces membrane depolarization which is believed to reduce the driving force of calcium during SOCE (Figure 3b). All these mechanisms participate in ending SOCE to prevent a sustained calcium entry which could lead to deleterious effects as previously discussed.

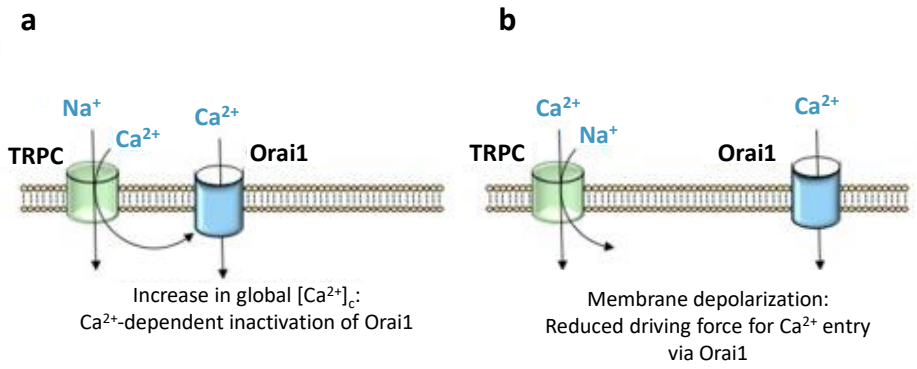

Figure 3: Overview of the modulation of Orai1 by TRPC channels.

Orai1 channel function might be positively or negatively regulated by TRPC channels in the vicinity. (a) Ca^{2+} and Na^{+} entry through TRPC channels might lead to membrane depolarization and thus attenuation of the electrical gradient that favors Ca^{2+} influx via Orai1. (b) Ca^{2+} entry via TRPC channels participates in global rises in $[Ca^{2+}]_c$, thus leading to Ca^{2+}-dependent inactivation of Orai1 channels.

Modified from Lopez et al. 2020, Cell

c. Molecular determinants diversity of SOCE

Since the discovery of STIM1 and ORAI1, new genes and isoforms have been identified and characterized. Some isoforms exhibit a cell type specificity and allow cells to adapt SOCE pathways to their needs. The original STIM1 protein discovered in 2007 is sometimes referred to as STIM1-Short in opposition to the STIM1-Long isoform discovered in 2011 while studying muscle development {Darbellay et al. 2011, JCB}. STIM1-Long is generated by an alternative splicing of the stim1 gene and

has an additional 106 amino acids arranged in an actin-binding domain (ABD). ABD maintains STIM1-Long within the ER-PM junctions to allow a fast activation of ORAI1 channels as illustrated by fluorescence microscopy {Sauc et al. 2015, JCS}. Compared to STIM1-Short, clusters formed by STIM1-Long are much smaller but still provide a stronger calcium influx upon store depletion. A recent study shined light on the activation of ORAI1 and TRPC1 by the two STIM1 isoforms {Dyrda et al. 2020, Cell Calcium}. The longer isoform is more prone to activate TRPC1 compared to ORAI1 whereas STIM1-Short shows the opposite. This preferred activation of TRPC1 by STIM1-Long is suggested to be responsible for higher calcium influx compared to the classic STIM1 isoform. Recently, more STIM1 isoforms have been discovered, among which, the first STIM1 inhibitory isoform found, for example, in testes and called STIM1A {Knapp et al. 2020 unpublished, bioRxiv}. Patch clamp and calcium imaging have shown that STIM1A acts as a dominant-negative isoform on SOCE. The same group just released a study about STIM1B, another isoform which is even shorter than the classic one and only expressed within neurons {Ramesh et al. 2021, Cell Reports}. STIM1B expression reduces SCDI compared to STIM1-Short and exhibit a slower kinetic of recruitment to ER-PM junctions.

STIM2 is the homolog of STIM1 and codes for a protein with a less sensitive EF-hand domain (affinities of 400 µM and 200 µM for STIM2 and STIM1, respectively) which allows STIM2 to be recruited to ER-PM junction with faster kinetics after ER depletion {Brandman et al, 2007, Cell; Zheng et al. 2008, Biochem Biophys Res Commun}. To better understand the recruitment of STIM2 to ER-PM junctions, a chimeric protein was generated from Kir6.2, an ER membrane protein, and the C-terminal (C-term) portion of either STIM1 or STIM2. Only chimeras containing the C-term of STIM2 was constitutively recruited to ER-PM junctions which was attributed to higher PIP_2 affinity of the K-rich domain of STIM2 {Ercan et al. 2009, Traffic}. So far, three isoforms of STIM2 have been identified and knockdown experiments helped to understand the way they modulate SOCE. The most common one is STIM2.2 or STIM2 alpha which preferentially acts as an activator compared to the less common STIM2.1 or STIM2 beta isoform shown to inhibit the SOCE {Soboloff et al. 2006, Current Biology; Miederer et al. 2015, Nature Comm}. The third isoform denominated STIM2.3 is shorter than the classic STIM2.2 but has not been extensively characterized.

The ORAI family is composed of three homologs: ORAI1, ORAI2 and ORAI3. ORAI1 is the only member with two identified isoforms both ubiquitously expressed and generated from an alternative translation initiation. ORAI1 alpha is the classic isoform identified as the main ORAI channel involved during SOCE. The second isoform, ORAI1 beta was identified in 2012 and also activates SOCE in a similar manner as ORAI1 alpha {Fukushima et al. 2012, JCS}. The main difference is that ORAI1 alpha contains a poly-arginine sequence which favors binding to PM phospholipids. Fluorescence recovery

after photobleaching (FRAP) experiments revealed that ORAI1 beta which lacks this poly-arginine sequence is able to travel faster within the PM and therefore favor ORAI1 clustering. ORAI2 and ORAI3 also bind to STIM and exhibit a high calcium entry but their current gets inactivated faster than ORAI1 {Lis et al. 2007, Curr Biol; Lee et al. 2009, PNAS}. ORAI2 has been found to modulate SOCE in T cells, driving immune response {Vaeth et al. 2017, Nat Commun}. Deletion of ORAI1 in T cells reduced SOCE, whereas deletion of ORAI2 increased calcium entry. This observation has been attributed to the fact that ORAI1 and ORAI2 are forming heteromeric channels and that ORAI2 attenuates heteromeric channel activity. The role of ORAI3 has been studied in the dorsal root ganglion neurons and it was shown that neuronal excitability was dependent on SOCE mediated by ORAI1 and ORAI3 {Wei et al. 2017, Front Cell Neurosci}. Recently, heart-specific deletion of ORAI3 led to heart failure in mice. This was associated with upregulation of TRPC6 and regulator of calcineurin 1 (RCAN1), indicating a profonde alteration of calcium signaling {Gammons et al. 2021, JAHA}.
The variety of ORAI1 proteins plays a role in fine tuning SOCE within different cell types and extracellular environments. This adaptation can be highlighted by the response to oxidative stress. Reactive oxygen species (ROS) such as H_2O_2 are toxic compound as they induce oxidation. Cysteine residues of proteins react particularly to ROS and form disulfide bonds with another cysteine residue, a reversible mechanism. Overall, oxidative stress has an inhibitory effect on SOCE and cell pretreatment with H_2O_2 inhibits SOCE when ORAI1 or ORAI2 but not ORAI3 is overexpressed in HEK cells stably expressing STIM1 {Bogeski et al. 2010, Sci Signal}. ORAI1 and ORAI2 both have a C195 which is absent in ORAI3. Investigation of redox sensitivity of each isoform revealed that C195 is critical in the ROS sensing property of ORAI channel. The addition of a cysteine in the equivalent position of ORAI3 conferred it a H_2O_2 sensitivity, whereas the replacement of the ORAI1 C195 by a non-oxidable residue made it partially H_2O_2 resistant. This difference in oxidative stress sensitivity is physiologically relevant, as during T cell activation, the expression of ORAI1 is replaced by ORAI3. A higher redox resistance has been observed in activated T cells upon H_2O_2 treatment (40% of SOCE inhibition against 87%) {Bogeski et al. 2010, Sci Signal}. This is a nice illustration of how T cells adapt to the oxidative environment during inflammation by expressing a more ROS-resistant ORAI protein.

3) Membrane contact sites (MCS)

ER-PM junctions discussed during SOCE are part of a more general type of junctions called membrane contact sites (MCS). The general definition of MCS is a close apposition of at least two membranes tethered together and involved in an inter membrane communication without fusion {reviewed in Scorrano et al. 2019, Nature Communications}. First descriptions of MCS originate from observations of the ER and mitochondria membranes in close apposition using electron microscopy

(EM) {Berhard and Rouillet, 1956, J Biophys Biochem Cytol; Copeland and Dalton, 1959, J Biophys Biochem Cytol}. The research field started to gain popularity when scientists discovered a functional role associated to MCS. First evidence came from phospholipid biosynthesis and transfer between ER and mitochondria {Vance, 1990, J Biol Chem}. Since then, more contacting organelles have been identified and associated with various cellular functions. To show how different these processes can be, we can cite regulation of mitochondrial fission {Friedman et al, 2011, Science}, calcium exchange between ER and mitochondria {Rizzuto et al. 1998, Science} or lipid transfer between ER and PM {Schauder et al, 2014, Nature}. It is now described that close proximity of membranes is maintained by tether proteins in most, if not all MCS {reviewed in Eisenberg-Bord et al. 2016, Developmental Cell}. It is expected that knockout of these tethers induces organelle mislocalization but in almost all cases, there is no strong alteration of organelle distribution. The main reason is the multitude of tethers involved in each MCS {De Brito and Scorrano, 2008, Nature; De Vos et al. 2012, Hum Mol Genet}.

a. Mitochondria associated membranes (MAM)

i. MAM in calcium signaling

ER generates MCS with all other organelles and ER-mitochondria is among the most studied. ER-mitochondria, also called MAM for mitochondria-associated membranes, have been extensively characterized, given the metabolic potential of mitochondria. The ultrastructure of MAM has been described using the gold standard technique in the field of MCS, electron microscopy which allows acquisition to the nanometer resolution at the cost of working with fixed samples. MAM are structures of approximately 200 nm in length for a gap distance between ER and outer mitochondrial membrane of 10 to 25 nm {Csordas et al, 2006, J Cell Biol}. Multiple roles have been attributed to MAM, their role in lipid transfer and metabolism was discussed earlier, but they are also relevant for calcium signaling. Calcium transfer from ER to mitochondria was first proposed when mitochondria-targeted aequorin allowed measurement of calcium elevation in mitochondrial matrix upon IP_3R activation {Rizzuto et al. 1993, Science}. Later, calcium transfer has been associated to a stimulation of ATP production by mitochondria {Jouaville et al. 1999, PNAS}. Calcium transfer to the mitochondrial matrix is mediated by MCU in the inner mitochondrial membrane. Its calcium affinity is pretty low (K_D of 10-30 µM). Because of this property, it was hard to understand how mitochondria could take up calcium under physiological stimulation where global calcium rises to only a few micromolar {Gunter and Gunter, 1994, J Bioenerg Biomembr}. A first answer came from observation that calcium elevations induced by IP_3R stimulation appeared to be higher around mitochondria than

in the cell bulk. This revealed that IP_3R in close proximity of mitochondria is critical for calcium elevation to reach a sufficiently high concentration to enter mitochondria matrix {Rizzuto et al. 1998, Science}. Moreover, VDAC, responsible for calcium transfer from cytosol to intermembrane space of mitochondria is enriched in MAM {Szabadkai et al. 2006, JCB}. All together, these studies highlighted the essential role of MAM in calcium transfer from ER to mitochondria and their functional role in ATP production.

ii. MAM morphology versus function

How MCS regulate physiological processes is suggested to be directly through their ultrastructure. To further understand how MCS morphology plays a role in signaling, it is interesting to look at the importance of MAM in calcium signaling. A study started to investigate the role of MAM ultrastructure and modified the intermembrane distance by expression of a tether protein. The shortening of ER-mitochondria distance from 24 nm to 6 nm strongly increased lateral dimension of MAM from 221 nm to 977 nm. How the intermembrane distance at MCS is linked to its lateral dimensions is not well understood and we do not know whether they are tightly associated with one another or if they are independently regulated. However, this modification of MAM morphology was associated with a sensitization of Tg-induced calcium overload and mitochondria membrane permeabilization {Csordas et al, 2006, J Cell Biol}. These results suggest that MAM ultrastructure is playing a role in the efficiency of the physiological response and its regulation could present a fine-tuning mechanism for cells.

Interestingly, another study highlighted the importance of ER-mitochondria distance in the efficient calcium transfer from ER to mitochondria. They found that expression of FATE1, a cancer-testis antigen, is associated to cancer development and exhibits an "anti-tether" role by uncoupling ER and mitochondria which in turn reduces calcium uptake by mitochondria {Doghman-Bouguerra et al. 2016, EMBO Rep}.

Overall, MAM play a critical role in calcium exchange from ER to mitochondria and MAM ultrastructure is directly modulating the calcium transfer efficiency. One could extend this regulatory aspect of MAM to other MCS and investigate if MCS ultrastructure is directly linked to their function.

b. ER-PM contact site

ER-PM contact sites have been extensively studied and they have been reported to play an important role in lipid homeostasis and calcium signaling. Ultrastructure of ER-PM shows a distance ranging from 10 nm to 30 nm which makes it permissive to protein interaction as we saw with STIM1 during SOCE. ER-PM junctions are dynamic structures which are evolving and adapting with cell needs and

upon physiological stimulation {reviewed in Li et al. 2021, Front Cell Dev Biol}. Interestingly, ER-PM contact sites come in very different shape as described by Orci and colleagues {Orci et al. 2009, PNAS} and cER usually does not exhibit ribosomes on the contact face to PM. In this introduction, we are going to focus on the role of ER-PM junction in calcium signaling but it is good to keep in mind that they also play a part in other mechanisms. In exocytosis, they serve as gateway to prevent PM access and for example restrict exocytosis for polarized morphogenesis of the yeast {Yunn Ee Ng et al., 2018, Current Biology}. ER-PM junctions have recently been described to help in the total cell cholesterol regulation as sensing platform for PM cholesterol level and induced the increase of cholesterol uptake and synthesis when needed {Infante and Radhakrishnan, 2017, eLife}.

i. PIP_2 homeostasis to sustain calcium entry

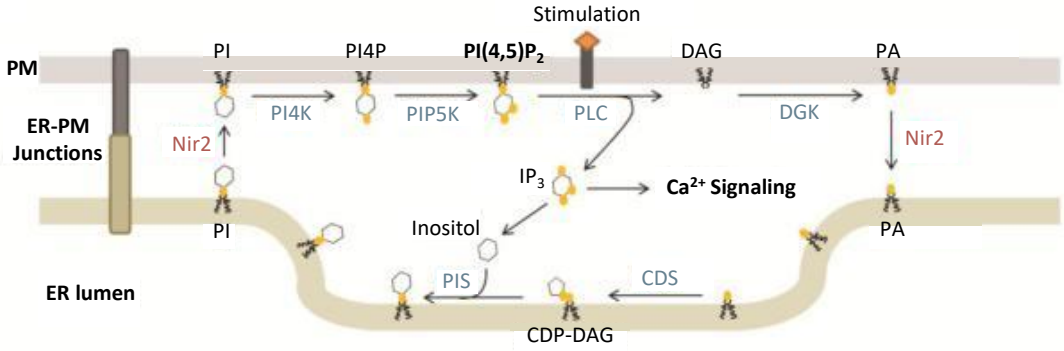

Figure 4: Updated model of the PI cycle with Nir2 mediating PI-PA exchange at ER-PM junctions.

PI4K: PI-4 kinase; PIP5K: PI4P-5 kinase; CDS: CDP-DAG synthase; PIS: PI synthase.

Modified from Chang and Liou, 2016, BBA

Regulation of lipid homeostasis by ER-PM junctions to sustain calcium signaling is a beautiful example of MCS communication. During SOCE, PIP_2 is hydrolyzed in PM to generate IP_3 which in turn mediates calcium entry though ER depletion. To sustain calcium entry and maintain PIP_2 homeostasis, it is vital to quickly restore PM PIP_2 levels, but the cell faces a challenge. Phosphatidylinositol (PI), the PIP_2 precursor, is synthetized in the ER membrane by a series of enzymatic reactions {Agranof et al. 1958, J Biol Chem}. How PI is then transferred to PM for PIP_2 synthesis was for a long time believed to be exclusively vesicular dependent. However, in 2015, discovery of Nir2, a cytosolic lipid transfer proteins (LTP) helped to better understand the inter-organelle PI cycle {Kim et al. 2011, Dev Cell; Cockcroft and Garner, 2013, Adv Biol Regul}. Nir2 is enriched in ER-PM contact sites upon receptor stimulation and its knockdown impairs calcium signaling {Chang et al. 2013, Cell Rep; Kim et al. 2013, EMBO Rep; Chang and Liou, 2015, J Biol Chem; Kim et al. 2015, Dev Cell}. PI cycling between PM and

ER is now well characterized (Figure 4). After PLC activation and DAG production, diacylglycerol kinase (DGK) mediates conversion of DAG into phosphatidic acid (PA) within the PM. The LSN2 domain of Nir2 binds PA and its PI transfer protein (PITP) domain clears PA from the PM by transferring it to the ER. PA is then transformed intp cytidine diphosphate diacylglycerol (CDP-DAG) and an inositol group is added by the PI synthase (PIS) to generate PI. Finally, Nir2 transfers PI back to PM where it is phosphorylated in a two-step process to regenerate PIP_2. There are still unanswered questions on this subject, such as how Nir2 transfers PI and PA between ER and PM. We do not know whether PI is exchanged to PA or if only one of the two can be transferred at once. Overall, PI cycle maintained by ER-PM junctions through Nir2 activity is essential for maintenance of calcium signaling during SOCE.

ii. Regulation of ER-PM distance during SOCE

ER-PM contact sites are highly dynamic during SOCE, and we do not fully understand the relationship between their ultrastructure and regulation of calcium entry. Ultrastructure of MCS is usually defined by two main parameters extracted from EM images, intermembrane distance, and length of the contact. ER-PM gap distance is controlled by tether proteins, and spans from 10 nm to 25 nm based on EM data of resting Jurkat and HeLa cells {Wu et al. 2006, JCB; Chang et al. 2013, Cell Rep}. During SOCE stimulation, this distance is regulated by the extended synaptotagmin (ESyt) protein family, ER-resident tethers. Under resting conditions, total internal reflection fluorescence (TIRF) microscopy revealed that ESyt1 is found deeper inside the ER membrane compared to ESyt2 and Esyt3 which are localized in cER {Giordano et al. 2013, Cell}. cER localization of ESyt2/3 depends on their C2C domain which is responsible for binding of PIP_2 on the PM. During SOCE, ESyt1 is recruited from ER to cER by a calcium-mediated process dependent on C2 domains of ESyt1 {Idevall-Hagren et al, 2015, EMBO J; Giordano et al, 2013, Cell}. Recruitment of ESyt1 induces a shortening of ER-PM gap distance from 21.8 nm to 14.8 nm in COS-7 cells {Fernandez-Busnadiego et al, 2015, PNAS}. ESyt1 knockdown causes a defect in replenishment of PM PIP_2 {Chang et al. 2013, Cell Rep}. This phenotype could be rescued by expressing wild type ESyt1 but not ESyt1-D724A mutant which fail to translocate to ER-PM junction. ESyt1 recruitment is associated with the accumulation of Nir2 within ER-PM junctions. From these observations, Chang and colleagues suggested that distance shortening induced by ESyt1 was key to PIP_2 replenishment through Nir2 recruitment to ER-PM junctions. Using artificial ER-PM tether proteins they investigated if shortening the ER-PM distance independently of ESyt1 is sufficient to recruit Nir2. The artificial tether MAPPER-L does not alter the 10 nm to 25 nm ER-PM distance and upon histamine treatment, Nir2 is not recruited to ER-PM junctions. Upon expression of MAPPER-S, a shorter artificial tether fixing distance to 10 nm, agonist stimulation with histamine induced recruitment of Nir2. This evidence strongly suggests that the ultrastructure of ER-

PM junction is directly involved in the recruitment of Nir2 and PIP_2 replenishment. Recently, ESyt1 was also shown to stabilize ER-PM junctions and favor ER refilling during calcium entry {Kang et al. 2019, Scientific Reports}.

Other studies suggest that ER-PM distance is plays a role during SOCE. Increasing ER-PM distance by ~6 nm using a synthetic form of Sec22b, a tether protein bridging ER-PM, reduced ER calcium content and delayed calcium refilling {Petkovic et al. 2014, Nat Cell Biol}. On the other hand, ER-PM distance shortening to less than 6 nm by artificial tethers restricted access of ORAI1 but not STIM1 to ER-PM junctions {Varnai et al. 2007, J Biol Chem}. Both STIM1 and ORAI1 could populate MCS when the distance was set to 11-13 nm by a more permissive artificial tether. Altogether, these data support a pivotal role of ER-PM distance in regulation of calcium fluxes during SOCE.

iii. Regulation of ER-PM size during SOCE

We saw that intermembrane distance decreases during SOCE with the binding of the ER-STIM1 and PM-ORAI, but ER-PM junctions are also dynamic regarding cER length which dramatically increases during SOCE. First observation of cER size increase upon a calcium dependent process was reported in 1983 in xenopus oocytes. Fully grown but immature oocyte exhibits about 2% of membrane coverage by cER against 25-30% in the animal hemisphere of mature oocyte. During oocyte maturation, cytosolic calcium elevations have been reported and suggested to be responsible for increase of cER membrane coverage {Gardiner and Grey, 1983, J Cell Biol; Moreau and al. 1980, Dev Biol; Wasserman et al. 1980, PNAS}.

More recent studies revealed that cER coverage of PM increases upon ER calcium depletion in a STIM1 dependent manner. PM coverage increases up to 5.3-fold from 0.23% to 1.24% in HeLa cells treated with Tg, a SERCA blocker inducing ER depletion. This mechanism has been attributed to STIM1 as its overexpression brings the resting coverage to 1.40% {Orci et al, 2009, PNAS}. In Jurkat cells, about a third of final ER-PM junctions form in response to ER calcium depletion and increases the cER coverage by 55%. In cells overexpressing STIM1, this increased coverage was more prominent and individual cER structures were longer {Wu et al. 2006, J Cell Biol}.

STIM1-dependent increase of cER structures is regulated in an isoform-dependent manner as the STIM1-Long isoform shows a different puncta pattern than the classic STIM1-Short isoform. STIM1-Long is recruited to the cER at rest and forms puncta which are smaller than with STIM1-Short after ER depletion {Sauc et al. 2015, JCS}. Furthermore, STIM1-Long does not induce an increase of cER size upon ER depletion by Tg. This evidence supports the role of STIM1-Short but not STIM1-Long in remodeling of ER-PM junctions during SOCE. Interestingly, calcium entry evoked by STIM knockout cells re-expressing STIM1-Short was lower than that of STIM1-Long re-expression. This suggest that cER could have a role in calcium entry regulation. However, another study of calcium elevation

evoked by STIM1-Long suggests that it is because TRPC1 is more activated by STIM1-Long than STIM1-Short {Dyrda and al. 2020, Cell Calcium}.

A few other proteins have been shown to alter cER length such as ER-resident calcium binding protein Junctate. Knockdown of Junctate reduced MCS size from 218 nm to 139 nm and decreases calcium entry through SOCE. On the other hand, overexpression of Junctate, increased cER length up to 339 nm and increased SOCE {Treves et al. 2004, JCB}. Association of increased cER size and higher calcium entry suggest that during SOCE, cER elongation plays a role in the development of a robust calcium entry.

During the study of the role of ESyt2 and ESyt3 during SOCE, an interesting observation was made as their overexpression leads to massive generation of closely apposed ER-PM junction with an intermembrane distance of ~10 nm {Giordano et al. 2013, Cell}. It is not clear whether this is just an artefact from overexpression or if ESyt2/3 have the potential to generate strong modification of ER-PM ultrastructure.

Overall, the role of ER-PM junction size in regulation of calcium entry is still unclear. Evidence points out that long cER structures tend to enhance SOCE efficiency, but no studies directly investigated how modifying cER size affects calcium entry or ER refilling.

V) Aim of the study

The goal of my PhD thesis was to investigate how the calcium fluxes of ER-PM junctions are regulated by the ultrastructure of the contact sites. As we discussed in the introduction, MCS are important player of the calcium signaling either in the MAM or the ER-PM junctions. The morphology of the ER-PM contacts is highly dynamic during calcium signaling, especially during SOCE. Studies are pointing out the role of the MCS ultrastructure in the regulations the calcium entry. However, no studies have looked at both the cER length and the ER-PM distance of corresponding ER-PM junctions and how these two parameters can be modulated by the expression of tether proteins and in turn how it modulates SOCE. By associating electron microscopy and calcium imaging, I extracted and correlate both ultrastructural parameters and calcium fluxes during SOCE.

A second part of my thesis was to develop new analytic tools using programming in ImageJ, VBA and Matlab. The tools I developed were initially aimed to be used for my own daily analysis but over time they became part of the routine analysis pipeline of many people in our lab and of some collaborators.

VI) Scientific article

This scientific article is submitted to Journal of Cell Science. The authors are Christopher Henry (CH), Amado Carreras-Sureda (ACS) and Nicolas Demaurex (ND). CH designed the strategy, acquired, analyzed, and interpreted all the data (electron microscopy and calcium imaging included). CH developed the softwares/scripts, prepared the figures, and wrote the manuscript. ACS analyzed and interpreted calcium imaging data and corrected the manuscript. ACS also supervised me and provided technical and methodological advice for calcium imaging. ND supervised me, raised funds and wrote the manuscript. ND designed the strategy, analyzed, and interpreted data.

Store-operated calcium entry (SOCE) is an essential calcium signaling pathway found in most human cells. Upon extracellular stimulation, inositol trisphosphate (IP_3) is generated and induces depletion of endoplasmic reticulum (ER) calcium store through IP_3 receptor. The drop of calcium concentration within the ER lumen is sensed by the ER calcium sensor STIM1. This triggers a conformational rearrangement of STIM1 exposing key cytosolic domains which favor its oligomerization and translocation to cortical ER (cER) regions. Within cER, STIM1 binds and gates the ORAI1 calcium channel on the plasma membrane (PM), leading to cytosolic calcium entry. Calcium elevation leads to inactivation of ORAI1 channel though calcium dependent inactivation (CDI) processes. Fast CDI happens in ms range mainly from electrochemical changes due to calcium elevation at the channel mouth. Slow CDI takes place few seconds after calcium entry and involves activation of accessory proteins such as calmodulin which help to detach STIM-ORAI complexes. Ultimately, refilling of ER calcium and CDI mechanisms are responsible for SOCE termination.

Interaction between STIM and ORAI takes place in close apposition of the cER and the PM, the so called ER-PM contact sites, where intermembrane distance ranges from 10 nm to 25 nm. This short distance, permissive to intermembrane protein interaction, is regulated during SOCE. ESyt1 protein is recruited to ER-PM junctions upon calcium entry and is associated with a shortening of gap distance from 21.8 nm to 14.8 nm. During SOCE, ER-PM junctions size is also dynamically regulated. cER lateral dimensions as well as its overall PM coverage is drastically increased in a STIM1 dependent manner. Electron microscopy (EM) imaging reported that during SOCE, the overall cER coverage of the PM goes from 0.23% to 1.24%.

Ultrastructure of ER-PM contact sites has been suggested to play an important role in regulation of SOCE. Gap distance is thought to regulate access of partner proteins to STIM-ORAI complex and shortening of intermembrane distance to 5 nm exclude accumulation of ORAI1 to contact sites.

Recruitment of ESyt1 is associated with a stabilization of ER-PM junctions, suggested to favor ER calcium refilling.

In this publication, we study the relationship between ER-PM contact sites ultrastructure and SOCE. We genetically modulated ER-PM junctions with endogenous and artificial tethers then used calcium imaging to measure the endogenous response. Using EM, we revealed that while cER increases during store depletion, intermembrane distance is not much affected, and that the following calcium addition did not modify ER-PM ultrastructure. By expressing the tether ESyt2 or the synthetic MAPPER-Long, we observed very long cER cisternae, at rest. Interestingly, after ER depletion, formation of longer cER was dramatically increased in number and size when any tether was expressed. This was particularly striking with ESyt2 and MAPPER-Long which generated some ER-PM junctions 4.2 times longer than the longest in control (434 nm for control against 1813 nm for MAPPER-Long). Interestingly, despite having longer contact sites generated by ESyt2 or MAPPER-Long we reported a ~50% reduction in SOCE. Manganese quench experiments suggest that long cER structures totally abrogate calcium influx 2 min after calcium entry. Additionally, extension of cER reduces calcium mobilized by agonist stimulation through IP_3R without reducing global ER calcium content.

Enforced tethering elongates the cortical endoplasmic reticulum and limits store-operated calcium entry

Christopher Henry[1], Amado Carreras-Sureda[1], & Nicolas Demaurex[1]

[1]Department of Cell Physiology and Metabolism, University of Geneva, Geneva, 1211, Switzerland.

Corresponding Author:

Nicolas Demaurex

Department of Cell Physiology and Metabolism,

Rue Michel-Servet, 1

University of Geneva,

Switzerland.

Abstract

Recruitment of STIM proteins to cortical ER (cER) domains forming membrane contact sites (MCS) mediate the store-operated Ca^{2+} entry (SOCE) pathway essential for human immunity. The cER is dynamically regulated by STIM and tethering proteins during SOCE, but the ultrastructural rearrangement and functional consequences of cER remodelling are unknown. Here, we express natural (E-Syt1/2) and artificial (MAPPER-S/L) protein tethers in HEK-293T cells and correlate the changes in cER length and gap distance measured by electron microscopy with ionic fluxes. Native cER cisternae extended during store depletion and remained elongated at constant ER-PM gap distance during subsequent Ca^{2+} elevations. Tethering proteins enhanced store-dependent cER expansion, anchoring the enlarged cER at tether-specific gap distances of 12-15nm (E-Syts) and 5-9nm (MAPPERs). Cells with artificially extended cER had reduced SOCE and reduced agonist-induced Ca^{2+} release. SOCE remained modulated by calmodulin and exhibited enhanced Ca^{2+}-dependent inhibition. We propose that cER expansion mediated by ER-PM tethering negatively regulates SOCE by confining STIM-ORAI complexes to the periphery of enlarged cER sheets, a process that might participate in the termination of store-operated Ca^{2+} entry.

Introduction

Store operated calcium entry (SOCE) is a ubiquitous signaling mechanism that plays an essential role in immunity and muscle function in humans by mediating long-lasting calcium signals that control gene expression and cell proliferation (Vaeth et al., 2017). Upon agonist stimulation, G-coupled receptors generate inositol trisphosphate (InsP3) that mobilize Ca^{2+} from the endoplasmic reticulum (ER). The ensuing Ca^{2+} depletion of the ER is sensed by the ER membrane-resident protein stromal interaction molecule 1 (STIM1) (Liou et al., 2005; Roos et al., 2005; Zhang et al., 2005) via its luminal EF-hand and sterile alpha motif (SAM) domains (Stathopulos et al., 2006). This initiates a conformational change that releases an intramolecular clamp between cytosolic coiled-coil domains, leading to STIM1 extension and oligomerization (Hirve et al., 2018; Schober et al., 2019). The switch into an elongated conformation unveils STIM1 channel activating domain (CAD) and exposes a K-rich polybasic C-terminal tail that binds to negatively charged lipids (Stathopulos and Ikura, 2010; Stathopulos et al., 2006; Zhang et al., 2005). Tail and CAD exposure promote the translocation of STIM1 oligomers to cortical ER (cER) regions and enable STIM1 to trap and gate the ORAI family of Ca^{2+}-selective channels (Feske et al., 2006; Vig et al., 2006; Zhang et al., 2006). The flow of Ca^{2+} ions across ORAI channels sustains long-lasting cytosolic Ca^{2+}signals and enables the refilling of ER calcium stores by sarco/ER Ca^{2+}-ATPase (SERCA) pumps (Chang et al., 2013; Malli et al., 2007; Mullins et al., 2009), thereby terminating SOCE. Excessive Ca^{2+} entry is prevented by fast (ms) and slow (sec) calcium dependent inactivation (CDI) mechanisms mediated in part by calmodulin and SARAF, which interact with STIM-ORAI complexes to regulate channel activity (Bhardwaj et al., 2020; Jardin et al., 2018; Palty et al., 2012).

The SOCE process relies on the generation and maintenance of ER-PM membrane contact sites (MCS) (Gudlur et al., 2019) that enable productive interaction between STIM and ORAI proteins by maintaining an appropriate gap distance ranging from 10 to 30 nm between the cER and the PM (Scorrano et al., 2019; Wu et al., 2017). The MCS morphology evolves during the SOCE process as STIM

and other tethering proteins are recruited to the cER and reversibly bind to PM lipids and interact with cognate PM proteins. In HeLa cells the surface covered by MCS increases ~5-fold (from 0.23% to 1.24%) upon calcium depletion, a remodeling that is recapitulated by STIM1 expression in cells with replete stores (Orci et al., 2009). Expression of STIM1, but not of the muscle-specific STIM1L isoform, increases MCS coverage in mouse embryonic fibroblasts (MEF) and in myoblasts, indicating that distinct STIM1 isoforms have different membrane-shaping functions (Sauc et al., 2015). Other tethering proteins were also reported to participate in the dynamic formation of MCS during SOCE. Junctate stabilizes the intracellular MCS generated by STIM1, thereby contributing to prophagocytic Ca^{2+} signals by recruiting inositol-trisphosphate receptors (InsP3R) to phagosomes (Guido et al., 2015). The extended synaptotagmin 1 (E-Syt1) is recruited to the cER upon Ca^{2+} elevations (Giordano et al., 2013; Idevall-Hagren et al., 2015), and its expression induces a shortening of the ER-PM gap distance from 21.8 nm to 14.8 nm in COS-7 cells (Fernandez-Busnadiego et al., 2015). The two other E-Syt isoforms, E-Syt2 and E-Syt3 are already localized within MCS at rest and do not promote gap shortening upon calcium entry (Giordano et al., 2013). The maintenance of an appropriate ER-PM gap distance at MCS was proposed to regulate SOCE by enabling the access of additional molecular components to STIM1-Orai1 complexes (Varnai et al., 2007), while the Ca^{2+}-dependent E-Syt1 recruitment was proposed to facilitate the recruitment of the phosphatidylinositol transfer protein Nir2 to replenish PM PIP2 following receptor-induced hydrolysis (Chang et al., 2013). A subsequent super-resolution microscopy study showed that the Ca^{2+}-dependent recruitment of E-Syt1 stabilizes ring-shaped MCSs forming around STIM1/ORAI1 MCSs, a process proposed to facilitate local ER Ca^{2+} replenishment (Kang et al., 2019).

The importance of MCS in Ca^{2+} signaling and lipid trafficking motivated several groups to develop artificial ER-PM tether proteins to label and manipulate MCS. Using the TM domain of STIM for ER retention and the polybasic motif of the small G protein Rit for constitutive binding to PM phosphoinositides, the group of Jen Liou developed a genetically encoded marker for ER-PM junctions termed “MAPPER” for “membrane-attached peripheral ER” (Chang et al., 2013). Two versions were

generated: a long version (MAPPER-L) bearing flexible cytosolic linkers meant to preserve the endogenous 10-25 nm ER-PM gap distance and a shorter version (MAPPER-S) designed to restrict the gap distance of the labeled junctions to 10 nm. MAPPER-L was enriched in the cER independently of the ER Ca^{2+} concentration while STIM1 and E-Syt1 translocated into MAPPER-L-labeled structures following agonist stimulation of Ca^{2+} store depletion. MAPPER-L labeling did not perturb the endogenous ER-PM junctions and did not impact SOCE while E-Syt1 recruitment to MCS shortened the ER-PM gap without altering the sizes and shapes of individual junctions (Chang et al., 2013). The MAPPERs were subsequently used to study the distribution of ER proteins populating ER-PM junctions (Thillaiappan et al., 2017; Zewe et al., 2018) and to study MCS dynamics (Poteser et al., 2016). The later study revealed that the junctional ER expands during SOCE in RBL-2H3 cells in a process that requires external Ca^{2+} (Poteser et al., 2016). In several instances however, expression of mCherry-tagged MAPPER-L induced the formation of abnormally large MCS (Besprozvannaya et al., 2018; Thillaiappan et al., 2017), suggesting that MAPPER-L is not simply labeling cER structures but modifying their morphology.

To better understand the role of MCS morphology during SOCE, we expressed the natural and artificial tether proteins E-Syt1, E-Syt2 and MAPPERs in HEK-293T cells and measured the ER-PM gap distance and cER length by electron microscopy (EM). Quantification of the cER morphometric parameters revealed that very large cER structures were generated by the expression of E-Syt2 or MAPPER-L during ER Ca^{2+} depletion, a process that was partly reverted upon Ca^{2+} entry. Fura-2 recordings revealed that SOCE was reduced in cells expressing either E-Syt2 or MAPPER-L, suggesting that the cER length negatively regulates SOCE efficiency.

Results

Ca^{2+} stores depletion enlarges natural and artificial cortical ER cisternae

To establish how ER-PM tethering alters the structure and dynamics of the cER, we transiently transfected HEK-293T cells with a plasmid expressing GFP-tagged versions of natural (E-Syt1/2) or artificial (MAPPER-S/L) tether proteins. We first verified by total internal reflection fluorescence (TIRF) microscopy that our tether proteins are recruited to regions of the ER close to the PM using thapsigargin (Tg) to deplete ER Ca^{2+} stores and favor the formation of STIM1-mediated ER-PM MCS. GFP-E-Syts and GFP-MAPPERs were detected in the TIRF plane as punctate fluorescent structures of similar appearances (Fig. S1A). The individual puncta were outlined with a custom Fiji/ImageJ script to determine morphometric parameters and the footprint of single cells manually outlined to calculate the MCS density (Fig. S1B). The individual MCS area averaged was 0.3 µm² and these structures covered 5-10% of the PM surface, without significant differences in these parameters between each pair of tether proteins (Fig. S1C). These data indicate that all 4 tether proteins accumulate in the TIRF plane into structures of similar apparent size when observed by optical microscopy.

To resolve the ultrastructure of the MCS forming during Ca^{2+} store depletion, we analyzed by EM the morphology of individual cER structures in cells fixed and embedded in Epon in situ. This procedure optimally preserves cellular architecture and maintains the orientation of cells relative to the substrate. Cells were sorted by flow cytometry to ensure that equal amounts of tether proteins were expressed (Fig. S2) and were divided in three conditions: 1) naïve, untreated cells, 2) cells exposed to 1 µM Tg for 10 min in the absence of Ca^{2+} to induce the depletion of ER Ca^{2+} stores and elicit SOCE, and 3) cells treated with Tg as in 2) and re-exposed to 1 mM Ca^{2+} for 2 min to enable Ca^{2+} influx and evaluate the impact of Ca^{2+} elevations on MCS morphology (Fig. 1A). cER structures were identified on the EM images as ER sheets located <30 nm from a continuous segment of the PM (Fig. 1B), and each contiguous cER unit was manually outlined to determine two parameters: the ER-PM gap distance and the length of single cER units. The ER-PM distance was extracted using a custom Matlab script

measuring the average distance between each pixel from 2 lines manually created along each membrane. The cER length was obtained in Fiji using the segmented line tool to follow the cER with accuracy (Fig. 1C). In non-treated HEK-293T cells the average gap distance and cER length were 17 nm and 66 nm, respectively (Fig. 1D, top panel and Table 1). In cells treated with Tg, a massive elongation of the cER was observed, the average length increasing by 2.3-fold, from 66 to 156 nm, while the ER-PM gap distance remained unchanged (Fig. 1D, middle panel and Table 1-2). We then calculated the volume of the cytosolic cleft contained between the cER and PM membranes, assuming that cER sheets form cylindric structures close to the PM (Fig. S3D). The cleft volume increased by 4.8-fold upon Tg treatment (Fig. 1D, bottom panel and Tables 1-2). Interestingly, the gap distance, cER length, and cleft volume were not impacted by the readmission of Ca^{2+} to cells treated with Tg (Fig. 1D). These ultrastructural observations indicate that cER are dynamic structures that elongate during store depletion, as previously shown for cells overexpressing STIM proteins (Orci et al., 2009; Sauc et al., 2015; Wu et al., 2006), but that the ER-PM gap distance remains constant during SOCE activation and Ca^{2+} entry. Furthermore, the length of native cER structures and their gap distance are not affected by cytosolic Ca^{2+} elevations occurring during SOCE.

E-Syts and MAPPERs expression generates large cER upon Ca^{2+} store depletion

We then assessed the impact of E-Syts or MAPPERs expression on MCS ultrastructure. In resting cells, the average gap distance and cER length were not impacted by the expression of any of the tether proteins (Tables 1-2), but MAPPER-L and E-Syt2 induced the apparition of cER cisternae longer than 300 nm (Fig. 2A). These elongated cER structures stabilized at specific gap distance of 5.2 nm and 13.5 nm, respectively, clearly apparent on the gap vs. length scatter plots (Fig. 2B). Following Ca^{2+} store depletion with Tg, the elongation of the cER was greatly potentiated in cells expressing any of the tether proteins, the average length increasing by 4.5-fold in cells expressing MAPPER-L, from 117 to 521 nm (Fig. 3 and Table 1). Interestingly, as the length of individual cER structures increased, the gap distance decreased to values specific for each family of tether protein, of 12-15 nm for the E-

Syts and 5-9 nm for the MAPPERs (Fig. 3B). Ca^{2+} store depletion was associated with a shortening of the averaged ER-PM distance in cells expressing all tethers except E-Syt2, the averaged gap decreasing from 17.3 nm to 14.9 nm in cells expressing E-Syt1 upon Tg addition (Tables 1-2). After readmission of Ca^{2+} to enable Ca^{2+} influx, the cER length decreased significantly in cells expressing all tethers except MAPPER-S, while the gap distance returned to pre-stimulatory values in cells expressing E-Syt1 (Fig. S3 and Tables 1-2). In cells expressing the other tethers, the gap distance remained unchanged and cER cisternae longer than 300 nm were still clustered at gap distances specific for each tether (Fig. 3C). As the cER expanded, the cleft volume increased upon Tg treatment in all conditions by up to 16.9-fold, with the largest volumes observed in cells expressing E-Syt2 and MAPPER-L (Fig. S3 and Tables 1-2). These observations indicate that ER-PM tethering enhances cER expansion during store depletion by anchoring elongated cER cisternae at fixed gap distances, and that this elongation process is partly reversed during the Ca^{2+} entry phase. The expanded cER sheets are anchored at 12-15 nm from the PM by E-Syts and at 5-9 nm by MAPPERs and these gap distances are minimally affected by changes in cytosolic Ca^{2+} concentration.

Effect of ER-PM tethering on Ca^{2+} store homeostasis and SOCE

To assess whether the cER expansion facilitated by ER tethering impacts SOCE, we measured the cytosolic Ca^{2+} elevations during the Tg/readmission protocol with Fura-2 in cells expressing E-Syts or MAPPERs at equivalent levels. The Ca^{2+} elevations evoked by Tg in Ca^{2+}-free medium were comparable in all conditions, indicating that the global ER Ca^{2+} content is not impacted by ER tethering (Fig. S4A). The SOCE responses, however, were significantly reduced by ER tethering and the Ca^{2+} entry rates measured following readmission of 1 mM Ca^{2+} were decreased by 60 and 40 % in cells expressing E-Syt2 and MAPPER-L, respectively (Fig. 5A-B). We confirmed that SOCE was still reduced in cells expressing E-Syt2 or MAPPER-L after they were FACS sorted for EM experiment (Fig. S4B). Since these two protein tethers induce a maximal cER expansion that is Ca^{2+}-dependent, we tested whether the SOCE defect is also Ca^{2+} dependent by varying the concentration of Ca^{2+} readded following Tg exposure.

The SOCE defect associated with MAPPER-L expression persisted when the Ca^{2+} concentration was decreased to 0.5 mM or increased to 2 mM Ca^{2+}, but when the Ca^{2+} concentration was increased to 10 mM comparable rates of Ca^{2+} entry were recorded in cells expressing or not the ER-PM tethers. (Fig. 5C). Interestingly, at 2 mM Ca^{2+} we observed a slight increase of the calcium entry rate when MAPPER-S was expressed. These data indicate that the expression of tethering proteins that promote cER expansion inhibit SOCE, and that the associated ultrastructural and functional effects are both Ca^{2+}-dependent.

To clarify the Ca^{2+} signaling defect associated with ER tethering, we expressed the two MAPPER constructs in different cell types. The SOCE defect associated with MAPPER-L expression was recapitulated in MEF cells, while a reduced SOCE was observed in HeLa cells expressing either the long or short MAPPER constructs (Fig. S5B-C). This indicates that the SOCE defect associated with ER tethering is not restricted to a specific cell type or to proteins tethering the ER at a specific gap distance, but is likely related to the cER expansion. To better assess the contribution of local Ca^{2+} fluxes in the functional effects of the MAPPERs, we then used the reversible SERCA inhibitor cyclopiazonic acid (CPA) to allow the refilling of depleted ER Ca^{2+} stores during Ca^{2+} readmission. SOCE was equally reduced by the two MAPPERs when CPA was used to transiently deplete ER Ca^{2+} stores in HEK-293T cells (Fig. 6A), uncovering a defect associated with MAPPERs that was not observed when Tg was used to irreversibly deplete Ca^{2+} stores (Fig. 5B).

To evaluate the impact of the MAPPERs on ER Ca^{2+} homeostasis we recorded the changes in the ER Ca^{2+} concentration with the ER-targeted Ca^{2+} probe R-CEPIA1$_{ER}$ during CPA-induced Ca^{2+} stores depletion and subsequent refilling. A faster ER Ca^{2+} depletion was observed in cells expressing MAPPER-L while no differences in the refilling kinetics were observed in cells expressing the MAPPERs (Fig. 6B). Unaltered refilling kinetics were also observed with the ratiometric ER calcium probe D1$_{ER}$ (Fig. S5). To test whether the faster ER Ca^{2+} leak impacts physiological Ca^{2+} fluxes, we then exposed cells to the InsP3-generating agonist ATP to promote the rapid release of Ca^{2+} from ER stores. The

amplitude of the ATP-induced Ca^{2+} elevations recorded in the absence of Ca^{2+} was reduced by ~20% when either of the two MAPPER construct was expressed (Fig. 6C). These data indicate that the expression of tethering proteins that promote cER expansion accelerates ER Ca^{2+} leak, thereby reducing the ability of cells to release Ca^{2+} from InsP3-sensitive stores.

To get insight into the underlying mechanism, we then investigated the impact of ER tethering on cytosolic Ca^{2+} extrusion by removing Ca^{2+} shortly after its readmission to cells treated with Tg. The Ca^{2+} concentration decreased rapidly following Ca^{2+} removal and the decay rates were not altered by the expression of the MAPPER proteins (Fig. 7A). This indicates that the cER expansion associated with ER tethering does not impact Ca^{2+} efflux at the PM, a process mediated by PMCA. The increased ER-PM cleft volume associated with ER tethering could promote the accumulation of STIM1-ORAI1 interactors that negatively regulate SOCE. To test this possibility, we overexpressed wild type or dominant-negative fluorescent calmodulin (CaM) constructs together with the MAPPER tethers. In control cells, expression of WT CaM decreased SOCE while DN CaM increased SOCE (compare Figs 7B-C and 5B), confirming that CaM negatively regulates STIM-ORAI1 interactions as previously reported (Singh et al., 2012; Bhardwaj et al., 2020). In these settings, SOCE remained reduced in cells expressing MAPPER-L (Fig. 7B-C), indicating that the negative regulation of SOCE associated with ER tethering is not relieved by preventing the activity of calmodulin.

To verify that cER tethering altered the permeability of SOCE channels, we added the divalent cation Mn^{2+}, which permeates SOCE channels and quenches the fluorescence of fura-2, measured at the isosbestic wavelength of 360 nm. The basal rates of Mn^{2+} quenching recorded in Ca^{2+}-containing medium prior to cell stimulation were slightly increased by the expression of MAPPER-L (Fig. 8A-B). Tg exposure increased the quench rates by 2.4-fold in control cells and by 1.8-fold in cells expressing the MAPPER constructs, whose response was reduced by 25% (Fig. 8A-B). Unexpectedly, following readmission of 1 mM Ca^{2+} the quench rates were reduced by 85 and 97 % in cells expressing MAPPER-S and MAPPER-L, respectively (Fig. 8A-B). Correlation of Mn^{2+} quench rates with cER length confirmed

that Mn^{2+} entry increases as the cER extends in store-depleted untreated cells while enforced cER extension conferred by tether expression does not potentiate store-operated ionic fluxes (Fig. 8C). These data indicate that the artificial elongation of the cER occurring during ER-PM tethering is associated with a near-complete abrogation of store-operated cation entry in the presence of Ca^{2+}.

Discussion

In this study, we correlate the morphological and topological changes in cortical ER structures occurring during SOCE in HEK-293T cells expressing natural or artificial ER-PM tethers with the ionic fluxes generated by interactions between endogenous signaling proteins at these membrane contact sites. We found that native cER cisternae expand during ER Ca^{2+} depletion and remain elongated during subsequent Ca^{2+} entry while their ER-PM gap distance remains constant in non-transfected cells. STIM1 was previously shown to recruit and to expand cER structures upon store depletion (Orci et al., 2009; Sauc et al., 2015; Wu et al., 2006) while E-Syt1 is recruited to MCS and was reported to reduce the ER-PM gap distance by up to 12 nm during the Ca^{2+} entry phase (Fernandez-Busnadiego et al., 2015; Giordano et al., 2013; Kang et al., 2019). However, these studies were performed in cells overexpressing STIM1 or E-Syts, in which the expressed proteins are likely the dominant tethers. Here we show that the only apparent ultrastructural change occurring during SOCE in naïve HEK-293T cells is a cER elongation that is likely mediated by endogenous STIM proteins, indicating that the cER gap distance is not dynamically regulated by the activity of endogenous E-Syt1.

Expression of E-Syt1 or of MAPPER-S had no significant impact on cER structures in non-treated cells, but the expression of E-Syt2 and MAPPER-L induced the apparition of abnormally elongated cER cisternae reaching a length of up to 900 nm. This is consistent with the potent tethering function of E-Syt2 (Fernandez-Busnadiego et al., 2015; Idevall-Hagren et al., 2015) and indicates that MAPPER-L is not an innocuous cER marker but alters its ultrastructure. This remodelling effect might be related to the very high avidity of the polybasic tail of the chimeric MAPPER proteins for phosphoinositides and

indicates that MAPPER should not be used to label the cER. In an earlier cryo-ET study large ER–PM contacts were observed in COS-7 cells overexpressing E-Syt3 and occasionally in cells overexpressing E-Syt1. These contacts resemble the elongated cER cisternae that we observed in cells overexpressing E-Syt2 and MAPPER-L, suggesting that by sorting cells for intermediate amounts of expressed proteins we may have avoided structures generated by high amounts of E-Syt1. The lack of effect of E-Syt1 in non-treated cells is expected given the reliance of this protein on Ca^{2+} elevations for its recruitment to MCSs.

Following Ca^{2+} stores depletion with Tg, the cER elongation was greatly potentiated by the expression of any of the 4 tether proteins. The strongest effects were observed with E-Syt2 and MAPPER-L, in-line with their effects in non-treated cells. Interestingly, the ER-PM gap distance stabilized at a fixed distance specific for each tether family as the cER cisternae elongated, around 12-15 nm for the E-Syts and 5-9 nm for the MAPPERs. This pattern contrasts sharply with the variability of the gap distances observed in smaller (<300 nm long) cER cisternae, which ranged from 5 to 30 nm regardless of tether expression. Another unexpected finding was that the cER elongation was reversed during the Ca^{2+} influx phase for all tethers except MAPPER-S, while the ER-PM gap distances remained unaffected. E-Syt1 expression in HEK-293T cells was previously reported to reduce the ER-PM gap distance by 12 nm upon Ca^{2+} entry, as estimated from changes in fluorescence intensity occurring in 50 nm near-PM optical sections in variable-angle TIRF imaging (Kang et al.). We propose that the increased fluorescence intensity reported in this study instead reflects the increased concentration of fluorescent molecules in contracting cER structures remaining anchored at a fixed distance of 12-15 nm to the PM.

The average ER–PM distance of native contacts was 25.4 nm in a cryo-electron tomography study of COS-7 cells (Fernandez-Busnadiego et al.), significantly higher than the averaged gap distance of 16.8 nm that we report by scoring >100 contacts in Epon-embedded HEK-293T cells. This difference might reflect differences between cell type or in the EM procedures as in our case the osmium labeling

of membranes and embedding in resin might reduce the apparent gap distance in our 30 nm-thick slices. In COS-7 cells overexpressing E-Syt1, the averaged gap distance in cryo-ET was 21.8 nm and decreased to 14.8 nm following Tg-induced SOCE with 2 mM external Ca^{2+} (Fernandez-Busnadiego et al.). In our HEK-293T cells expressing E-Syt1 the ER-PM gap decreased from 17.3 to 14.9 nm during Tg addition and to 12.8 nm if considering only the longest cER structures. Thus, the gap distance was reduced at an earlier step during the SOCE protocol, suggesting that the Ca^{2+} elevation generated by the release of Ca^{2+} from ER stores during Tg application is sufficient to recruit E-Syt1 to the PM and to induce a shortening of the ER–PM gap distance. This is consistent with the reported Ca^{2+}-dependent tethering function of E-Syt1 (Fernandez-Busnadiego et al., 2015; Giordano et al., 2013).

Counterintuitively, the cER expansion imparted by the expressed tether did not enhance SOCE but instead reduced the incoming fluxes of ions generated by STIM-ORAI interactions at MCS. In cells expressing E-Syt2 and MAPPER-L, which caused maximal cER expansion, the rates of Ca^{2+} influx evoked by the Tg-readmission protocol were reduced by ~50%. The effect was observed in several cell types and persisted when the Ca^{2+} concentration was reduced to 0.5 mM but disappeared at 10 mM Ca^{2+}, the highest concentration tested. MAPPER-S expression also reduced SOCE in HeLa cells or when the reversible SERCA inhibitor CPA was used to evoke SOCE. CPA enables store refilling which would further reduce the cytosolic Ca^{2+} concentration during the influx phase. These data thus indicate that the expression of tethering proteins that promote cER expansion reduce SOCE and that this effect is preferentially detected at low cytosolic Ca^{2+} concentrations with the depletion-readmission protocol. The cER expansion also impacted the Ca^{2+} homeostasis of intracellular Ca^{2+} stores, reducing the amount of Ca^{2+} mobilized by an InsP3-mediated agonist and accelerating the rates of Ca^{2+} store depletion upon SERCA inhibition. Interestingly, the kinetics of ER refilling, which reflect the activity of SERCA, were unaffected despite the reduced Ca^{2+} entry (Fig. 6A and 6B), indicating that most of the incoming Ca^{2+} ions were recaptured into the ER. The activity of the PMCA also remained unaffected and Ca^{2+} influx remained sensitive to the expression of CaM mutants, indicating that the regulation of STIM-ORAI complexes by accessory proteins is conserved. Using Mn^{2+}, we could quantify the effect of ER tethering

on store-operated cationic fluxes recorded before and after Ca^{2+} readmission, and correlate these PM fluxes with the cER size measured in the same experimental conditions. These experiments revealed that MAPPERs expression reduces Mn^{2+} entry marginally after store depletion and maximally at the peak of the cytosolic Ca^{2+} elevation. These data indicate that cER tethering reduces the activity of STIM-ORAI complexes formed upon store depletion and greatly amplifies their Ca^{2+}-dependent inhibition.

Based on our morphological observations, we propose that during STIM1 recruitment to the PM the cER expands as new interactions are formed between incoming STIM1 proteins and phospholipids. In the presence of an excessive amount of tethers, the newly formed STIM1-PM interactions are replaced by more stable interactions between the PM and the expressed tethers, which have a higher affinity for phospholipids (Heo et al., 2006), thereby promoting cER expansion and stabilization at a fixed distance (Fig. 8D). Upon Ca^{2+} elevations, the electrostatic interactions between negatively charged phospholipids and the tethers are weakened, reversing the elongation process, while the interactions between STIM and ORAI proteins are disrupted by Ca^{2+}-bound CaM and by other Ca^{2+}-dependent negative regulators like SARAF (Fig. 8D). Our functional observations further suggest that the artificially elongated cER cisternae do not allow productive STIM-ORAI interactions in their centre since the cER length was not correlated with the SOCE amplitude. This suggests that the elongated cERs are populated predominantly by the exogenous tethers, with STIM-ORAI complexes restricted to the periphery of the MCS, consistent with an earlier report that STIM1-ORAI1 complexes accumulate at the periphery of cER cisternae artificially tethered 4–6 nm from the PM (Varnai et al., 2007). Alternatively, STIM proteins might populate the expanded structures but revert to a globular, resting conformation, thereby reducing the amount of extended STIM1 proteins available for gating. This would be consistent with our previous observation that overexpressed YFP-STIM is concentrated in thin regions of the cER close to the PM (Orci et al., 2009).

In summary, we show that native cER cisternae expand during store depletion in HEK-293T cells and that this elongation persists during subsequent Ca^{2+} elevations. Enforced expression of ER-

PM tethers maximizes cER expansion and fixes the enlarged cisternae at specific gap distances in a process partially reversed by Ca^{2+} elevations. cER enlargement negatively regulates Ca^{2+} release and SOCE, likely by sequestering STIM-ORAI complexes and possibly InsP3 receptors at the periphery of the enlarged cER sheets. These findings indicate that ER-PM tethering negatively regulates SOCE by promoting cER expansion, a remodelling that likely participates in the termination of store-operated Ca^{2+} entry.

Materials and Methods

Reagents. The following reagents were used in this manuscript; Thapsigargin (T9033/CAY10522, Sigma), cyclopiazonic acid from Penicillium cyclopium, (C1530, Sigma), Mg-ATP (Sigma), $MnCl_2$ (Sigma), Fura-2-AM (F1201, Invitrogen), Deep Red CellMask and Lipofectamine 2000 (ThermoFisher Scientific). Ca^{2+} recording buffers contained (in mM): NaCl 140, KCl 5, $MgCl_2$ 1, Hepes 20, Glucose 10, supplemented with 1 mM EGTA or 0,5-10 mM $CaCl_2$ as indicated.

Plasmids. pEGFP-C1 was purchased from ClonTech (#6084_1), pcDNA-$D1_{ER}$ (#36325), EGFP-ESyt1 (#66830) and EGFP-ESyt2 (#66831) from Addgene. MAPPER constructs were a kind gift from Jen Liou, UT Southwestern, TX, CaM constructs were gifts from Rajesh Bhardwaj, University of Bern.

Cell culture and transfections. Human embryonic kidney (HEK-293T) cells were obtained from ATCC (CRL-11268, Manassas, VA, USA) maintained in Dulbecco's modified Eagles medium (cat. no. 31966-021) supplemented with 10% fetal bovine serum and 1 % penicillin/streptomycin, grown at 37°C and 5% CO_2 and regularly tested for mycoplasma. MEF cells were grown in identical conditions, HeLa cells purchased from the European collection of cell culture (ECACC) were grown in MEM Gibco (41090). Prior to experiments, cells were seeded on cover glass of 25 mm + poly-L-lysine (P4832, Sigma-Aldrich) and transfected 1-day post-seeding using 200 ng of plasmids for HEK-293T, 0.5 µg for MEF and 1 µg for HeLa cells mixed with 3 µL lipofectamine 2000. The DNA-Lipofectamine mix was added to cells for 4 h and the culture medium was replaced.

Transmission electron microscopy (TEM). Cells were sorted by flow cytometry (MoFlo Astrios, Beckman) for similar GFP fluorescence levels 24h post-transfection and re-seeded for 24h on plastic dishes treated with poly-L-lysine. Cells were exposed to NT, CF, or CA conditions, fixed with 2.5% glutaraldehyde, stained with uranyl acetate, postfixed with osmium tetroxide, and embedded in Epon. After sectioning at 30 nm, samples were imaged on a Technai 20 transmission electron microscope (FEI, Eindhoven, Netherlands) at 92 000 times magnification. For each cell identified on the grid every ER structure located within 30nm of the PM was imaged. The cER length and the ER-PM gap distance were determined on EM images using ImageJ/Fiji and Matlab, respectively. A segmented line was drawn in ImageJ/Fiji across the cER long axis to extract the cER length. The ER-PM gap distance was obtained from two lines drawn on the PM and proximal cER membranes whose pixel-to-pixel geodesic distance were extracted and averaged for each cER. Only structures located at less than 30 nm from the PM were analyzed.

Ca^{2+} imaging. Ca^{2+} imaging was performed as described previously (Sauc et al., 2015). Briefly, cells were loaded with 4 μM Fura-2-AM in CA medium for 25 min at room temperature (25°C) before imaging on a Nikon Eclipse Ti microscope (Nikon Instruments), equipped with a Lambda DG4 illumination system (Sutter Instrument) and a 16-bit CMOS camera (pco.Edge sCMOS, Visitron Systems). Cells were selected for similar GFP fluorescence and the following filter sets were used (all from Chroma Technology Corp.): For fura-2 ratio recordings: ET340x-ET380x-ET510/80m-T400lp, for Mn^{2+} quench: ET365/10x, for R-CEPIA1$_{ER}$ recordings: ET572/35x–69002bs–ET630/75m. We piloted the setup with Visiview software (Visitron) using a python script to better control the time resolution during the protocol (https://github.com/Carandoom/VisiviewFura2). Ca^{2+} images were analyzed using a ImageJ script (https://github.com/Carandoom/Fura2Analysis DOI: https://zenodo.org/badge/latestdoi/373477639). Using regions drawn on the background and on each cell of interest, the script removes the mean background fluorescence and extracts the mean fluorescence of each cell region for each frame to calculate the fluorescence ratio and graph it as R/R0 in Excel. The rates of Ca^{2+} entry were calculated with a Matlab script

(https://github.com/Carandoom/SlopeFromLinearRegression DOI: https://zenodo.org/badge/latestdoi/373492736) . Briefly, the script plots the recording, allowing the user to analyze a positive or negative slope within a given range of timepoints. The script calculates the first derivative to define a region to fit a linear regression and extracts a slope parameter.

Total internal reflection fluorescence (TIRF). TIRF imaging was performed on a Nikon Eclipse Ti microscope equipped with a Perfect Focus System (PFS III) and a 100x oil CFI Apochromat TIRF Objective (NA 1.49; Nikon Europe B.V.). For 488 nm excitation the filter cube contained a ZET488/10 excitation filter (Chroma) a 502 nm dichroic mirror (H 488 LPXR superflat) and a 530/43 Bright Line HC emission filter (Semrock, Inc.). For CellMask imaging we used a 640 nm laser and Cy5 700/75 emission filter. The fluorescence was collected by an EMCCD camera cooled at -80°C (iXon Ultra 897, Andor Technology Ltd) piloted with NIS-Elements Ar software V4.13 (Nikon). The PM was labelled with deep red CellMask (1:10 000 in CA for 10 min at RT) and used to adjust the TIRF angle. Fluorescence puncta on TIRF images were segmented using a custom ImageJ/Fiji script available on GitHub (https://github.com/Carandoom/STIM-ORAI-Segmentation DOI: https://zenodo.org/badge/latestdoi/373828941)

Data analysis. Statistical analysis was performed with GraphPad Prism 9, *P* values are labelled: * $P \leq 0.05$, ** $P \leq 0.01$, *** $P \leq 0.001$ and **** $P \leq 0.0001$.

Data availability

The data that support the findings of this study are present in the supplementary figures, with number of experiments and statistical tests applied.

Acknowledgements

We are grateful to Cyril Castelbou for the technical assistance, the bioimaging, READS and flow cytometry facilities (Geneva Medical Centre). This work was funded by the Swiss National Foundation [grant number 310030_189042 (to ND)

Author contributions

CH, Conception and design, Acquisition of data, Analysis and interpretation of data, Drafting or revising the article; ACS, Acquisition of data, Analysis and interpretation of data; ND, Conception and design, Analysis and interpretation of data, Drafting or revising the article.

Competing Financial Interests

The authors declare no competing financial interests.

Figures Legends

Figure 1: Ca^{2+} depletion promotes the elongation of the native cortical ER.

A) Ca^{2+} recording illustrating the conditions used for EM analysis during the Tg-readmission protocol. HEK-293T cells were either untreated (NT), treated for 10 min with 1 µM Tg in Ca^{2+}-free medium to deplete ER Ca^{2+} stores (CF) or subsequently re-exposed to 1 mM Ca^{2+} for 2 min to allow Ca^{2+} entry (CA). They were then fixed, embedded in Epon resin, sectioned and observed. B) Representative electron micrographs showing the morphology of cortical ER sheets at membrane contact sites (white arrows) in the three conditions. Scale bar: 100 nm. C) Zoomed image of a cER sheet from the CF condition in B. The lines drawn to extract the ER-PM distance (i) and cER length (ii) are shown. D) Quantification of the ER-PM gap distance (top), cER length (middle) and cleft volume (bottom) in the three conditions. Cleft volume was calculated from the cER gap and length values assuming a cylindric shape. Data are mean±SEM of 105, 89, and 146 quantified structures, ****p<0.0001 ***p<0.001, one-way ANOVA.

Figure 2: Effect of E-Syts and MAPPERs expression on cER morphology in naïve HEK-293T cells

A) Representative electron micrographs of cER sheets in cells expressing the indicated ER-PM tethers, before store depletion. B) Scatter plots of ER-PM gap distances as a function of cER length in each condition. E-Syt2 and MAPPER-L expression induced the apparition of elongated cER sheets anchored at a fixed distance from the PM, dotted lines, and values (in nm) indicate the average gap distance at cER length >300 nm. The corresponding quantitative analysis is presented in the Tables.

Figure 3: E-Syts and MAPPERs expression augments the cER elongation during Ca^{2+} store depletion

A) Representative electron micrographs of cER sheets in cells expressing the indicated ER-PM tethers, 10 min after Tg addition in Ca^{2+}-free medium. B) Scatter plots of ER-PM gap distances as a function of cER length in each condition. Expression of each tether induced the apparition of elongated cER sheets anchored at a fixed distance from the PM (dotted lines and values). The corresponding quantitative analysis is presented in the Tables.

Figure 4: The cER elongation persists in E-Syts and MAPPERs cells after store-operated Ca^{2+} influx.

A) Representative electron micrographs of cER sheets in cells expressing the indicated ER-PM tethers, 2 min after Ca^{2+} readmission. B) Scatter plots of ER-PM gap distances as a function of cER. Elongated cER sheets persisted in cells expressing the tethers, anchored at a fixed distance from the PM (dotted lines and values). The corresponding quantitative analysis is presented in the Tables.

Figure 5*: E-Syt2 and MAPPER-L expression inhibits store-operated Ca^{2+} entry*

A) Left: Averaged fura-2 recordings of Ca^{2+} elevations evoked by the Tg-readmission protocol in cells expressing the E-Syts or a control plasmid. Right: Quantification of the Ca^{2+} entry rates. B) Averaged Ca^{2+} recordings (left) and Ca^{2+} entry rates (right) in cells expressing the MAPPERs or a control plasmid. C) Ca^{2+} entry rates recorded at varying Ca^{2+} concentration in cells expressing the indicated tether. Data are mean±SEM of 39-110 cells from 5-9 independent recordings, *p<0.05, **p<0.01, ***p<0.001, ****p<0.0001, one-way ANOVA.

Figure 6: MAPPERs expression perturbs ER Ca^{2+} store homeostasis

A) Averaged Ca^{2+} recordings (left) and Ca^{2+} entry rates (right) in cells expressing MAPPERs or a control plasmid, transiently exposed to the reversible SERCA inhibitor CPA to enable store refilling during Ca^{2+} readmission. Both versions of the MAPPER tethers decreased Ca^{2+} entry rates in these conditions. B) Left: averaged changes in free ER Ca^{2+} concentration recorded with R-CEPIA1$_{ER}$ during transient CPA exposure followed by Ca^{2+} readmission, as in A). Right: Quantification of the rates of ER Ca^{2+} depletion and refilling. MAPPER-L expression accelerated the Ca^{2+} depletion of the ER. C) Averaged Ca^{2+} recordings of cells expressing MAPPERs or a control plasmid, exposed to 100 µM ATP in Ca^{2+}-free medium. Right: Quantification of the peak amplitude of the evoked responses. Data are mean±SEM of 30-166 cells from 6-9 independent recordings, **p<0.01, ***p<0.001, ****p<0.0001, one-way ANOVA.

Figure 7: Calmodulin modulates SOCE independently of MAPPERs expression

A) Averaged Ca^{2+} recordings (left) and Ca^{2+} extrusion rates (right) of cells expressing MAPPERs or a control plasmid. Ca^{2+} was removed 2 min after readmission to assess PMCA-mediated Ca^{2+} extrusion. B, C) Averaged Ca^{2+} recordings (left) and Ca^{2+} entry rates (right) in cells expressing MAPPERs or a control plasmid together with WT-CaM (B) or dominant-negative DN-CaM (C). DN-CaM positively modulated SOCE independently of MAPPERs expression. Data are mean±SEM of 52-183 cells from 3-11 independent recordings, *p<0.05, **p<0.01, ****p<0.0001, one-way ANOVA.

Figure 8: MAPPERs expression inhibits store-operated Mn^{2+} entry

A) Averaged Mn^{2+} quench recordings in cells expressing MAPPERs or a control plasmid before stimulation (NT), after store depletion (CF), and following Ca^{2+} readmission (CA). Recordings in CF were in nominal Ca^{2+}-free medium without EGTA to avoid Mn^{2+} chelation. B) Statistical evaluation of the Mn^{2+} quenching rates. MAPPERs expression strongly reduced Mn^{2+} entry after Ca^{2+}readmission. Data are mean±SEM of 171-406 cells from 5-12 independent recordings, *p<0.05, **p<0.01, ****p<0.0001, one-way ANOVA. C) Mn^{2+} quench rates as a function of cER length for the NT and CA conditions. MAPPERs expression caused massive cER enlargement without enhancing SOCE.

Table 1: Quantification of cortical ER parameters

Epon sections were generated before stimulation (NT), after store depletion (CF), and following Ca^{2+} readmission (CA). The total number of contact sites measured is indicated for each condition.

Table 2: Statistical evaluation of cER morphological parameters.

Cells expressing E-Syts and MAPPER were imaged in NT, CF, and CA conditions. *p<0.05, **p<0.01, ***p<0.001, ****p<0.0001, one-way ANOVA.

Figure S1: E-Syts and MAPPERs populate similar near-PM clusters following store depletion.

A) Representative TIRF images of HEK-293T cells expressing the indicated GFP-tagged tether proteins. Cells were labelled with CellMask, treated 10 min with 1 µM Tg in Ca^{2+}-free, and fixed. B) CellMask

image of MAPPER-S-expressing cells from A, with the cell border (left) and GFP clusters (right) outlined in yellow. C) Quantification of the cluster area (left) and membrane coverage (right) in cells expressing the different tethers. Data are mean±SEM of 18-30 cells, ns: not significant, one-way ANOVA.

Figure S2: Sorting strategy of cells expressing ER-PM tether proteins.

Cells expressing GFP-tagged E-Syts and MAPPERs were sorted by flow cytometry for similar GFP fluorescence in NT, CF, and CA conditions.

Figure S3: E-Syts and MAPPERs expression augments the cER elongation during SOCE.

A-C) Quantification of the averaged ER-PM gap distance (A), cER length (B) and cleft volume (C) in cells expressing E-Syts and MAPPERs and imaged in NT, CF, and CA conditions. D) Cleft volume was calculated using cER length and gap values assuming a cylindric shape. Data are mean±SEM.

Figure S4: E-Syt2 and MAPPER-L expression inhibit store-operated Ca^{2+} entry.

A) Quantification of the amount of Ca^{2+} release by Tg in Ca^{2+}-free medium in cells expressing the indicated tether proteins. Data are mean±SEM of 83-248 cells, ns: not significant, one-way ANOVA. B) Quantification of Ca^{2+} entry rate in cells expressing GFP-tagged E-Syts and MAPPERs, sorted by flow cytometry for similar GFP fluorescence. Data are mean±SEM of 225-331 cells. *p<0.05, ***p<0.001, ****p<0.0001, one-way ANOVA. C, D) Averaged Ca^{2+} recordings (left) and Ca^{2+} extrusion rates (right) in MEF cells (C) and HeLa cells (D) expressing MAPPERs or a control plasmid. MAPPER-S expression negatively modulated SOCE in HeLa cells.

Figure S5: MAPPERs expression does not impact ER Ca^{2+} refilling.

Left: averaged $D1_{ER}$ recordings of the free ER Ca^{2+} concentration during Ca^{2+} readmission in cells transiently exposed to CPA. Right: Quantification of the rates of ER refilling in cells expressing the indicated tether proteins.

References

Besprozvannaya, M., Dickson, E., Li, H., Ginburg, K. S., Bers, D. M., Auwerx, J. and Nunnari, J. (2018). GRAM domain proteins specialize functionally distinct ER-PM contact sites in human cells. *Elife* 7.

Bhardwaj, R., Augustynek, B. S., Ercan-Herbst, E., Kandasamy, P., Seedorf, M., Peinelt, C. and Hediger, M. A. (2020). Ca(2+)/Calmodulin Binding to STIM1 Hydrophobic Residues Facilitates Slow Ca(2+)-Dependent Inactivation of the Orai1 Channel. *Cell Physiol Biochem* 54, 252-270.

Chang, C. L., Hsieh, T. S., Yang, T. T., Rothberg, K. G., Azizoglu, D. B., Volk, E., Liao, J. C. and Liou, J. (2013). Feedback regulation of receptor-induced Ca2+ signaling mediated by E-Syt1 and Nir2 at endoplasmic reticulum-plasma membrane junctions. *Cell Rep* 5, 813-25.

Fernandez-Busnadiego, R., Saheki, Y. and De Camilli, P. (2015). Three-dimensional architecture of extended synaptotagmin-mediated endoplasmic reticulum-plasma membrane contact sites. *Proc Natl Acad Sci U S A* 112, E2004-13.

Feske, S., Gwack, Y., Prakriya, M., Srikanth, S., Puppel, S. H., Tanasa, B., Hogan, P. G., Lewis, R. S., Daly, M. and Rao, A. (2006). A mutation in Orai1 causes immune deficiency by abrogating CRAC channel function. *Nature* 441, 179-85.

Giordano, F., Saheki, Y., Idevall-Hagren, O., Colombo, S. F., Pirruccello, M., Milosevic, I., Gracheva, E. O., Bagriantsev, S. N., Borgese, N. and De Camilli, P. (2013). PI(4,5)P(2)-dependent and Ca(2+)-regulated ER-PM interactions mediated by the extended synaptotagmins. *Cell* 153, 1494-509.

Guido, D., Demaurex, N. and Nunes, P. (2015). Junctate boosts phagocytosis by recruiting endoplasmic reticulum Ca2+ stores near phagosomes. *J Cell Sci* 128, 4074-82.

Heo, W. D., Inoue, T., Park, W. S., Kim, M. L., Park, B. O., Wandless, T. J. and Meyer, T. (2006). PI(3,4,5)P3 and PI(4,5)P2 lipids target proteins with polybasic clusters to the plasma membrane. *Science* 314, 1458-61.

Hirve, N., Rajanikanth, V., Hogan, P. G. and Gudlur, A. (2018). Coiled-Coil Formation Conveys a STIM1 Signal from ER Lumen to Cytoplasm. *Cell Rep* 22, 72-83.

Idevall-Hagren, O., Lu, A., Xie, B. and De Camilli, P. (2015). Triggered Ca2+ influx is required for extended synaptotagmin 1-induced ER-plasma membrane tethering. *EMBO J* 34, 2291-305.

Jardin, I., Albarran, L., Salido, G. M., Lopez, J. J., Sage, S. O. and Rosado, J. A. (2018). Fine-tuning of store-operated calcium entry by fast and slow Ca(2+)-dependent inactivation: Involvement of SARAF. *Biochim Biophys Acta Mol Cell Res* 1865, 463-469.

Kang, F., Zhou, M., Huang, X., Fan, J., Wei, L., Boulanger, J., Liu, Z., Salamero, J., Liu, Y. and Chen, L. (2019). E-syt1 Re-arranges STIM1 Clusters to Stabilize Ring-shaped ER-PM Contact Sites and Accelerate Ca(2+) Store Replenishment. *Sci Rep* 9, 3975.

Liou, J., Kim, M. L., Heo, W. D., Jones, J. T., Myers, J. W., Ferrell, J. E., Jr. and Meyer, T. (2005). STIM is a Ca2+ sensor essential for Ca2+-store-depletion-triggered Ca2+ influx. *Curr Biol* 15, 1235-41.

Malli, R., Frieden, M., Hunkova, M., Trenker, M. and Graier, W. F. (2007). Ca2+ refilling of the endoplasmic reticulum is largely preserved albeit reduced Ca2+ entry in endothelial cells. *Cell Calcium* 41, 63-76.

Mullins, F. M., Park, C. Y., Dolmetsch, R. E. and Lewis, R. S. (2009). STIM1 and calmodulin interact with Orai1 to induce Ca2+-dependent inactivation of CRAC channels. *Proc Natl Acad Sci U S A* 106, 15495-500.

Orci, L., Ravazzola, M., Le Coadic, M., Shen, W. W., Demaurex, N. and Cosson, P. (2009). From the Cover: STIM1-induced precortical and cortical subdomains of the endoplasmic reticulum. *Proc Natl Acad Sci U S A* 106, 19358-62.

Palty, R., Raveh, A., Kaminsky, I., Meller, R. and Reuveny, E. (2012). SARAF inactivates the store operated calcium entry machinery to prevent excess calcium refilling. *Cell* 149, 425-38.

Poteser, M., Leitinger, G., Pritz, E., Platzer, D., Frischauf, I., Romanin, C. and Groschner, K. (2016). Live-cell imaging of ER-PM contact architecture by a novel TIRFM approach reveals extension of junctions in response to store-operated Ca(2+)-entry. *Sci Rep* 6, 35656.

Roos, J., DiGregorio, P. J., Yeromin, A. V., Ohlsen, K., Lioudyno, M., Zhang, S., Safrina, O., Kozak, J. A., Wagner, S. L., Cahalan, M. D. et al. (2005). STIM1, an essential and conserved component of store-operated Ca2+ channel function. *J Cell Biol* 169, 435-45.

Sauc, S., Bulla, M., Nunes, P., Orci, L., Marchetti, A., Antigny, F., Bernheim, L., Cosson, P., Frieden, M. and Demaurex, N. (2015). STIM1L traps and gates Orai1 channels without remodeling the cortical ER. *J Cell Sci* 128, 1568-79.

Schober, R., Waldherr, L., Schmidt, T., Graziani, A., Stilianu, C., Legat, L., Groschner, K. and Schindl, R. (2019). STIM1 and Orai1 regulate Ca(2+) microdomains for activation of transcription. *Biochim Biophys Acta Mol Cell Res* 1866, 1079-1091.

Scorrano, L., De Matteis, M. A., Emr, S., Giordano, F., Hajnoczky, G., Kornmann, B., Lackner, L. L., Levine, T. P., Pellegrini, L., Reinisch, K. et al. (2019). Coming together to define membrane contact sites. *Nat Commun* 10, 1287.

Stathopulos, P. B. and Ikura, M. (2010). Partial unfolding and oligomerization of stromal interaction molecules as an initiation mechanism of store operated calcium entry. *Biochem Cell Biol* 88, 175-83.

Stathopulos, P. B., Li, G. Y., Plevin, M. J., Ames, J. B. and Ikura, M. (2006). Stored Ca2+ depletion-induced oligomerization of stromal interaction molecule 1 (STIM1) via the EF-SAM region: An initiation mechanism for capacitive Ca2+ entry. *J Biol Chem* 281, 35855-62.

Thillaiappan, N. B., Chavda, A. P., Tovey, S. C., Prole, D. L. and Taylor, C. W. (2017). Ca(2+) signals initiate at immobile IP3 receptors adjacent to ER-plasma membrane junctions. *Nat Commun* 8, 1505.

Vaeth, M., Maus, M., Klein-Hessling, S., Freinkman, E., Yang, J., Eckstein, M., Cameron, S., Turvey, S. E., Serfling, E., Berberich-Siebelt, F. et al. (2017). Store-Operated Ca(2+) Entry Controls Clonal Expansion of T Cells through Metabolic Reprogramming. *Immunity* 47, 664-679 e6.

Varnai, P., Toth, B., Toth, D. J., Hunyady, L. and Balla, T. (2007). Visualization and manipulation of plasma membrane-endoplasmic reticulum contact sites indicates the presence of additional molecular components within the STIM1-Orai1 Complex. *J Biol Chem* 282, 29678-90.

Vig, M., Peinelt, C., Beck, A., Koomoa, D. L., Rabah, D., Koblan-Huberson, M., Kraft, S., Turner, H., Fleig, A., Penner, R. et al. (2006). CRACM1 is a plasma membrane protein essential for store-operated Ca2+ entry. *Science* 312, 1220-3.

Wu, M. M., Buchanan, J., Luik, R. M. and Lewis, R. S. (2006). Ca2+ store depletion causes STIM1 to accumulate in ER regions closely associated with the plasma membrane. *J Cell Biol* 174, 803-13.

Wu, Y., Whiteus, C., Xu, C. S., Hayworth, K. J., Weinberg, R. J., Hess, H. F. and De Camilli, P. (2017). Contacts between the endoplasmic reticulum and other membranes in neurons. *Proc Natl Acad Sci U S A* 114, E4859-E4867.

Zewe, J. P., Wills, R. C., Sangappa, S., Goulden, B. D. and Hammond, G. R. (2018). SAC1 degrades its lipid substrate PtdIns4P in the endoplasmic reticulum to maintain a steep chemical gradient with donor membranes. *Elife* 7.

Zhang, S. L., Yeromin, A. V., Zhang, X. H., Yu, Y., Safrina, O., Penna, A., Roos, J., Stauderman, K. A. and Cahalan, M. D. (2006). Genome-wide RNAi screen of Ca(2+) influx identifies genes that regulate Ca(2+) release-activated Ca(2+) channel activity. *Proc Natl Acad Sci U S A* 103, 9357-62.

Zhang, S. L., Yu, Y., Roos, J., Kozak, J. A., Deerinck, T. J., Ellisman, M. H., Stauderman, K. A. and Cahalan, M. D. (2005). STIM1 is a Ca2+ sensor that activates CRAC channels and migrates from the Ca2+ store to the plasma membrane. *Nature* 437, 902-5.

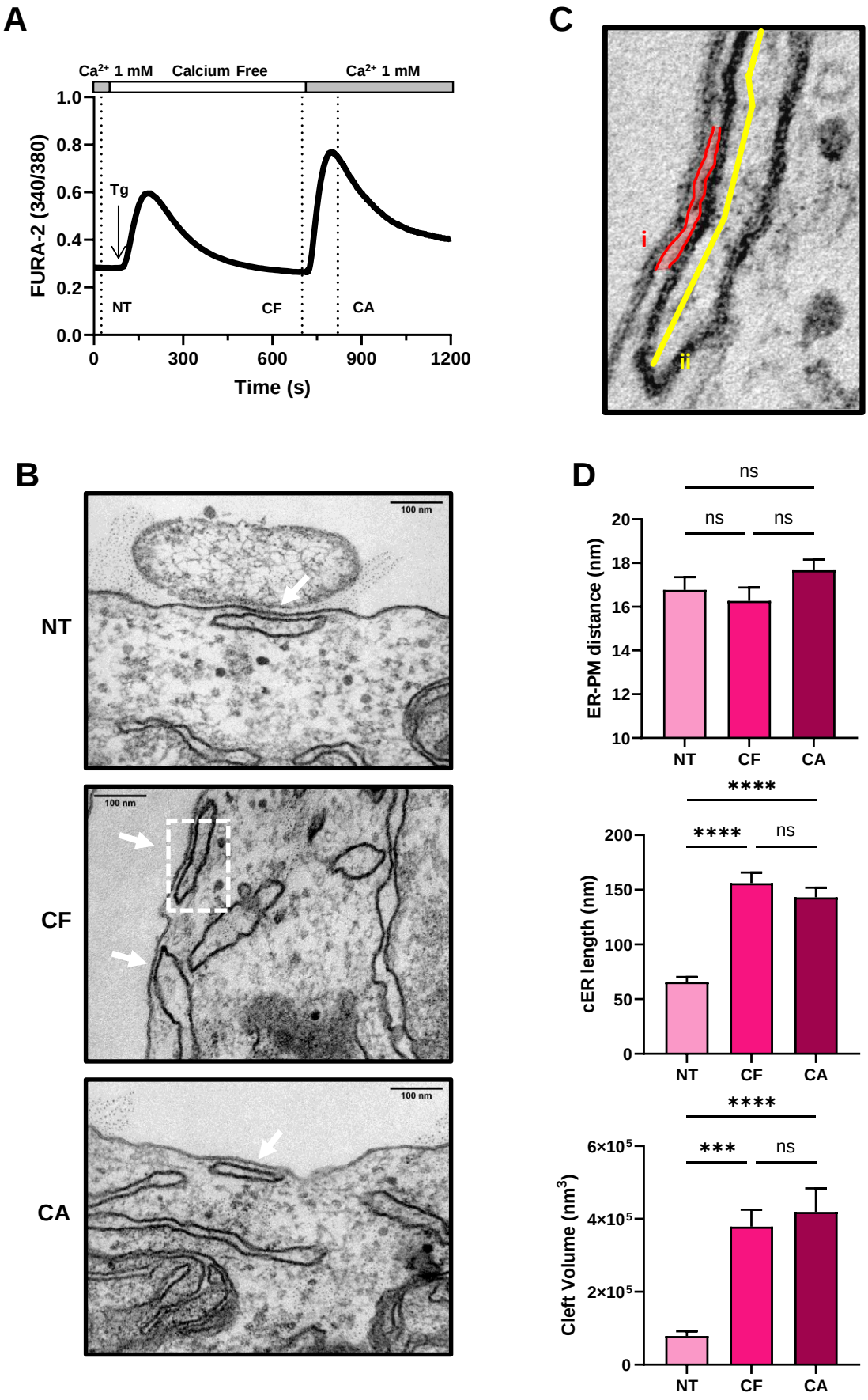
A
Ca2+ 1 mM
Calcium Free
Ca2+ 1 mM
FURA-2 (340/380)
Tg
NT
CF
CA
Time (s)
B
NT
CF
CA
100 nm
C
i
ii
D
ER-PM distance (nm)
cER length (nm)
Cleft Volume (nm3)
ns
****
***
NT
CF
CA

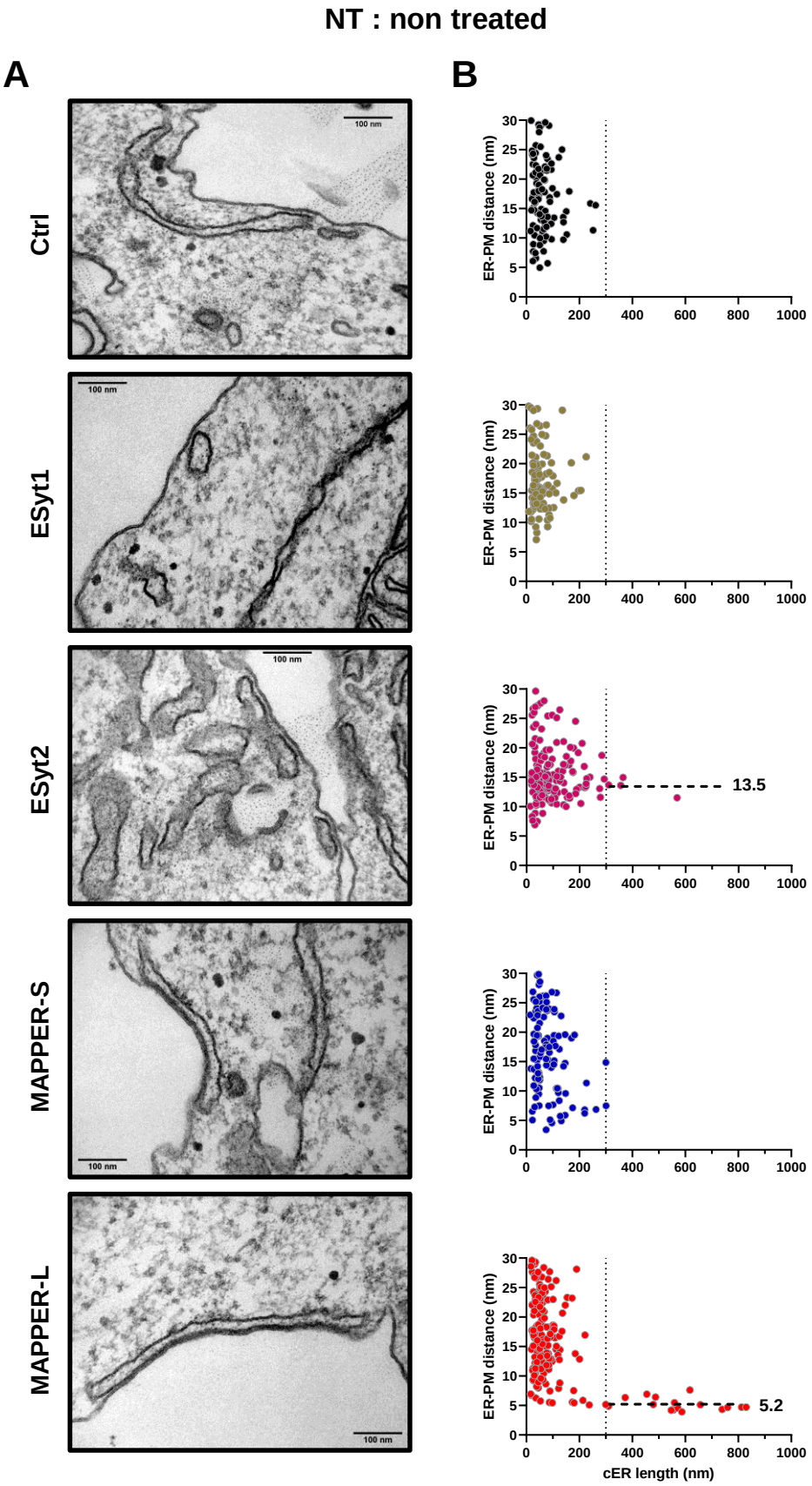
NT : non treated
A
B
Ctrl
ESyt1
ESyt2
MAPPER-S
MAPPER-L
100 nm
ER-PM distance (nm)
cER length (nm)
13.5
5.2

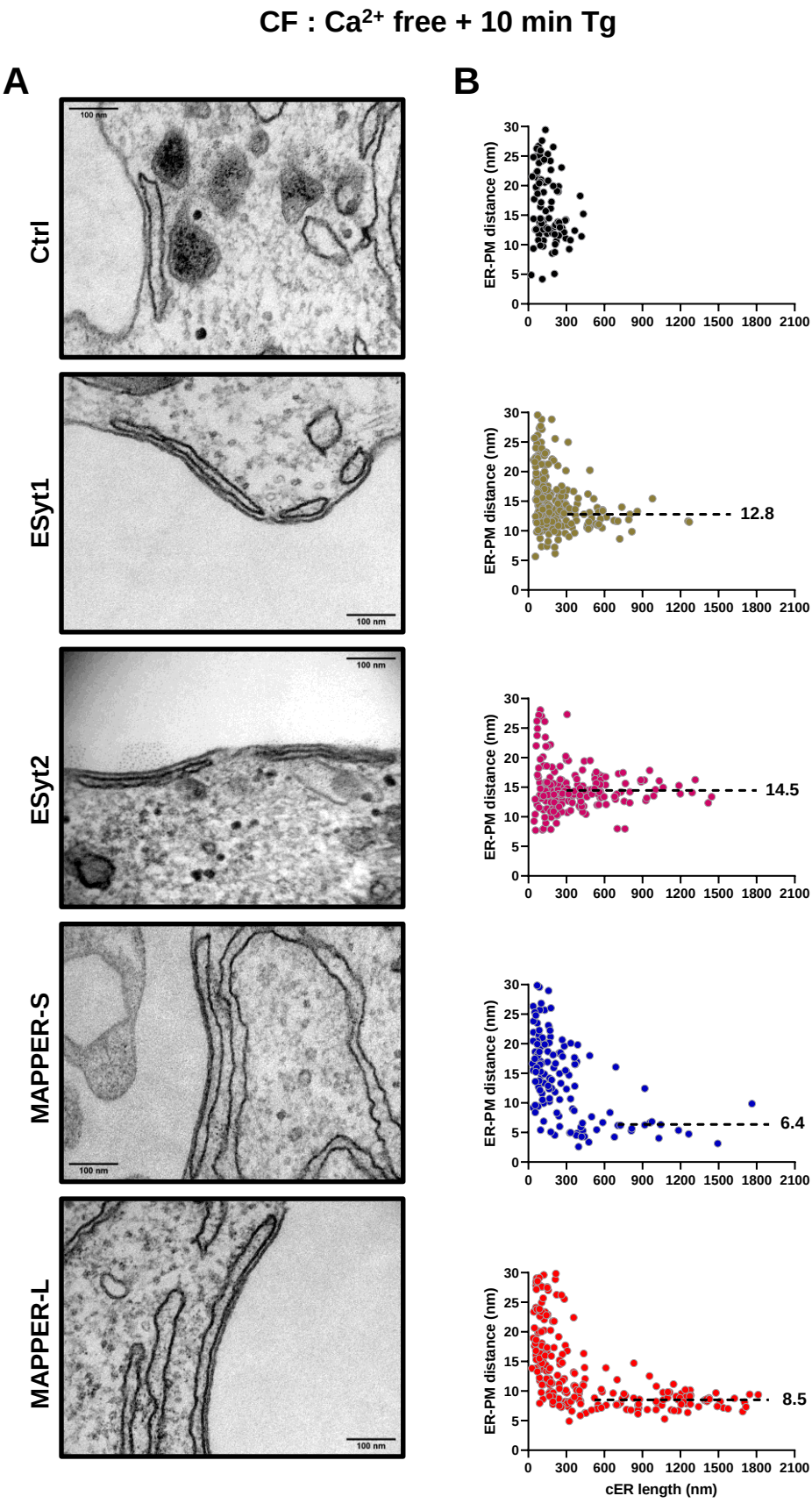
CF : Ca2+ free + 10 min Tg
A
B
Ctrl
ESyt1
ESyt2
MAPPER-S
MAPPER-L
100 nm
ER-PM distance (nm)
cER length (nm)
0
5
10
15
20
25
30
300
600
900
1200
1500
1800
2100
12.8
14.5
6.4
8.5

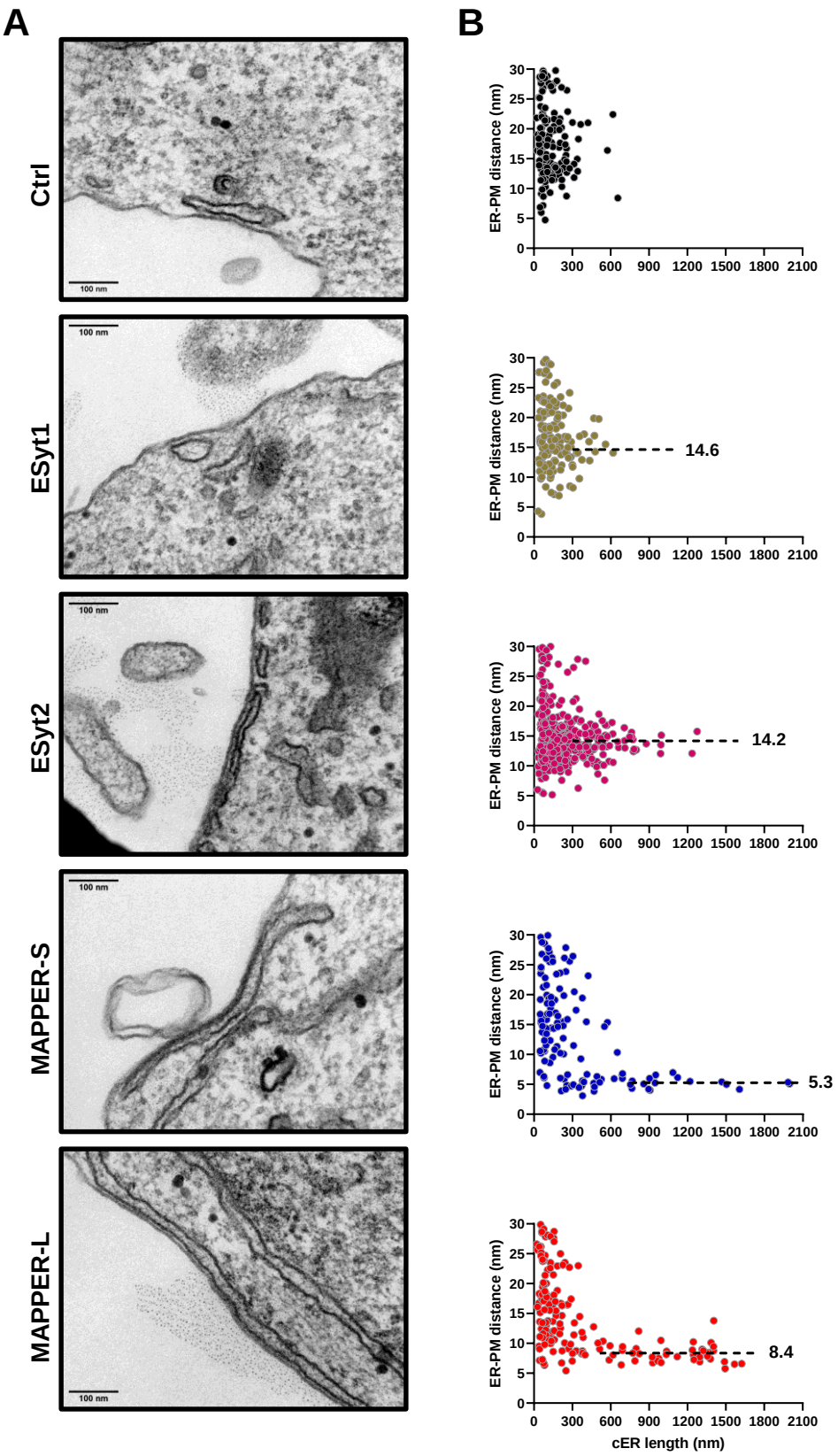
CA: 10 min Tg in CF then 2 min in 1 mM Ca2+
A
B
Ctrl
ESyt1
ESyt2
MAPPER-S
MAPPER-L
100 nm
ER-PM distance (nm)
cER length (nm)
0
300
600
900
1200
1500
1800
2100
5
10
15
20
25
30
14.6
14.2
5.3
8.4

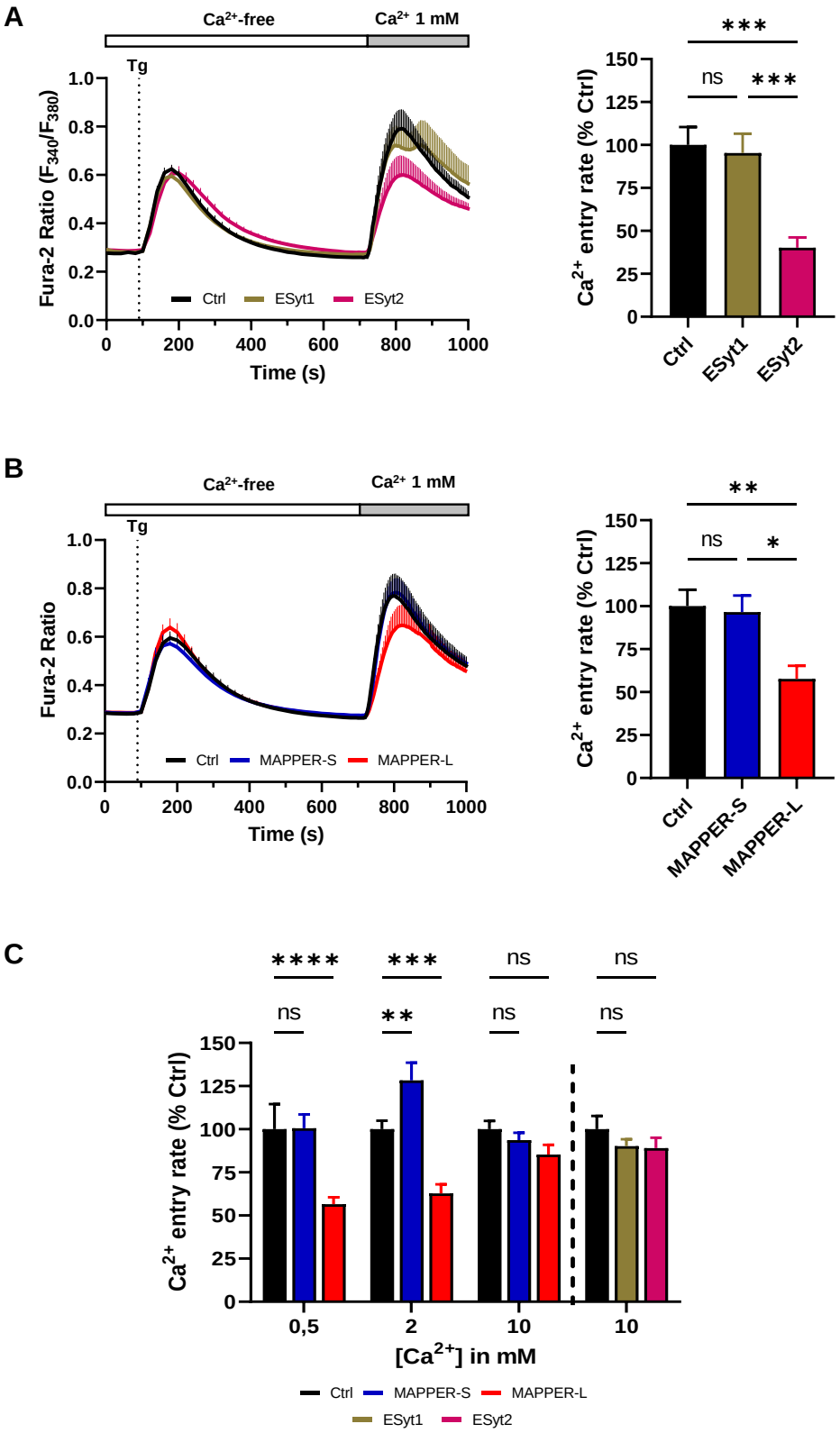
A
Ca2+-free
Ca2+ 1 mM
Tg
Fura-2 Ratio (F340/F380)
Time (s)
Ctrl
ESyt1
ESyt2
Ca2+ entry rate (% Ctrl)
***
ns
***
B
Ca2+-free
Ca2+ 1 mM
Tg
Fura-2 Ratio
Time (s)
Ctrl
MAPPER-S
MAPPER-L
Ca2+ entry rate (% Ctrl)
**
ns
*
C
****
***
ns
ns
ns
**
ns
ns
Ca2+ entry rate (% Ctrl)
0,5
2
10
10
[Ca2+] in mM
Ctrl
MAPPER-S
MAPPER-L
ESyt1
ESyt2

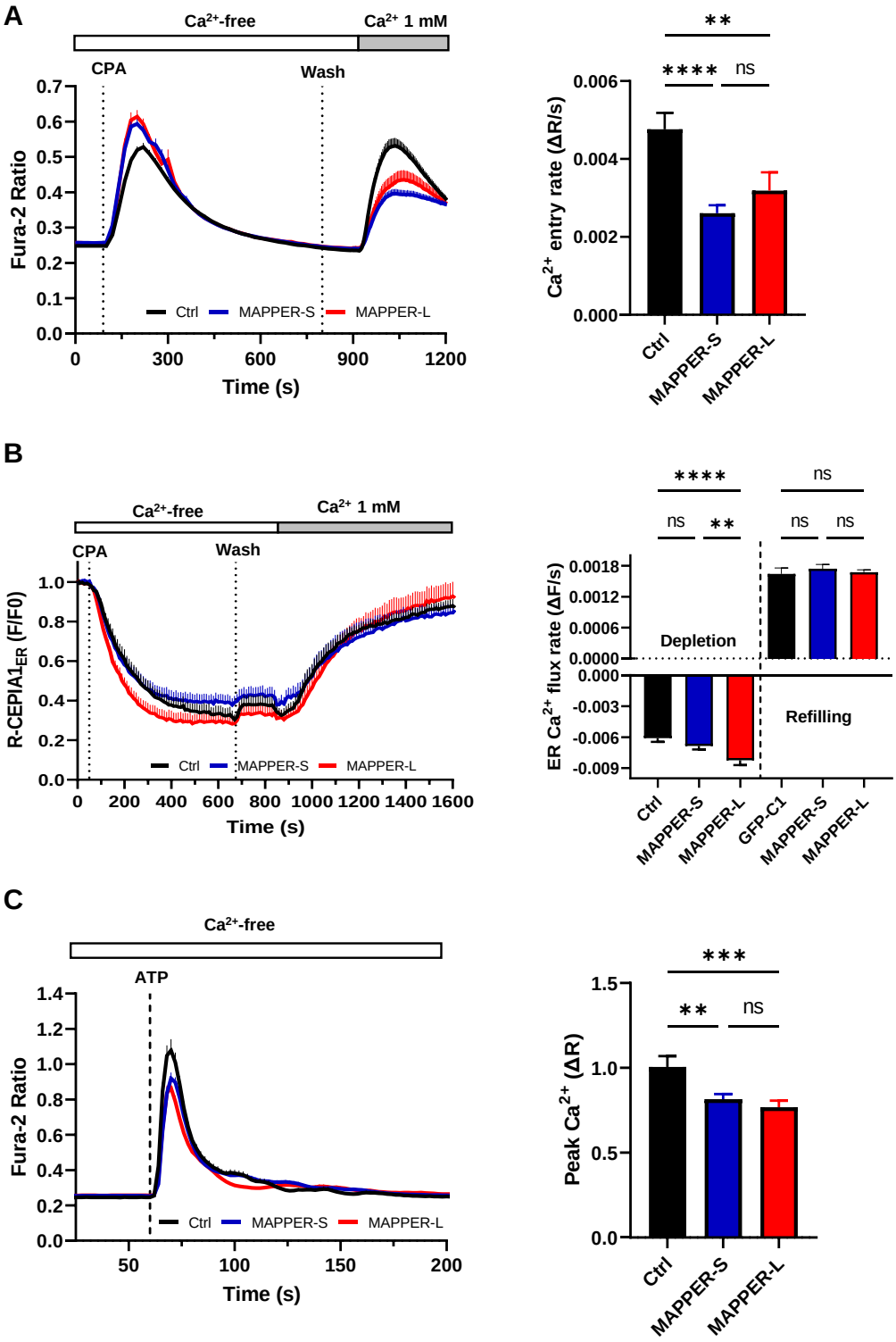
A
Ca2+-free
Ca2+ 1 mM
CPA
Wash
Fura-2 Ratio
Time (s)
Ctrl
MAPPER-S
MAPPER-L
Ca2+ entry rate (ΔR/s)
**
****
ns
B
R-CEPIA1ER (F/F0)
ER Ca2+ flux rate (ΔF/s)
Depletion
Refilling
GFP-C1
C
ATP
Peak Ca2+ (ΔR)
***

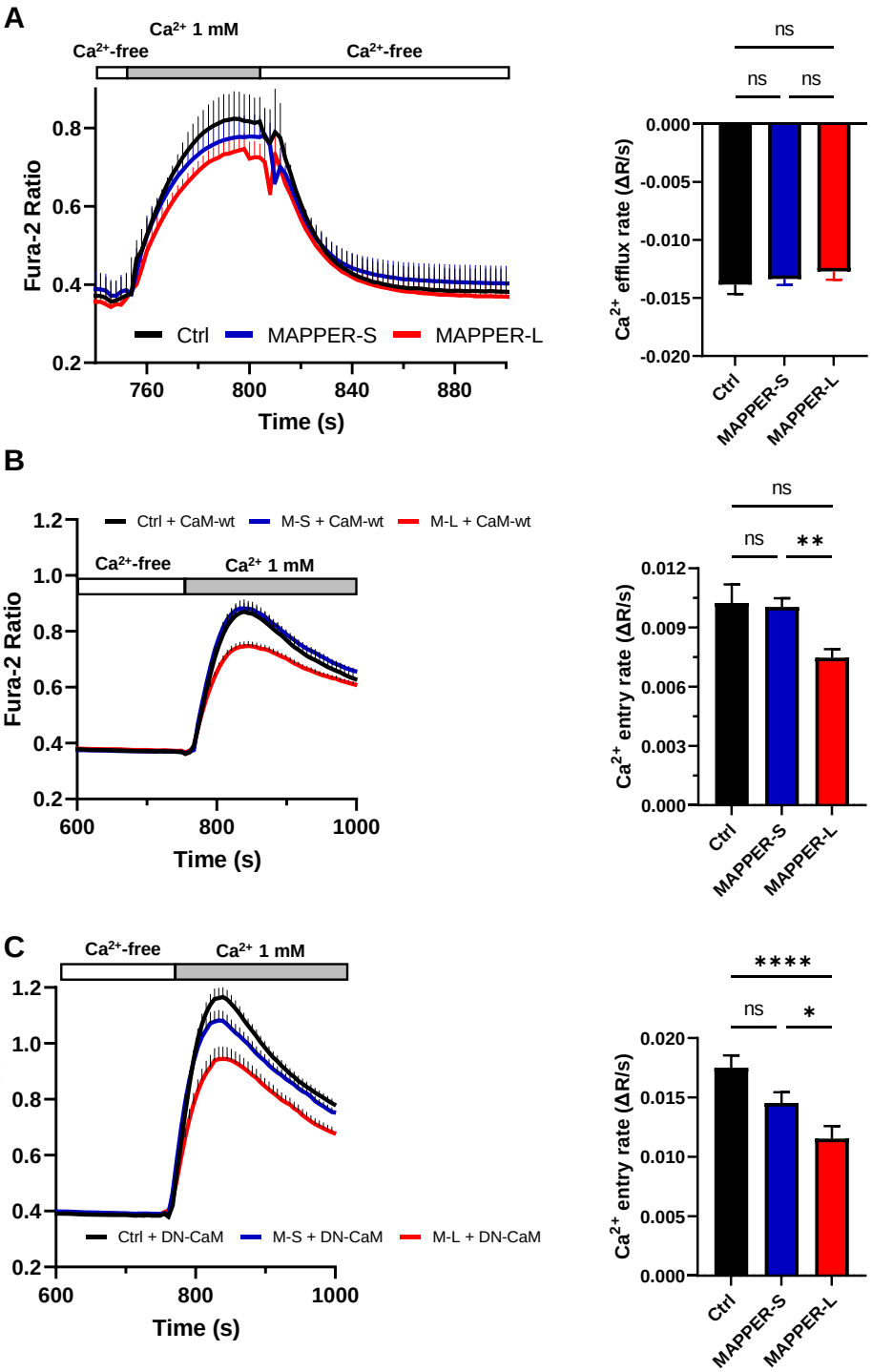
A
Ca2+ 1 mM
Ca2+-free
Ca2+-free
Fura-2 Ratio
0.8
0.6
0.4
0.2
760
800
840
880
Time (s)
Ctrl
MAPPER-S
MAPPER-L
ns
ns
ns
Ca2+ efflux rate (ΔR/s)
0.000
-0.005
-0.010
-0.015
-0.020
Ctrl
MAPPER-S
MAPPER-L
B
Ctrl + CaM-wt
M-S + CaM-wt
M-L + CaM-wt
Ca2+-free
Ca2+ 1 mM
Fura-2 Ratio
1.2
1.0
0.8
0.6
0.4
0.2
600
800
1000
Time (s)
ns
ns
**
Ca2+ entry rate (ΔR/s)
0.012
0.009
0.006
0.003
0.000
Ctrl
MAPPER-S
MAPPER-L
C
Ca2+-free
Ca2+ 1 mM
Fura-2 Ratio
1.2
1.0
0.8
0.6
0.4
0.2
Ctrl + DN-CaM
M-S + DN-CaM
M-L + DN-CaM
600
800
1000
Time (s)
****
ns
*
Ca2+ entry rate (ΔR/s)
0.020
0.015
0.010
0.005
0.000
Ctrl
MAPPER-S
MAPPER-L

Figure 8, Henry et al.

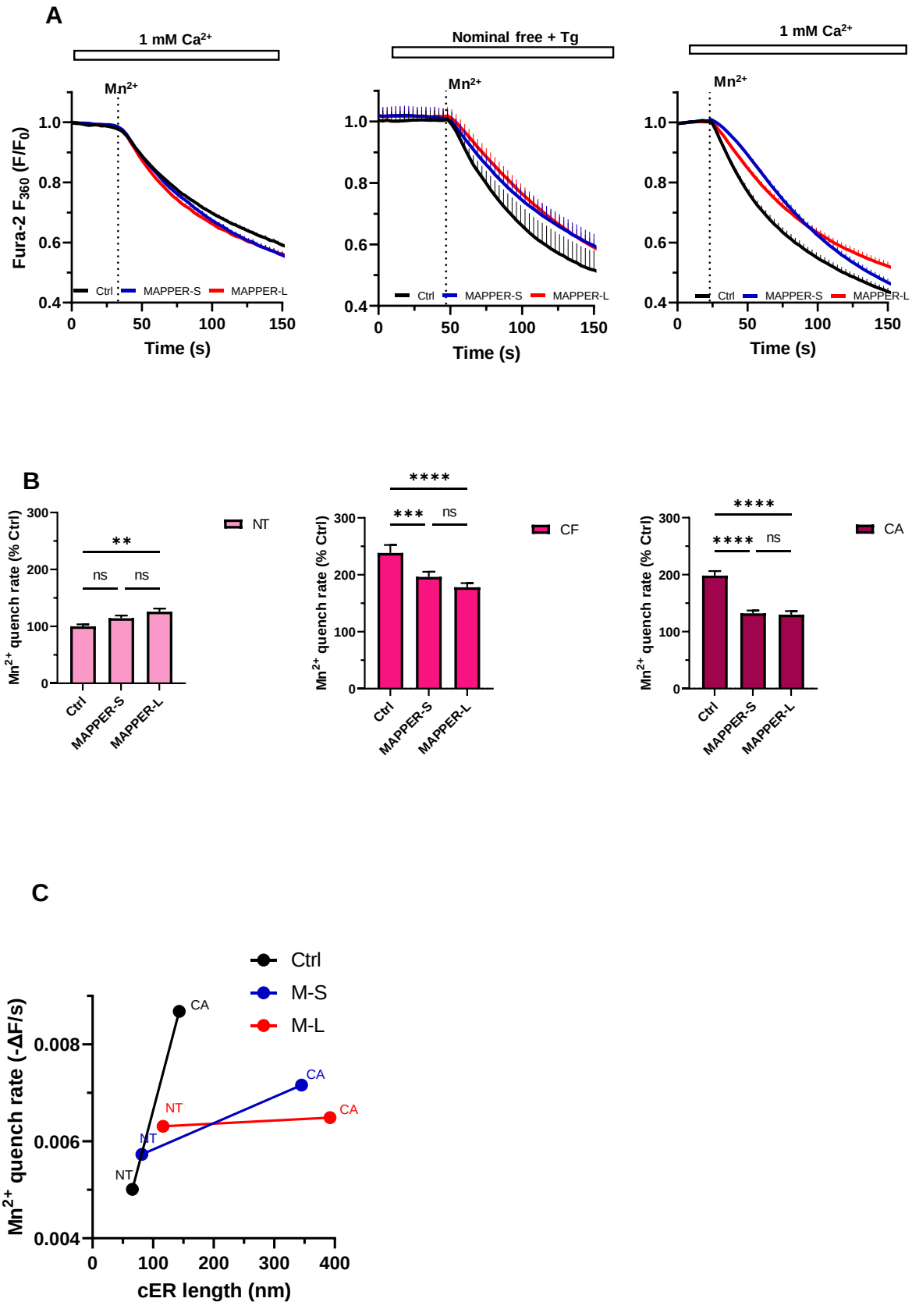

Table 1 (related to Figs. 1-4), Henry et al.

		ER-PM distance (nm)		cER length (nm)		
	Condition	Mean	SD	Mean	SD	N
Ctrl	NT	16,77	6,02	65,8	45,5	105
	CF	16,27	5,77	156,0	92,4	89
	CA	17,67	5,85	143,1	106,5	146
ESyt1	NT	17,27	5,33	56,8	42,3	100
	CF	14,92	4,78	234,2	206,2	226
	CA	16,88	5,38	161,9	115,7	149
ESyt2	NT	15,40	4,50	95,7	79,5	167
	CF	14,76	3,68	371,1	290,2	194
	CA	14,73	4,25	239,3	198,1	402
MAPPER-S	NT	16,28	6,70	81,4	57,6	110
	CF	13,99	6,74	294,5	309,2	133
	CA	13,54	7,74	345,3	384,6	127
MAPPER-L	NT	15,85	6,97	116,5	161,7	175
	CF	13,17	6,52	520,5	485,2	223
	CA	14,45	6,73	392,0	447,5	162

NT: Non treated
CF: EGTA 1 mM + Tg 10 min
CA: EGTA 1 mM + Tg 10 min then Ca^{2+} 1 mM for 2 min

Table 2 (related to Figs. 1-4), Henry et al.

		ER-PM distance		MCS length	
	Tukey's multiple comparisons test	Summary	Adjusted P Value	Summary	Adjusted P Value
Ctrl	NT vs. CF	ns	0.8148	*	0.0421
	NT vs. CA	ns	0.432	ns	0.0522
	CF vs. CA	ns	0.1602	ns	0.9275
ESyt1	NT vs. CF	**	0.0017	****	<0,0001
	NT vs. CA	ns	0.8565	**	0.005
	CF vs. CA	**	0.0032	*	0.0228
ESyt2	NT vs. CF	ns	0.5357	****	<0,0001
	NT vs. CA	ns	0.4073	****	<0,0001
	CF vs. CA	ns	0.998	****	<0,0001
MAPPER-S	NT vs. CF	**	0.0052	****	<0,0001
	NT vs. CA	***	0.0007	****	<0,0001
	CF vs. CA	ns	0.7995	ns	0.2558
MAPPER-L	NT vs. CF	****	<0,0001	****	<0,0001
	NT vs. CA	ns	0.0623	****	<0,0001
	CF vs. CA	ns	0.075	****	<0,0001
NT	Ctrl vs. ESyt1	ns	0.9705	ns	0.9992
	Ctrl vs. ESyt2	ns	0.3000	ns	0.8876
	ESyt1 vs. ESyt2	ns	0.0709	ns	0.7613
	Ctrl vs. MAPPER-S	ns	0.9701	ns	0.9921
	Ctrl vs. MAPPER-L	ns	0.6852	ns	0.5083
	MAPPER-S vs. MAPPER-L	ns	0.9718	ns	0.8010
CF	Ctrl vs. ESyt1	ns	0.3199	ns	0.1137
	Ctrl vs. ESyt2	ns	0.2323	****	<0,0001
	ESyt1 vs. ESyt2	ns	0.9985	****	<0,0001
	Ctrl vs. MAPPER-S	*	0.0286	***	0.0010
	Ctrl vs. MAPPER-L	***	0.0001	****	<0,0001
	MAPPER-S vs. MAPPER-L	ns	0.6818	****	<0,0001
CA	Ctrl vs. ESyt1	ns	0.7560	ns	0.9716
	Ctrl vs. ESyt2	****	<0,0001	**	0.0012
	ESyt1 vs. ESyt2	***	0.0008	*	0.0163
	Ctrl vs. MAPPER-S	****	<0,0001	****	<0,0001
	Ctrl vs. MAPPER-L	****	<0,0001	****	<0,0001
	MAPPER-S vs. MAPPER-L	ns	0.6603	ns	0.5510

NT: Non treated

CF: EGTA 1 mM + Tg 10 min

CA: EGTA 1 mM + Tg 10 min then Ca^{2+} 1 mM for 2 min

Figure S1 (related to Figs. 1-4), Henry et al.

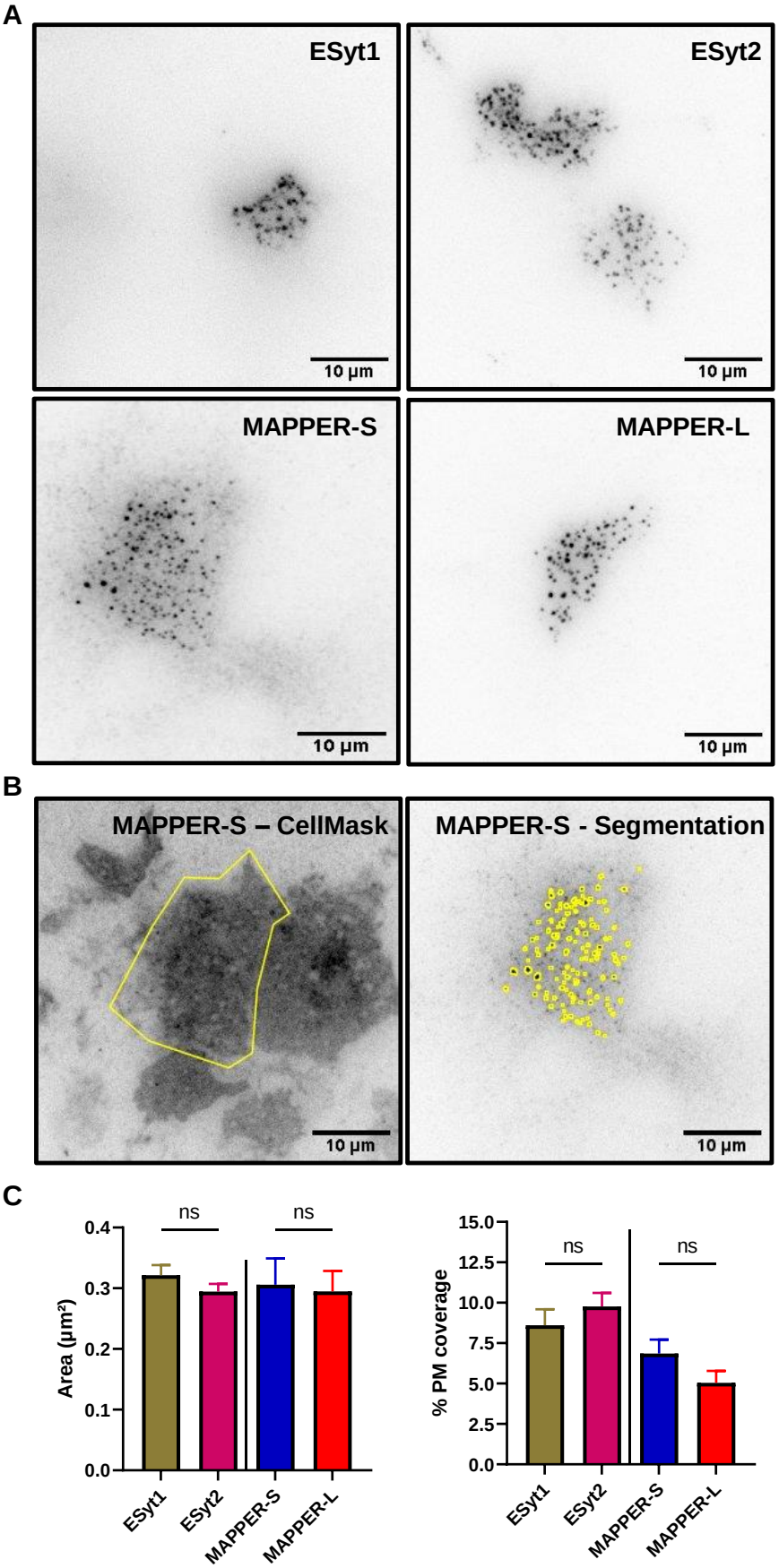

Figure S2 (related to Figs. 1-4), Henry et al.

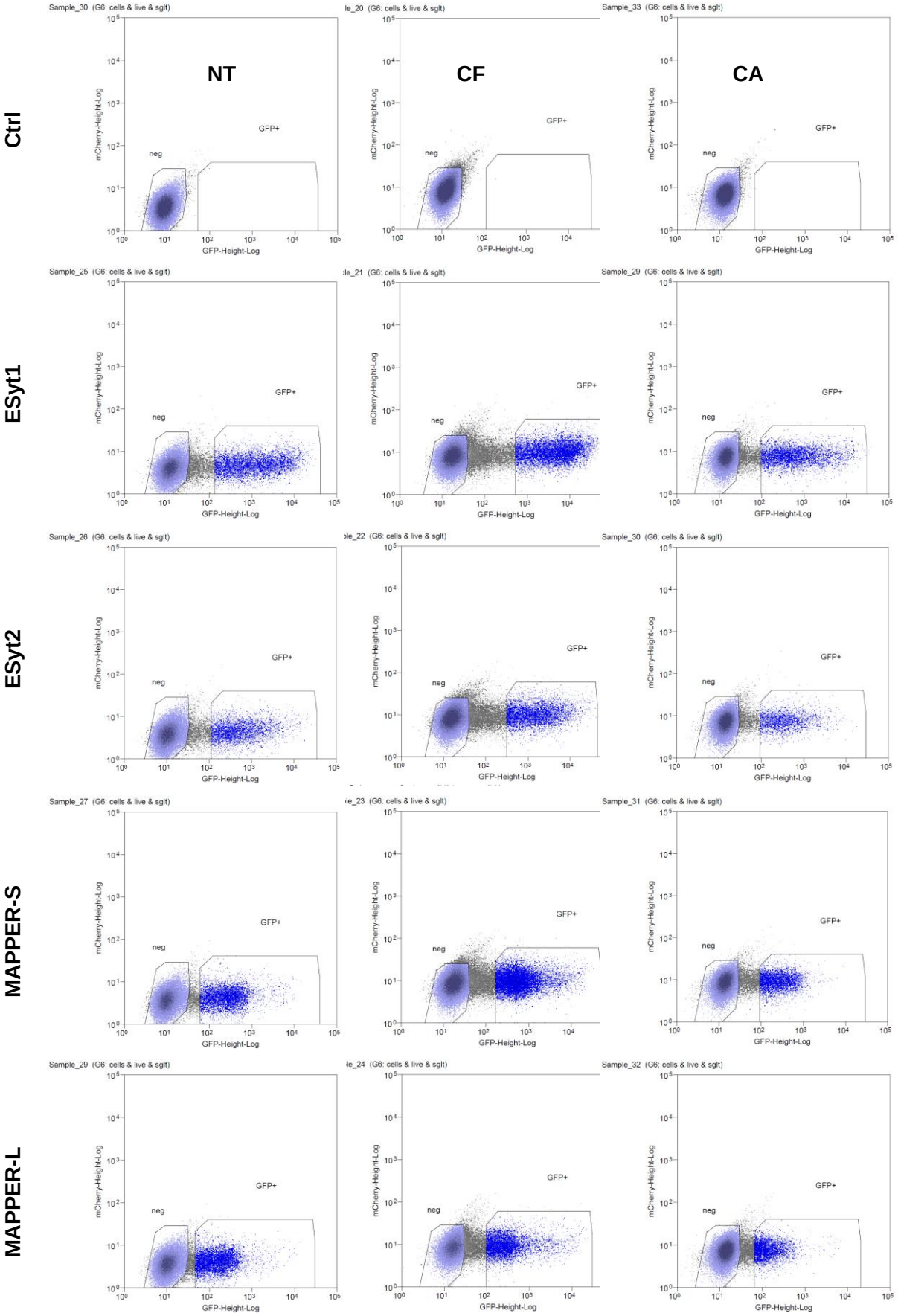

Figure S3 (related to Figs. 1-4), Henry et al.

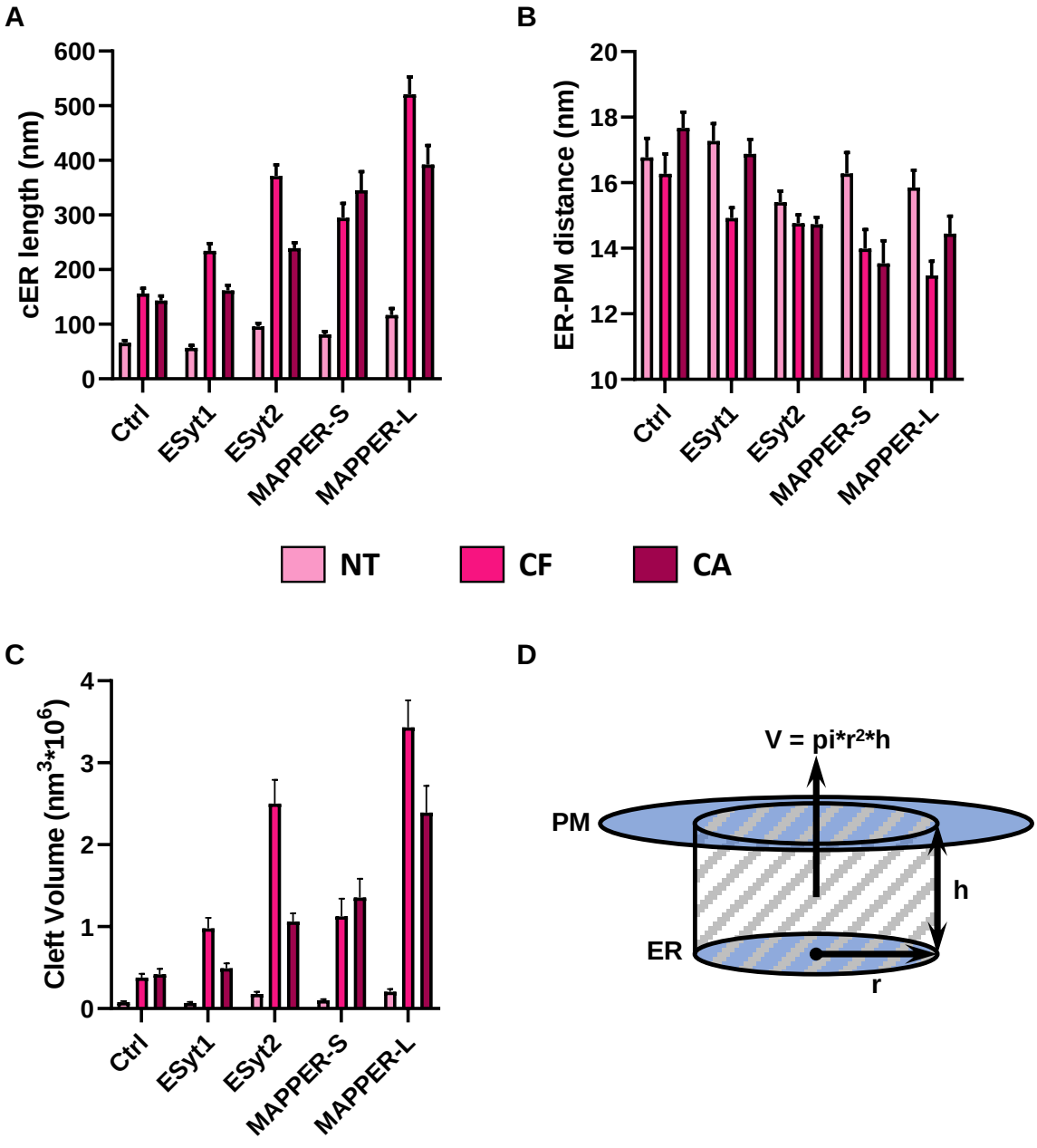

Figure S4 (related to Figs. 5-8), Henry et al.

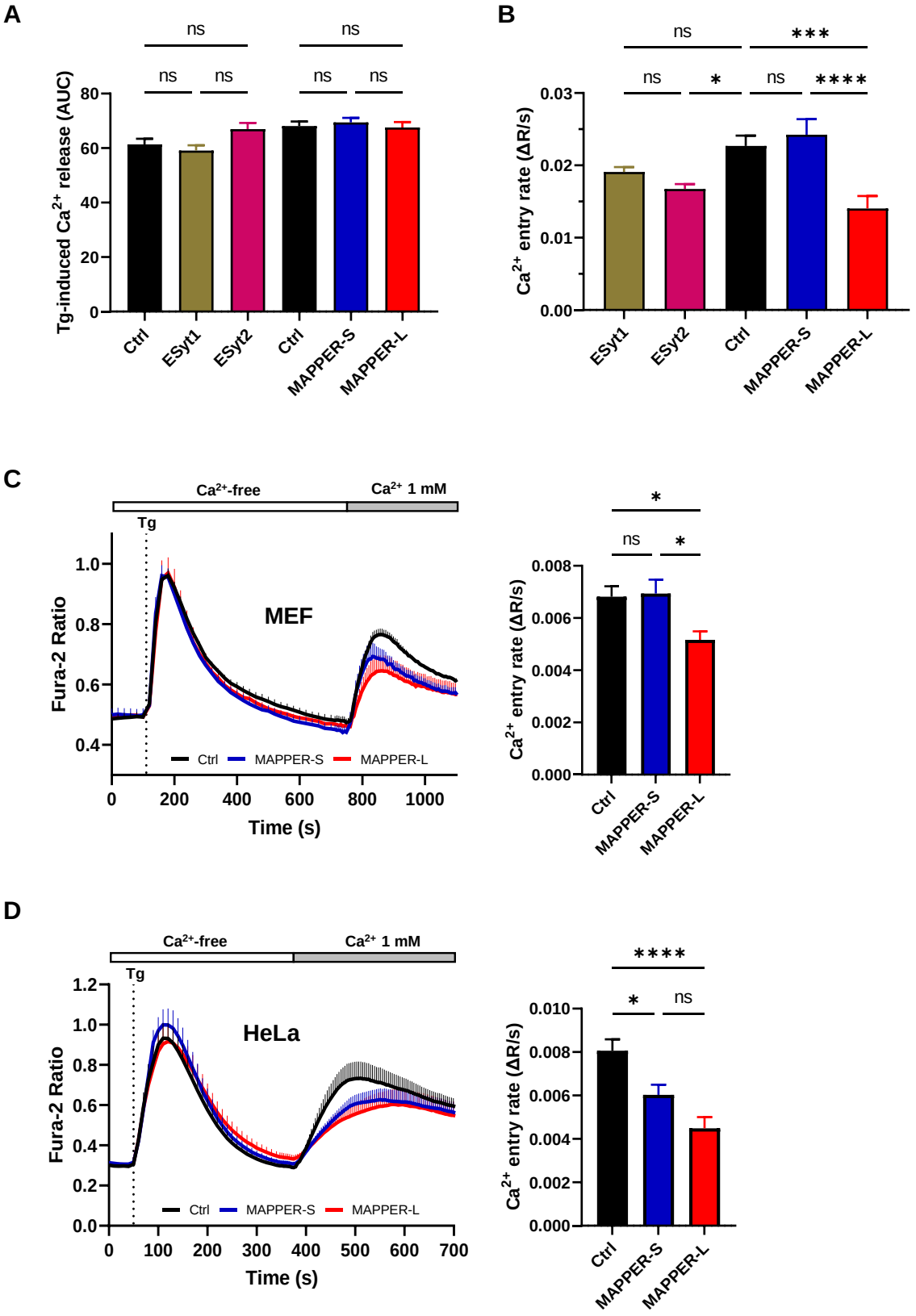

Figure S5 (related to Figs. 5-8), Henry et al.

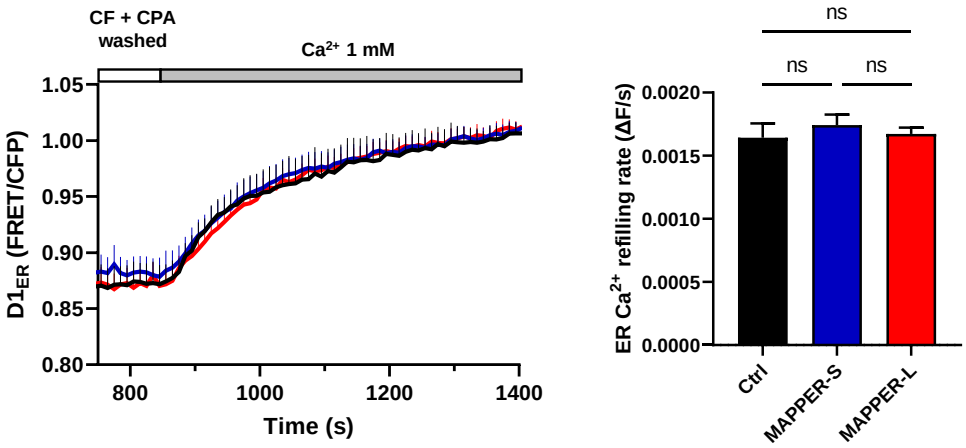

VII) Development of analytic tools

During my thesis, I realized that many tasks during analysis consisted of copy pasting or repeating same operations over and over. At some point, I figure out it was possible to automatize some aspects of data analysis in order to gain time and reliability. I started to learn how to code simple scripts using ImageJ such as removing background in all my images at once or separating and saving multiple channels from a single file. Over time, what started from removing image background became a fully developed pipeline covering from microscope control to extraction of biological information.

1) FURA-2 imaging pipeline

To measure cytosolic calcium, a common tool we use in our lab is FURA-2-AM dye, a ratiometric calcium sensor. Incubation of cells with this dye for 30 minutes allows its transfer and trapping into the cytosol. Following, cells are imaged under fluorescence microscopy using the two excitation wavelengths of FURA-2 (340 nm and 380 nm) which both emit at the same wavelength (~510 nm). Cells are usually challenged with drugs targeting different calcium related cellular components. To study SOCE, one of the classic protocols is depletion of ER calcium store using SERCA inhibitor such as Tg in a calcium-free medium. Following passive depletion of ER store, extracellular calcium is added, and a strong cytosolic elevation is observed, typical of SOCE (Figure 5). From this protocol, we usually extract fluorescence of each individual cells over time and plot it for visual interpretation. We also extract several characteristic parameters such as calcium entry slope which indicates calcium entry rate in the cell.

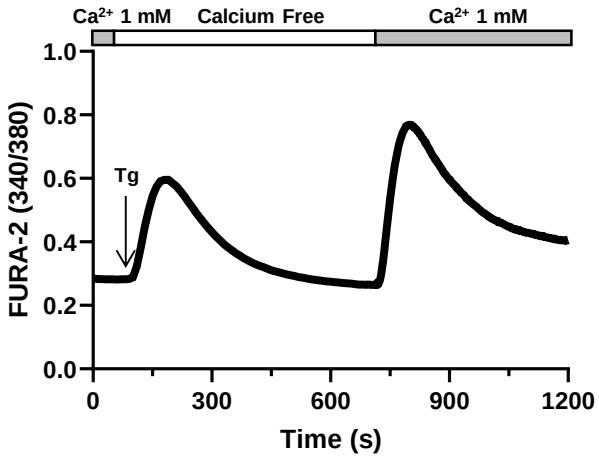

Figure 5: FURA-2 trace of SOCE protocol
FURA-2 loaded cells are imaged under fluorescence microscopy and FURA-2 ratio (340nm/380nm) represents calcium changes. Cell medium is changed from 1 mM calcium buffer to calcium free solution. It is followed by addition of thapsigargin (Tg) to block SERCA pumps which induce ER calcium depletion and elevation of cytosolic calcium. After ER full

depletion, calcium-containing buffer is added back to the cells and a strong cytosolic calcium elevation is observed.

a. Image acquisition

The pipeline I developed starts from the control of our wide field microscope acquisition software, Visiview from Visitron systems. Something important for our protocol is temporal resolution. Since we are investigating relatively fast events, it is key to precisely control image acquisition rate. To get best temporal resolution during calcium entry, we want to have one frame every two or three seconds. However, the total protocol last 10 to 20 min depending how many steps are added to the protocol. This is a relatively long imaging time involving an important cell phototoxicity as we need to illuminate them with a UV light to excite FURA-2. To go around this limitation, it is possible to reduce frame rate during the experiment when temporal resolution is not as critical. It is typically the case during Tg-induced calcium release which is a slow process, and acquisition rate can easily be set to one image every ten seconds. The issue we faced is that Visiview does not allow to program multiple frame rates during an experiment. What Visiview does allow is to use its Python API to control every acquisition element. Taking advantage of this tool, I created a script allowing me to change the frame rate at any time of acquisition by pre-programming it. The first part of acquisition is set to take an image every 10 seconds and after 10 min, once ER depletion is complete, a new file is created where frame rate automatically changes for one image every 3 seconds (https://github.com/Carandoom/VisiviewFura2 ; DOI: https://doi.org/10.5281/zenodo.5026893).
After image acquisition, I fuse the two protocol in one file using a custom script I wrote in ImageJ (https://github.com/Carandoom/FuseFilesFura2 ; DOI: https://doi.org/10.5281/zenodo.5168563).

b. Extraction of region of interest signal

Using ImageJ, I open the 2 channels and I create region of interest (ROI) inside cells. This part could be automatized for cells relatively individualized but for HEK cells growing in groups, it is much more difficult, especially without an additional marker such as DAPI. To ensure data high quality, I decided to keep cell selection manual.
Sometimes, we want to have a preview of the traces, so I use another custom script to generate FURA-2 ratio image and create a graph of ROIs signal over time (Figure 6) (https://github.com/Carandoom/PlotFromRoi ; DOI: https://doi.org/10.5281/zenodo.5168601).

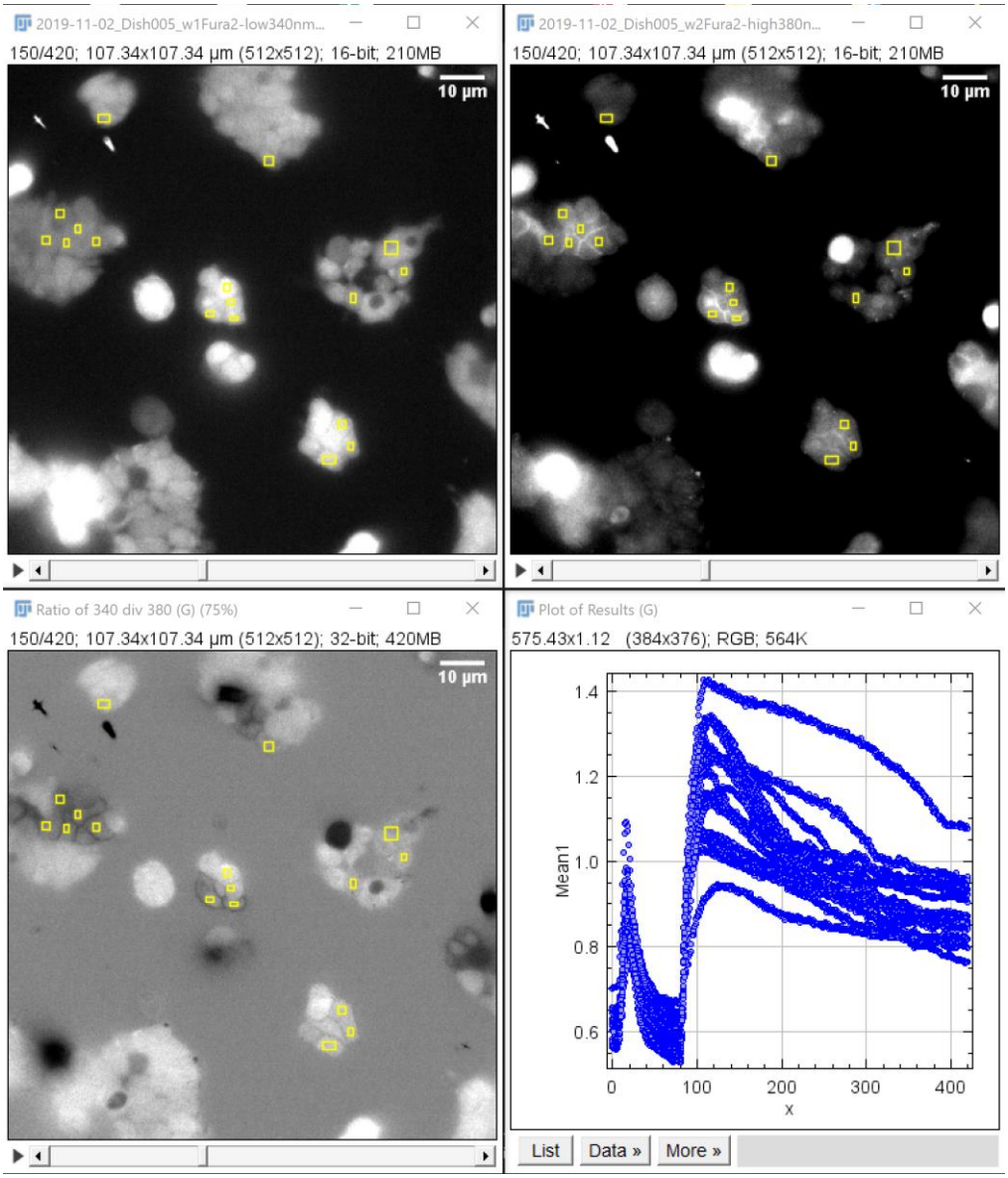

Figure 6: Ratio image and traces from region of interest in ImageJ
HEK-293T cells loaded with FURA-2-AM and imaged under fluorescence wide field microscope. Top left is 340 nm excitation channel and top right is 380 nm excitation channel. Bottom left is ratio image generated from pixel to pixel division of 340 nm by 380 nm images. Bottom right is the graph of the region of interest signal over time extracted from ratio image. To note on the graph, x axis represents frame number from the image and is not converted to time in seconds. On the 3 images, yellow rectangles represent region of interests used to extract ratio plotted on the graph.

I usually create an additional ROI in the background region to extract mean fluorescence of non-specific signal and remove it from the whole image later on.

After saving all regions, I start the main script, which is divided in 2 parts. The first one opens each channel image in ImageJ and its corresponding background ROI to subtract background for each time frame. Following, cell ROIs are opened, and average fluorescence is extracted over time and exported in text files (https://github.com/Carandoom/Fura2Analysis ; DOI: https://doi.org/10.5281/zenodo.5026897). The second part is coded in VBA, the programming language of Excel which gives a full control on import of data and generation of formula. The aim of

this part is to open each text files generated from the first part of the script and import them in an Excel file. The script creates a new Excel file with 4 tabs, the first two are used to import 340 nm and 380 nm channels. In the third one, the script generates formula to calculate 340 nm and 380 nm channels ratio. In the last one, I calculate the normalization to the first few time points for each trace for them to all start at 1 which makes it easier to compare when ratios are not starting at the same level. To facilitate data exploration, the script adds dish identification as "Dishxxx" in the first row. It also generates cell number based on ROI number from which cell signal has been extracted. I then export manually data in a Graphpad Prism template for data visualization and data cleaning if needed.

c. Calcium entry rate

Finally, we need to extract calcium entry rate during SOCE. To analyze this parameter, we can extract the maximal entry rate from the maximum of the first derivative. Another way is to describe global entry rate using the slope of a linear fitting on multiple points during calcium entry. The two ways are giving a slightly different information about entry rate and for our experiments we decided to rather analyze the slope from a linear fitting to integrate the full response. To define the fitting for each trace, I wrote a script in Matlab which uses the first derivative to find where to fit a linear regression and export the slope parameter (Figure 7) (https://github.com/Carandoom/SlopeFromLinearRegression ; DOI: https://doi.org/10.5281/zenodo.5026895).

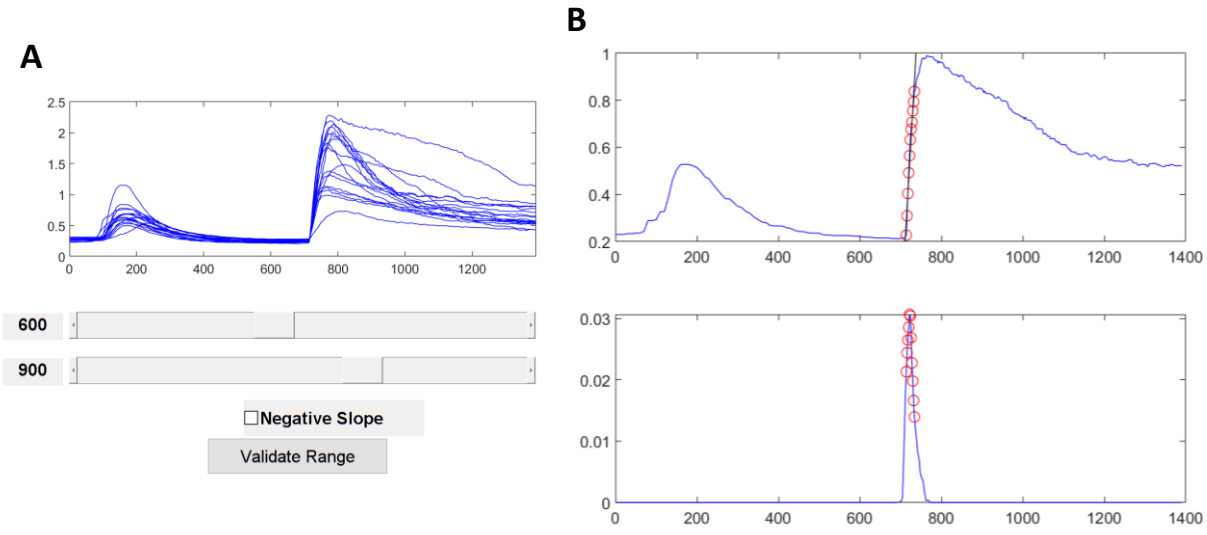

Figure 7: User interface of Matlab script to fit a linear regression
A) First interface shown to user, traces (y axis is FURA-2 ratio) are plotted with associated time (here in s). At the bottom are two sliders to select the range in which the algorithm is going to find the portion of the traces to fit. In case we would like to analyze a decreasing part of the traces, we can tick "Negative Slope". Once the interval is selected, the user press "Validate Range" and a second Interface appears. B) Second interface of the script which shows each trace one by one to allow user to manually check individual fitting. On top are the individual trace and linear regression drawn. The points taken into consideration for linear regression fitting are labelled in red. Those points are taken from the bottom graph which is the first derivative of the above trace only in the selected range (more details and video example on GitHub).

The main script allows me to gain time and reliability on cell signal extraction, import and organization of data in Excel. The second one extract calcium entry rate and allow me to easily fit a linear regression on the traces. Before using this script, I was extracting the slope using GraphPad Prism where I had to manually select the range to fit a linear regression for each trace. I ran a couple tests and concluded that this script made a 3h analysis only a 45 min analysis. Since this experiment is at the core of my thesis project and I performed it more than 100 times, the gain of time is substantial (Over 200h saved). Over time, this script has been updated and I have developed personalized versions for some colleagues. For example, I created an alternative background removal method based on a rolling ball method and extracted sum fluorescence instead of mean fluorescence. This script and its variations are currently used by most of our lab members and also by some collaborators that have published results using it (see acknowledgments of Dyrda et al. 2019, Cell Calcium).

2) Segmentation of MCS

Working with SOCE, our lab often performs TIRF microscopy to study STIM1 recruitment or ORAI1 clustering. Depending how precise we need to be, many options are available to study cER recruitment of STIM1. If we just need to know global STIM1 recruitment, mean fluorescence evolution over time is sufficient. However, is we want to study STIM1 puncta morphology throughout its recruitment, another approach is required. When we need to analyze individual STIM1 puncta using TIRF microscopy, the biggest challenge is to separate them accurately. Thresholding is key for selecting puncta and directly depends on local background. Often, separation of close puncta is difficult and there is need of sophisticated strategy to overcome this problem (Figure 8A). A very powerful method is to use a maxima map which detects local maximum and generate a binary mask separating each maximum. Combined with thresholding, it allows to have a very precise segmentation of STIM puncta. This process is not simple to automatize as from one image to another, they require different sensitivity to properly detect local maximum.

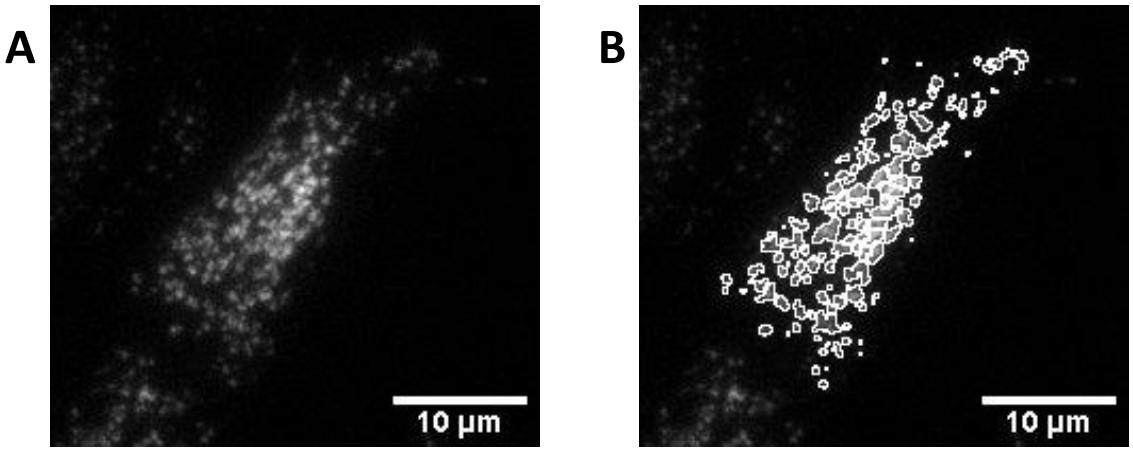

Figure 8: STIM1 puncta from TIRF segmented using custom ImageJ script
A) single TIRF image of fluorescently labelled STIM1 after Tg treatment. We can see formation of puncta structures close to each other's. B) Segmentation of STIM1 puncta using ImageJ script. Image from Amado Carreras-Sureda.

To accelerate the segmentation pipeline, I developed a script in ImageJ for user to navigate much faster between each different step (Video example available on GitHub: https://github.com/Carandoom/STIM-ORAI-Segmentation ; DOI: https://doi.org/10.5281/zenodo.5026889). This script does not remove background so each user can decide what works best for their data. The first image is opened, and the user manually outlined the cell in which to perform segmentation. The user is then prompted to enter a value for the maxima map sensitivity and can go back and forth to inspect maxima detection and obtain the best maxima map possible. Once the user is satisfied, the script starts the longest part of the work, it generates a maxima map for each time points. Following this procedure, the user can adjust the segmentation threshold of STIM1 puncta, and it will be applied to every frame. Maxima map and threshold mask are both binary images and are combined to separate each punctum in the most accurate way using both information. Region of interest are created based on this new map (Figure 8B) and their morphometric parameters are extracted and exported into a text file.
This script does not present a significant advantage for single time point images, but when working with many time points, the analysis time is rapidly reduced. I developed this script because I had to analyze the puncta formation over many time points and manual segmentation was highly time consuming. I used this script in a publication currently in revision at eLife (in revision Carreras-Sureda et al. 2021, eLife).

3) Colocalization

A very common question in biology is whether two proteins colocalize as it gives precious information about their potential interaction or coupling for a physiological process. This is of particular interest when studying STIM and ORAI since under TIRF microscopy, they form puncta structures in which STIM activates ORAI. There are already available softwares to measure colocalization of two channels in a single image. In our case, we wanted to easily measure colocalization throughout SOCE activation. This is something already implemented in Imaris software but to use it we need a license unavailable in our lab. However, our university give us access to Matlab license, so I could develop a colocalization software in Matlab, using a similar interface as Imaris (https://github.com/Carandoom/Coloc2ChannelsStackROI ; DOI: https://doi.org/10.5281/zenodo.5025988). This software allows us to restrict our analysis on a single cell which can strongly increase analysis reliability (Figure 9).

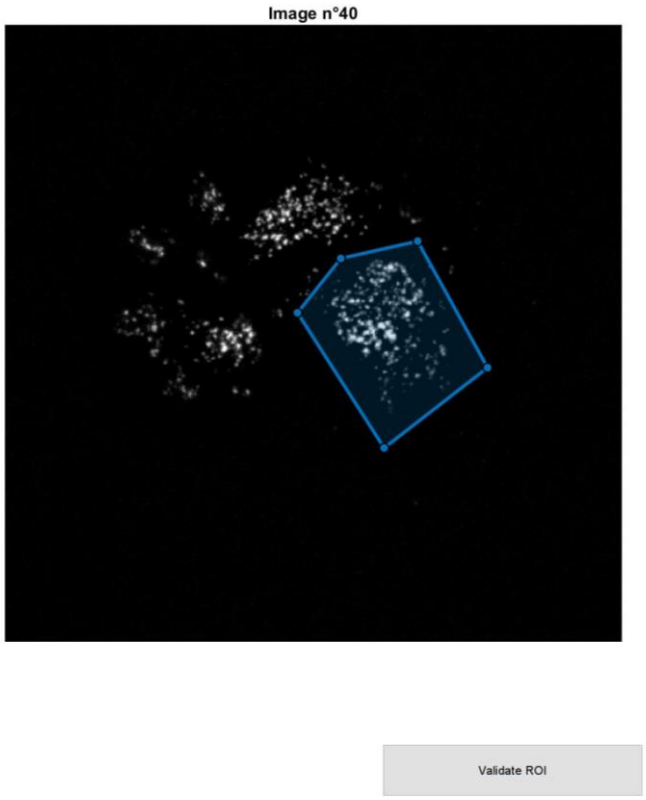

Figure 9: Restriction of image region to measure colocalization
User interface allowing to draw a region around area to analyze, typically around cell of interest. It is possible to navigate between all opened images using a slider (not shown on this example). Once the selection is done, the user press on "Validate ROI" and the software move on to the colocalization interface.

After selection process, region of interest is isolated to calculate colocalization parameters. This interface is then composed of 4 specialized blocs (Figure 10). The first one contains each channel and its applied threshold (Figure 10A) while the second bloc shows the composite image of the two channels displayed in Green/Red and a scatter plot of their pixel to pixel intensity (Figure 10B). The third part is composed of two histograms which allows the user to directly interact by clicking on it to set the desired threshold (Figure 10C). When the user clicks on the histogram, a yellow area highlights the selected pixel intensities and the thresholded image gets updated. The last section allows the user to apply selected thresholds to all the images and generate a table with colocalization parameters (Figure 10D).

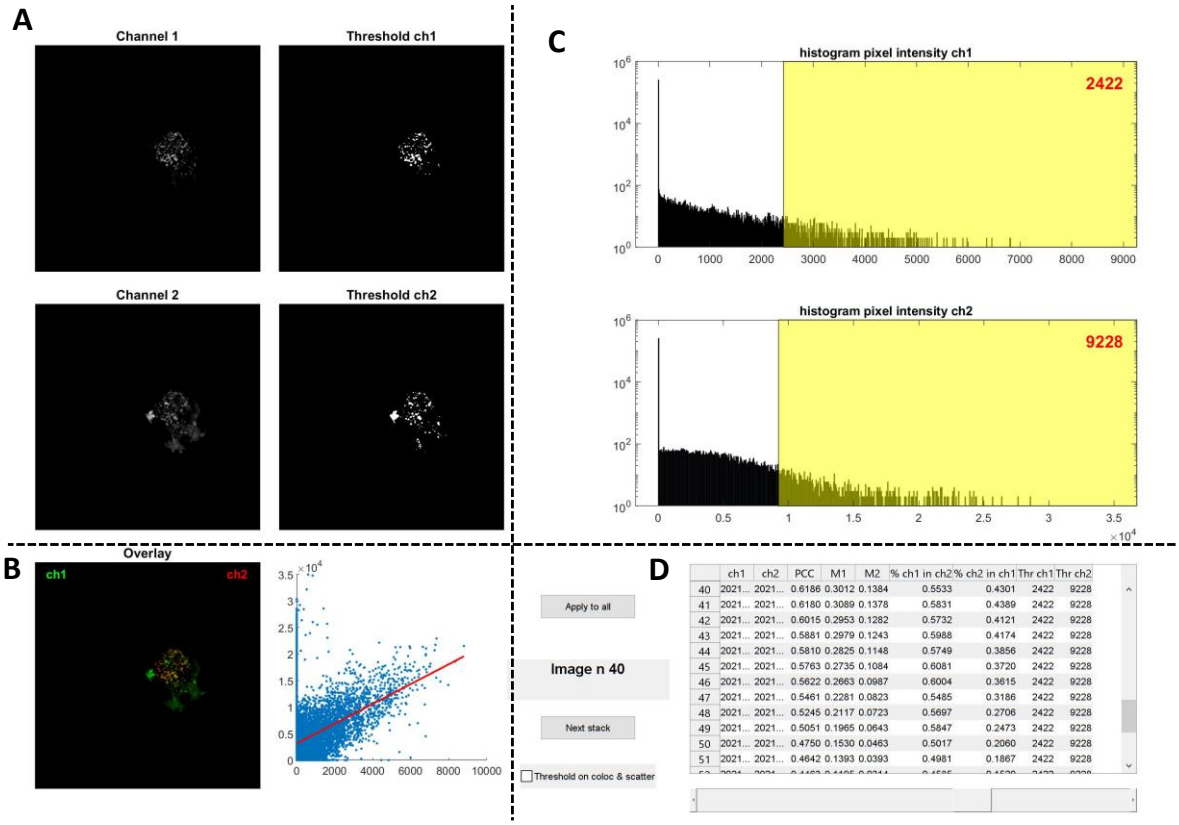

Figure 10: Colocalization software interface
A) On the left are the two channels isolated in the previously selected region. On the right is the thresholded image. B) The composite image containing both channels is displayed on the left and the pixel to pixel scatter plot for both channels is on the right. A linear regression is fitted as indication of the correlation between channel 1 and channel 2. C) histograms for pixel intensity distribution of each channel. Area highlighted in yellow represents the pixels selected by the threshold. D) "Apply all" button generates the table on the right which contain all the colocalization information (see GitHub for details). It is possible to navigate through the time points using the slider at the bottom. "Next stack" allows the user to restart the image selection process. "Threshold on coloc & scatter" is a yet non-implemented feature for a future release to limit B in the defined threshold. Ch1: channel 1; ch2: channel 2.

Overall, this script can be used either to get colocalization of two channels in a single dimension image as well as for 3D images (z-stacks or timelapses). This software has been used by a co-worker for a manuscript under submission to Journal of Biological Chemistry.

4) Nuclear translocation

Microscopy can be extremely informative when activation of a protein leads to a change in its compartmentalization pattern. NFAT is a typical example of a cytosolic protein which translocate to nucleus upon activation during SOCE. Its translocation is very good proxy to estimate NFAT activation status. To measure translocation of a protein from cytosol to nucleus, it is important to have a nuclear marker. A co-worker needed to analyze NFAT translocation upon cell stimulation and was manually defining cytosolic and nucleus regions from cells. He asked me if I could reliably detect the two compartments and measure percentage of NFAT translocation. To obtain a percentage of nuclear translocation, sum fluorescence of nuclear compartment is divided by sum fluorescence of

nuclear + cytosolic compartments. I could create a script in ImageJ which uses a nuclear marker and NFAT signal itself to define these two compartments (https://github.com/Carandoom/NuclearTranslocation ; DOI: https://doi.org/10.5281/zenodo.5176125). Nuclear segmentation using this script is accurate at 40x magnification (Figure 11) but with the current parameters it is not great with a 10x magnification. It is possible to change algorithm settings to go around this limitation. The script extracts the sum of fluorescence for both regions to know how much of NFAT is in the nucleus compared to the cytosol.

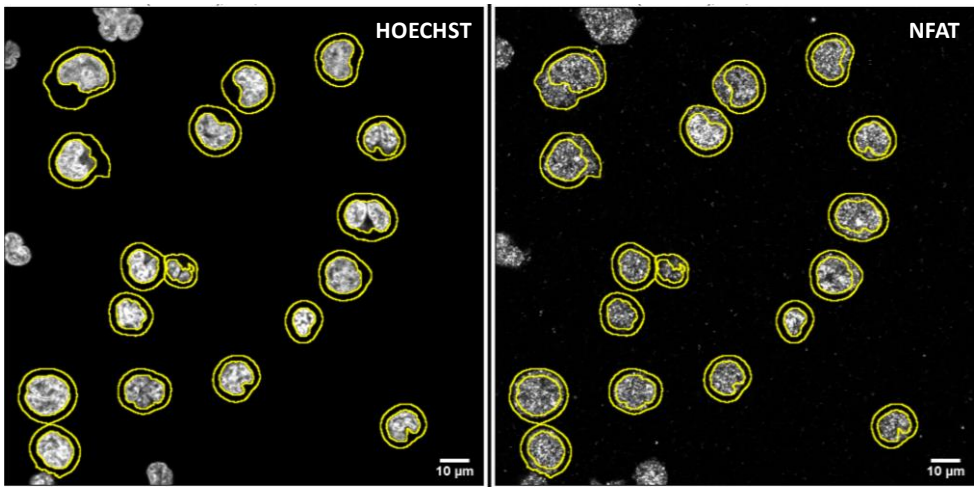

Figure 11: Segmentation of nucleus and nucleus+cytosolic compartments in Jurkat cells.
Jurkat cells treated 4h with thapsigargin then fixed for immunofluorescence. Left: Hoechst staining to label cell nucleus. Right: NFAT staining using antibody. Segmented regions are highlighted in yellow. Inner region corresponds to the nucleus and outer region delimits cytosol + nucleus (See GitHub for details on segmentation procedure).

After visual assessment of many regions generated by the script, we concluded that segmentation was accurate and in the few cases where it was not, cells were often automatically excluded. We also compared results obtained by manual analysis and from this script and concluded that they are similar (Figure 12). We did not publish results using this script yet, but we believe that it is a useful tool for the SOCE community and hope to see new studies taking advantage its availability.

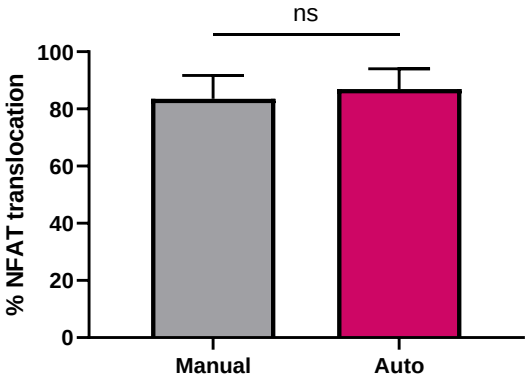

Figure 12: Comparison of the automatic and manual detection of the NFAT translocation to the nucleus.
Nuclear translocation of NFAT in Jurkat cells after 4h of thapsigargin treatment. Mean+/-s.d., student t-test.

VIII) Discussion

MCS are central structures for signaling pathways and to regulate cell homeostasis. Modulation of these platforms involve effector protein recruitment as well as morphological adaptation. ER-PM contact sites are at the core of SOCE, and studies suggest a role of ER-PM junctions morphology and their stability in regulation of SOCE {Varnai et al., 2007, J Biol Chem; Kang et al., 2019, Scientific Reports}. My thesis investigates the structure-function relationship between ultrastructure of ER-PM contact sites and SOCE. Using electron microscopy, I studied MCS morphology throughout SOCE by measuring ER-PM gap distance and cER length. I show that during ER calcium depletion, cER length increases and this is potentiated by expression of tether proteins. I investigated the impact of such potentiation on SOCE and found that generation of very long cER structures inhibit calcium entry. modulation of ER-PM contact sites morphology represents a simple yet powerful way for cells to regulate such crucial mechanism as SOCE.

During a second time, I developed tools to extract key information from our experiments either by accelerating a pipeline already existing or by creating a new way to obtain insights. The informatic era now allows scientists to go deeper in understanding of their data and help them to reach conclusions much faster.

1) ER-PM contact sites ultrastructure during SOCE

Investigating SOCE is commonly achieved by Tg application to induce ER store depletion. Morphological changes of ER-PM junctions upon Tg treatment have been reported and the amount of cER in contact with PM increased by 5.3-fold {Orci et al., 2009, PNAS}. This assessment is usually done in a calcium containing media where Tg is added for 10 min. However, calcium imaging often features a more complex protocol to isolate ER release from calcium entry through ORAI. The key difference is addition of thapsigargin in a calcium-free media for 10 min then calcium is added to the cells. So far, no one has looked at ER-PM ultrastructure at different timepoints of such protocol. Using electron microscopy, we assessed the ER-PM morphology at resting, after ER depletion in calcium-free and 2 minutes following calcium addition. We showed that cER length indeed increases upon ER depletion, but calcium addition does not significantly further modify this size. Suggesting cER elongation to be caused by ER depletion itself without need for calcium entry. The exact expansion mechanism is still unknown, but literature and our results point toward a STIM-mediated elongation {Orci et al. 2009, PNAS; Sauc et al., 2015, J Cell Science}. In literature, using CPA instead of Tg to wash it restore SERCA activity and allow ER refilling resulted in STIM1 clearing from ER-PM junctions as observed in TIRF. No electron microscopy data are available to support that cER itself is shrinking upon SOCE termination from calcium entry, but I expect that STIM1 clearing would revert

cER elongation to reach back a resting state. Moreover, I do not know if a more physiological stimulation, such as with an agonist to trigger the IP_3 pathway, would result in cER elongation. Because agonist induces a fast ER depletion compared to Tg, it is possible that cER expansion does not have time to fully develop before SOCE termination.

The question is now, why does cER length increase during ER depletion ? As ER depletion results in activation of SOCE one could expect that it is to favor calcium entry. As shown by Treves and colleagues {Treves et al., 2004, J Cell Biology}, expression of Junctate increased cER size from 218 nm to 339 nm and enhanced calcium entry. On the other hand, depletion of Junctate reduced cER to 139 nm and decreased SOCE. Together, these results suggest that cER expansion positively regulates calcium entry. But in my experiments, when I use tether to generate longer cER structures, I observe an inhibitory effect on SOCE. This discrepancy could come from the observation of Junctate induced cER at rest and not after ER depletion. In this study, it is not known how cER evolve upon STIM1 activation and therefore we cannot have the final cER length of those ER-PM junctions to compare with my results. My hypothesis is that since Junctate directly interacts with STIM1 through its C-term domains {Srikanth et al., 2012, PNAS}, its overexpression enhances STIM1 recruitment to ER-PM junctions. Whereas ESyts and MAPPERs both compete against STIM1 for PIP_2 binding on PM and since ESyt2 and MAPPERs are constitutively recruited to ER-PM junctions, they exclude STIM1 from the contact sites core. Therefore, STIM1 needs to further extend cER to populate ER-PM junctions {Giordano et al., 2013, Cell; Chang et al. 2013, Cell Rep}. Interestingly, Varnai and colleagues used tether proteins and restricted ER-PM junction access to ORAI1 but not STIM1. However, STIM1-ORAI1 accumulated on periphery of ER-PM contact sites, suggesting that excluding one of them from the contact core also displace the complex {Varnai et al., 2007, J Biol Chem}. They did not observe a modification in calcium entry upon STIM1-ORAI1 exclusion from ER-PM junction center which could be explained by the fact they overexpressed both STIM1 and ORAI1. This boost SOCE {Lee et al., 2013, J Cell Science} and potentially compensate for an inhibition of calcium entry caused by STIM1-ORAI1 peripherical accumulation.

Recently, Kang and colleagues have used super resolution TIRF microscopy to reveal that STIM1 rearrange from puncta to ring-like structures upon calcium entry {Kang et al., 2019, Sci Rep}. These structures were more stable and closer to the PM, and the more stabilized ones were associated with enhanced ER refilling. Kang and colleagues also suggested that ring-shaped STIM1 might disassemble faster than punctate ones as they are more exposed to the surrounding environment which ultimately dim calcium entry. I believe that STIM1 accumulates in similar ring-shape structures already during ER depletion when ESyt2 or MAPPERs are expressed. Our manganese quenching results suggest that after 2 min of calcium entry, without ER refilling, manganese entry is almost

completely abrogated. From this I tend to believe that CDI mechanisms are more efficient when STIM1 is accumulated in ring structures.

A previous EM study of MAPPER-L showed that its expression was neutral to ER-PM contact morphology as well as for SOCE {Chang et al., 2013, Cell Rep}. I do not fully understand how we can observe such difference between Chang and my experiments. Because their study was not focused on morphological characterization of ER-PM junctions, they did not discuss in great detail about their EM quantification. Since very large cER structures are a minority, they could have been missed if only a few contacts were investigated. In my non-treated MAPPER-L dataset, only 16 contacts out of 175 exhibited longer cER than control. For SOCE experiments, our stimulation protocol slightly differs as we used Tg alone where they used Tg + histamine. Stimulation of IP_3 pathway leads to hydrolysis of PIP_2, MAPPER-L ligand and therefore cancel out its tethering effect. Now I don't expect PIP_2 to be totally depleted as the cellular system will fight back with Nir2 and Nir3 proteins {Giordano et al. 2013, Cell}. So PIP_2 binding by MAPPER and STIM1 proteins will be exposed to a faster turnover but where MAPPER only uses PIP_2 binding as a stabilization mechanism, STIM1 also binds to ORAI1. Therefore, I believe that during the full treatment by Chang and colleagues, MAPPER-L is replaced by STIM1 and its inhibitory impact on SOCE is cancelled out. Sadly, they did not investigate SOCE in MAPPER-S expressing cells but, in my case, I see a similar inhibition of SOCE as with MAPPER-L.

Throughout SOCE, I did not observe significant ER-PM distance changes in control cells which was surprising to me since studies highlighted ESyt1 role in intermembrane shortening {Giordano et al., 2013, Cell; Fernandez-Busnadiego et al, 2015, PNAS}. Fernandez-Busnadiego and colleagues showed that treating ESyt1 expressing Cos7 cells with calcium induces a shortening of ER-PM gap distance from 21.8 nm to 14.8 nm. We can already say discuss that the average distance measured in my HEK-293T cells is ~17 nm at rest which could be due to cell type differences. Also, cell fixation was carried out in 1 mM Calcium containing buffer on my side against DMEM which contains 1.8 mM calcium for this study. Higher calcium concentration in the cell medium before fixation could affect the basal SOCE activation and therefore ER-PM distance. Fernandez-Busnadiego and colleagues used cryo EM which better preserve structures from radiation damages. Strong radiation from classic EM tends to increase sample deformation such as structure shrinking and therefore could reduce the apparent measured distances. In this study, ESyt1 was overexpressed when intermembrane shortening was observed. In my experiments, I see similar findings as ESyt1 expression and ER depletion also shorten gap distance. This suggest that ER depletion is sufficient to activate ESyt1 and favor ER-PM shortening without calcium entry. It is possible that calcium elevation from ER depletion is localized and coupled to ESyt1 to favor its activation. Since IP_3R are suggested to be responsible for ER leak

{Lemos et al., 2021, BBA Molecular Cell Research}, Tg treatment would result in long lasting (minutes) local calcium increase around IP_3R. Active IP_3R are enriched close to ER-PM junctions {Thilaiappan et al., 2017, Nature Communications} and could present a higher passive calcium leak which would favor ESyt1 activation as ESyt1 is also enriched close to ER-PM junctions {Kang et al., 2019, Sci Rep}. Such coupling would favor a rapid activation of ESyt1 upon physiological IP_3R stimulation which favors ER-PM junction stability and allow efficient refilling to avoid over activation of SOCE machinery.

Figure 13: Calmodulin binding site prediction for ESyt1
Using Calmodulin target database website I obtained the calmodulin binding site prediction of ESyt1. ESyt1 sequence id: Q9BSJ8-1. Score below amino acids range from 0 to 9 with 9 being the highest score associated to calmodulin binding prediction. Color code is associated with the likeness of calmodulin binding site from green to violet for not likely to very likely, respectively.

When I pursue my experiment by adding calcium for 2 minutes, I restore basal ER-PM distance in ESyt1 overexpressing cells proposing a calcium dependent mechanism for ESyt1-dependent ER-PM distance extension. This is counterintuitive as calcium binding to ESyt1 induces a conformational

change which rather reduce the protein span length. ER-PM junctions are complex signaling platform and calcium entry triggers many effectors such as calmodulin. By running a calmodulin binding prediction using "Calmodulin target database" {Yap et al., 2000, J Struct Funct Genomics}, I could detect multiple potential binding site of calmodulin within C2 domains of ESyt1 (Figure 13). C2A (312 to 433 a.a.) and C2E (971 to 1093 a.a.) have high score to be calmodulin binding sites and C2C (627 to 751 a.a.) presents a smaller score but worth to note. An extensive study of C2 domain importance for ESyt1 calcium-dependent recruitment to ER-PM junctions revealed that C2A is not important {Idevall-Hagren et al, 2015, EMBO J}. On the contrary, the main conclusion of this study is that C2C and C2E are critically required for the proper ESyt1 binding to PM PIP_2. My hypothesis is that upon calcium entry, calmodulin binds to ESyt1 and exclude it from ER-PM junctions, increasing gap distance and therefore destabilizing STIM1-ORAI1 interaction.

In my control cells, I do not see neither a shortening of ER-PM distance upon ER depletion nor an increase upon calcium entry. This suggests to me that endogenous level of ESyt1 is not sufficient to induce such strong ER-PM distance changes. Interestingly, I observe a trend in my data with a slight shortening of ER-PM distance with calcium depletion and back to basal level after calcium entry. To me, endogenous ESyt1 does affect intermembrane distance but to a lesser extent than in overexpression conditions. Because of my EM setup, I might not have sufficient resolution to detect refined changes in ER-PM distance cause by ESyt1 activity. Using cryo-EM as Fernandez-Busnadiego and colleagues could reveal this endogenous dynamism and help to better understand how ER-PM distance is regulated by ESyt1.

STIM protein diversity and the way they regulate SOCE has been studied in the different cellular systems where each isoform is preferentially expressed. I generated a summary table of the key characteristics I would like to discuss regarding the three main STIM1 isoforms (Table 1).

STIM1-S as ref	SOCE	Length (a.a.)	cER size	Main tissue expression
STIM1-S	**0**	**685**	**0**	All
STIM1-L	**+**	**791**	**-**	Skeletal muscle
STIM1-B	**-**	**540**	**-**	Brain

Table 1: Main characteristics of STIM1 isoforms
Using STIM1-S, classical isoform as reference I noted if STIM1-L or STIM1-B isoform is more (+) or less (-) for each parameter. Length corresponds to the protein sequence length. Sources: Darbellay et al., 2011, J Cell Biol ; Sauc et al., 2015, Journal of Cell Science; Ramesh et al., 2021, Cell Rep.

Expression of STIM1-S is ubiquitous, so I used it as a reference to compare STIM1-Long and STIM1-B calcium entry, protein length and cER size. STIM1-L is mostly found in skeletal muscle and plays a role in muscle development {Darbellay et al., 2011, J Cell Biology; Sauc et al., 2015, J Cell Science}. On the

other hand, STIM1-B is specifically expressed in neurons and is involved in synaptic plasticity {Ramesh et al., 2021, Cell Rep}. ECC is essential in skeletal muscle cells and this mechanism require fast calcium elevation to trigger muscle contraction. STIM1-S normally takes seconds to get recruited to ER-PM junctions whereas STIM1-L is constitutively concentrated in the cER {Sauc et al., 2015, J Cell Science}. This is an important advantage for a rapid activation of SOCE machinery upon stimulation. Interestingly, STIM1-L-populated cER is smaller than STIM1-S one and but exhibits stronger SOCE. This observation comforts my hypothesis that long cER yield smaller calcium influx and that ER-PM ultrastructure can regulate SOCE. However, it was showed that STIM1-L does not interact with ORAI and TRPC in the same way as STIM1-S and could in part explain the stronger influx {Dyrda et al., 2020, Cell Calcium}. Furthermore, STIM1-B generates smaller ER-PM contacts and also display smaller SOCE compared to STIM1-S. This would suggest that cER length is not critical to modulate calcium entry and that other parameters are more important. If we look into the protein length, no EM study investigated the ER-PM gap distance when one or another isoform is expressed. By looking the length of each isoform, I would correlate it with the ER-PM intermembrane distance. STIM1-L exhibits higher calcium entry and longer sequence where STIM1-B displays lower calcium influx for a smaller length. The correlation between protein length and calcium entry rate seems appealing. Conceptually, changing ER-PM distance would modify the calcium concentration within the ER-PM cleft. Increasing the intermembrane distance would result in a more diffuse calcium concentration in this volume where reducing it would have opposite effect. In turn, changing the local calcium concentration would result in modification of ORAI1 CDI and directly affect calcium entry. Some study questioned the role of ER-PM distance in calcium regulation, for example Petkovich and colleagues suggest that ER-PM distance modification affect regulation of ER and cytosolic calcium levels. They generated a longer form of Sec22b, a SNARE protein enriched in ER-PM contact sites {Petkovic et al. 2014, Nat Cell Biol}. This longer isoform increased ER-PM gap distance by ~6 nm and decreased ER calcium level at rest. This was associated with higher cytosolic calcium level, expected when ER calcium is lower. However, CPA-induced calcium entry was not impacted by ER-PM distance change. Suggesting that regulation of ER-PM distance is not a crucial mechanism to modulate SOCE and that the differential calcium entry from one STIM isoform to another is mediated by other means. Different channel gating affinities as shown for STIM1-L which preferentially binds to TRPC over ORAI are one way to explain the higher calcium entry of STIM1-L isoform.

2) Programming as a tool for data analysis in biology

For people who never learned how to do programming, it is often seen as a black box in which magic is happening. But the truth is, since the development of internet and the availability of online libraries, learning programming as never been easier. Today it is possible to be self-taught

programmer and even if it is not done in a month, it is doable. It is actually how I learned coding, by scrapping off internet for answers to my questions in the search of improving my data analysis. But now, why most scientists should be encouraged to learn basic programming skills ? In our current biology era, data volumes are continuously increasing, to the point that no human can manually handle some type of data due to their absurd dimension. My favorite example is that one human genome sequencing can generate over 100 billion bases of sequence data {Pelak et al., 2010, PLOS Genetics}. This crazy amount of data, of course apply more to some field than other but with time, an increasing number of scientists are going to face the challenges of handling large datasets. Smaller data set also create challenges; repetitive tasks such as copy paste or extracting information from a region of interest are time consuming and sometimes prone to error. Luckily, they are relatively simple to automatize, and it is now more and more common for scientists to create small scripts for example in ImageJ to perform some routine tasks. Imagine this kind of process as the equivalent of when people discovered the copy/paste function in their computer: no need to manually enter a value to duplicate.

Because I faced similar trouble with my data, I came to realize that programming could really improve my daily analysis. To this end, I started to learn how to automatically perform routine tasks such as separation of channels from one file to individual ones. And with time I successfully created a full analysis pipeline for calcium imaging. This pipeline performs routine tasks such as copy and paste but also more advanced ones like fitting a linear regression on a nonlinear trace. I encountered a lot of challenges during the design and implementation of this pipeline, from people not trusting a script doing things alone to harmonizing each part to work together. As I said earlier, programming is a black box, sometimes scary and it is not easy to trust it, sometimes for good reason. Scripts need to be extensively tested before release to make sure it does what it is intended to. Generating artefacts and drawing false conclusions are risks we do not want to take. And this is why releasing a pipeline spanning the full experiment process is taking time. I had to make sure every part was working properly and capable to handle errors.

As discussed, the pipeline strongly reduces the needed time for each experiment analysis with over 200h saved on my side. To save time with this script, it costed me time to develop the scripts and it span over months as it was a side project. I cannot say how much time I invested in the creation of the full pipeline, but I can say it is more than 200h. The question is now, was it worth it ? With more than a year of existence, this script saved me a lot of time but also to my colleagues. We are four people to use it systematically and when I will leave the lab, people will still be able to use it as it is well stored on GitHub with a full documentation. Plus, I used the opportunity to learn programming while creating these scripts and applied this knowledge to other data analysis situations.

Looking back to the strategies used for this pipeline, I can see some points I would improve. For example, the acquisition script for Visiview can be simplified. Currently, I set the acquisition to a giving time frame and wait for the desired number of timepoints to be imaged before starting a new recording. This approach involves the duplication of a big section which requires to set up each parameter again (exposure, channels, …). I discovered later the existence of a specific coding tool which detects in real time which timepoint is currently being imaged. Using this approach, I could change only the frame rate when the timepoint reaches the one I want. This would reduce by more than half the length of the code for this script. However, it would not change execution speed but improve code readability and stability.

A criticized I often received from the users is that they need multiple scripts in different programming environments. To use the full pipeline, users have to use Visiview, ImageJ, Excel and Matlab which in the end, is a lot of different interfaces and require some training. It would be possible to combine all the scripts in a unique file, but it would be long to create, hard to read and to maintain. I would have considered to create a single script if I was doing a PhD focusing on computer science.

Another advantage of programming nowadays is the source code accessibility online. On one hand it ensures that everyone has access to the tools and can use it for their own needs. On the other side, it allows people to interact with the creator and ask technical questions or participate collaboratively to improve the scripts.

Overall, programming is a tool I learned and used to facilitate the daily work of scientists. But learning how to code also helped me a lot with problem solving and dedication. It may feel overwhelming when you do not know anything about a topic and struggle to understand its basic concepts. Because of that, programming taught me go from the beginning, step by step and to think before rushing.

To conclude, during this thesis I investigated how structure-function relate when it comes to ER-PM junctions and calcium signaling. I found that cER length is important for the regulation of SOCE but there are still grey zones on how it does so. I exposed some ideas and discussed important aspects of ER-PM ultrastructure and how they relate to SOCE in the current view of the literature. In a second part, I learned how to create new analytical tools and helped the scientific community with new analysis pipeline.

IX) References

Abdullaev, I. F., Bisaillon, J. M., Potier, M., Gonzalez, J. C., Motiani, R. K. and Trebak, M. (2008). Stim1 and orai1 mediate crac currents and store-operated calcium entry important for endothelial cell proliferation. *Circ. Res.* 103, 1289–1299.

AGRANOFF, B. W., BRADLEY, R. M. and BRADY, R. O. (1958). The enzymatic synthesis of inositol phosphatide. *J. Biol. Chem.* 233, 1077–1083.

Antigny, F., Sabourin, J., Saüc, S., Bernheim, L., Koenig, S. and Frieden, M. (2017). TRPC1 and TRPC4 channels functionally interact with STIM1L to promote myogenesis and maintain fast repetitive Ca2 + release in human myotubes. *Biochim. Biophys. Acta - Mol. Cell Res.* 1864, 806–813.

Arnaudeau, S., Kelley, W. L., Walsh, J. V. and Demaurex, N. (2001). Mitochondria Recycle Ca2+ to the Endoplasmic Reticulum and Prevent the Depletion of Neighboring Endoplasmic Reticulum Regions. *J. Biol. Chem.* 276, 29430–29439.

Berna-Erro, A., Braun, A., Kraft, R., Kleinschnitz, C., Schuhmann, M. K., Stegner, D., Wultsch, T., Eilers, J., Meuth, S. G., Stoll, G., et al. (2009). STIM2 regulates capacitive Ca2+ entry in neurons and plays a key role in hypoxic neuronal cell death. *Sci. Signal.* 2, 1–11.

Bernhard, W. and Rouiller, C. (1956). Close topographical relationship between mitochondrai and ergastoplasm of liver cells in a definite phase of cellular activity. 2, 73–77.

Berridge, M. J. (2009). Pl-2: Inositol Trisphosphate and Calcium Signalling. *Eur. J. Endocrinol.* 130, SS4.

Besprozvannaya, M., Dickson, E., Li, H., Ginburg, K. S., Bers, D. M., Auwerx, J. and Nunnari, J. (2018). GRAM domain proteins specialize functionally distinct ER-PM contact sites in human cells. *Elife* 7, 1–25.

Bezprozvanny, I. B., Ondrias, K., Kaftan, E., Stoyanovsky, D. A. and Ehrlich, B. E. (1993). Activation of the calcium release channel (ryanodine receptor) by heparin and other polyanions is calcium dependent. *Mol. Biol. Cell* 4, 347–352.

Bhardwaj, R., Augustynek, B. S., Ercan-Herbst, E., Kandasamy, P., Seedorf, M., Peinelt, C. and Hediger, M. A. (2020). Ca2+/calmodulin binding to STIM1 hydrophobic residues facilitates slow Ca2+-dependent inactivation of the ORAI1 channel. *Cell. Physiol. Biochem.* 54, 252–270.

Boczek, T., Sobolczyk, M., Mackiewicz, J., Lisek, M., Ferenc, B., Guo, F. and Zylinska, L. (2021). Crosstalk among calcium atpases: Pmca, serca and spca in mental diseases. *Int. J. Mol. Sci.* 22, 1–23.

Bogeski, I., Kummerow, C., Al-Ansary, D., Schwarz, E. C., Koehler, R., Kozai, D., Takahashi, N., Peinelt, C., Griesemer, D., Bozem, M., et al. (2010). Differential redox regulation of ORAI ion channels: A mechanism to tune cellular Calcium signaling. *Sci. Signal.* 3, 1–10.

Brandman, O., Liou, J., Park, W. S. and Meyer, T. (2007). STIM2 Is a Feedback Regulator that Stabilizes Basal Cytosolic and Endoplasmic Reticulum Ca2+ Levels. *Cell* 131, 1327–1339.

Bulla, M., Gyimesi, G., Kim, J. H., Bhardwaj, R., Hediger, M. A., Frieden, M. and Demaurex, N. (2019). ORAI1 channel gating and selectivity is differentially altered by natural mutations in the first or third transmembrane domain. *J. Physiol.* 597, 561–582.

Burgoyne, R. D. and Clague, M. J. (2003). Calcium and calmodulin in membrane fusion. *Biochim. Biophys. Acta - Mol. Cell Res.* 1641, 137–143.

Cai, X., Nwokonko, R. M., Loktionova, N. A., Abdulqadir, R., Baraniak, J. H., Wang, Y., Trebak, M., Zhou, Y. and Gill, D. L. (2018). Pore properties of Orai1 calcium channel dimers and their activation by the STIM1 ER calcium sensor. *J. Biol. Chem.* 293, 12962–12974.

Cai, X., Zhou, Y., Nwokonko, R. M., Loktionova, N. A., Wang, X., Xin, P., Trebak, M., Wang, Y. and Gill, D. L. (2016). The Orai1 store-operated calcium channel functions as a hexamer. *J. Biol. Chem.* 291, 25764–25775.

Camello, C., Lomax, R., Petersen, O. H. and Tepikin, A. V. (2002). Calcium leak from intracellular store - The enigma of calcium signalling. *Cell Calcium* 32, 355–361.

Carafoli, E. (1991). Calcium pump of the plasma membrane. *Physiol. Rev.* 71, 129–153.

Carreras-Sureda, A., Pihán, P. and Hetz, C. (2017). The unfolded protein response: At the intersection between endoplasmic reticulum function and mitochondrial bioenergetics. *Front. Oncol.* 7, 1–7.

Chang, C. L., Chen, Y. J., Quintanilla, C. G., Hsieh, T. S. and Liou, J. (2018). EB1 binding restricts STIM1 translocation to ER-PM junctions and regulates store-operated Ca2+ entry. *J. Cell Biol.* 217, 2047–2058.

Chang, C. L., Hsieh, T. S., Yang, T. T., Rothberg, K. G., Azizoglu, D. B., Volk, E., Liao, J. C. and Liou, J. (2013). Feedback regulation of receptor-induced ca2+ signaling mediated by e-syt1 and nir2 at endoplasmic reticulum-plasma membrane junctions. *Cell Rep.* 5, 813–825.

Chang, C. L., Hsieh, T. S., Yang, T. T., Rothberg, K. G., Azizoglu, D. B., Volk, E., Liao, J. C. and Liou, J. (2013). Feedback regulation of receptor-induced ca2+ signaling mediated by e-syt1 and nir2 at endoplasmic reticulum-plasma membrane junctions. *Cell Rep.* 5, 813–825.

Chang, C. L. and Liou, J. (2015). Phosphatidylinositol 4, 5-bisphosphate homeostasis regulated by Nir2 and Nir3 proteins at endoplasmic reticulum-plasma membrane junctions. *J. Biol. Chem.* 290, 14289–14301.

Chang, C. L. and Liou, J. (2016). Homeostatic regulation of the PI(4,5)P2-Ca2+ signaling system at ER-PM junctions. *Biochim. Biophys. Acta - Mol. Cell Biol. Lipids* 1861, 862–873.

Chang, C. L. and Liou, J. (2015). Phosphatidylinositol 4, 5-bisphosphate homeostasis regulated by Nir2 and Nir3 proteins at endoplasmic reticulum-plasma membrane junctions. *J. Biol. Chem.* 290, 14289–14301.

Choi, D. W. (1988). Glutamate neurotoxicity and diseases of the nervous system. *Neuron* 1, 623–634.

Cockcroft, S. and Garner, K. (2013). Potential role for phosphatidylinositol transfer protein (PITP) family in lipid transfer during phospholipase C signalling. *Adv. Biol. Regul.* 53, 280–291.

COPELAND, D. E. and DALTON, A. J. (1959). An association between mitochondria and the endoplasmic reticulum in cells of the pseudobranch gland of a teleost. *J. Biophys. Biochem. Cytol.* 5, 393–396.

Covington, E. D., Wu, M. M. and Lewis, R. S. (2010). Essential role for the CRAC activation domain in store-dependent oligomerization of STIM1. *Mol. Biol. Cell* 21, 1897–1907.

Csordás, G., Renken, C., Várnai, P., Walter, L., Weaver, D., Buttle, K. F., Balla, T., Mannella, C. A. and Hajnóczky, G. (2006). Structural and functional features and significance of the physical linkage between ER and mitochondria. *J. Cell Biol.* 174, 915–921.

Cunningham, K. W. and Fink, G. R. (1994). Calcineurin-dependent growth control in Saccharomyces cerevisiae mutants lacking PMC1, a homolog of plasma membrane Ca2+ ATPases. *J. Cell Biol.* 124, 351–363.

Darbellay, B., Arnaudeau, S., Bader, C. R., Konig, S. and Bernheim, L. (2011). STIM1L is a new actin-binding splice variant involved in fast repetitive Ca 2+ release. *J. Cell Biol.* 194, 335–346.

Darbellay, B., Arnaudeau, S., Bader, C. R., Konig, S. and Bernheim, L. (2011). STIM1L is a new actin-binding splice variant involved in fast repetitive Ca 2+ release. *J. Cell Biol.* 194, 335–346.

Darbellay, B., Arnaudeau, S., Bader, C. R., Konig, S. and Bernheim, L. (2011). STIM1L is a new actin-binding splice variant involved in fast repetitive Ca 2+ release. *J. Cell Biol.* 194, 335–346.

De Brito, O. M. and Scorrano, L. (2008). Mitofusin 2 tethers endoplasmic reticulum to mitochondria. *Nature* 456, 605–610.

De vos, K. J., Mórotz, G. M., Stoica, R., Tudor, E. L., Lau, K. F., Ackerley, S., Warley, A., Shaw, C. E. and Miller, C. C. J. (2012). VAPB interacts with the mitochondrial protein PTPIP51 to regulate calcium homeostasis. *Hum. Mol. Genet.* 21, 1299–1311.

Doghman-Bouguerra, M., Granatiero, V., Sbiera, S., Sbiera, I., Lacas-Gervais, S., Brau, F., Fassnacht, M., Rizzuto, R. and Lalli, E. (2016). FATE 1 antagonizes calcium- and drug-induced apoptosis by uncoupling ER and mitochondria . *EMBO Rep.* 17, 1264–1280.

Dyrda, A., Koenig, S. and Frieden, M. (2020). STIM1 long and STIM1 gate differently TRPC1 during store-operated calcium entry. *Cell Calcium* 86, 102134.

Eisenberg-Bord, M., Shai, N., Schuldiner, M. and Bohnert, M. (2016). A Tether Is a Tether Is a Tether: Tethering at Membrane Contact Sites. *Dev. Cell* 39, 395–409.

El-Dairi, M. and House, R. J. (2019). Optic nerve hypoplasia. *Handb. Pediatr. Retin. OCT Eye-Brain Connect.* 285–287.

Ercan, E., Momburg, F., Engel, U., Temmerman, K., Nickel, W. and Seedorf, M. (2009). A conserved, lipid-mediated sorting mechanism of yeast Ist2 and mammalian STIM proteins to the peripheral ER. *Traffic* 10, 1802–1818.

Ercan, E., Momburg, F., Engel, U., Temmerman, K., Nickel, W. and Seedorf, M. (2009). A conserved, lipid-mediated sorting mechanism of yeast Ist2 and mammalian STIM proteins to the peripheral ER. *Traffic* 10, 1802–1818.

Fernández-Busnadiego, R., Saheki, Y. and De Camilli, P. (2015). Three-dimensional architecture of extended synaptotagmin-mediated endoplasmic reticulum–plasma membrane contact sites. *Proc. Natl. Acad. Sci.* 112, E2004–E2013.

Feske, S., Gwack, Y., Prakriya, M., Srikanth, S., Puppel, S. H., Tanasa, B., Hogan, P. G., Lewis, R. S., Daly, M. and Rao, A. (2006). A mutation in Orai1 causes immune deficiency by abrogating CRAC channel function. *Nature* 441, 179–185.

Feske, S., Picard, C. and Fischer, A. (2010). Immunodeficiency due to mutations in ORAI1 and STIM1. *Clin. Immunol.* 135, 169–182.

Fierro, L. and Parekh, A. B. (1999). Fast calcium-dependent inactivation of calcium release-activated calcium current (CRAC) in RBL-1 cells. *J. Membr. Biol.* 168, 9–17.

Friedman, J. R., Lackner, L. L., West, M., DiBenedetto, J. R., Nunnari, J. and Voeltz, G. K. (2011). ER tubules mark sites of mitochondrial division. *Science (80-.).* 334, 358–362.

Fukushima, M., Tomita, T., Janoshazi, A. and Putney, J. W. (2012). Alternative translation initiation gives rise to two isoforms of Orai1 with distinct plasma membrane mobilities. *J. Cell Sci.* 125, 4354–4361.

Gammons, J., Trebak, M. and Mancarella, S. (2021). Cardiac-specific deletion of orai3 leads to severe dilated cardiomyopathy and heart failure in mice. *J. Am. Heart Assoc.* 10,.

Gardiner, D. M. and Grey ., D. (1983). Membrane junctions in Xenopus eggs: Their distribution suggests a role in calcium regulation. *J. Cell Biol.* 96, 1159–1163.

Gees, M., Colsoul, B. and Nilius, B. (2010). The role of transient receptor potential cation channels in Ca2+ signaling. *Cold Spring Harb. Perspect. Biol.* 2,.

George Thompson, A. M., Ursu, O., Babkin, P., Iancu, C. V., Whang, A., Oprea, T. I. and Choe, J. Y. (2016). Discovery of a specific inhibitor of human GLUT5 by virtual screening and in vitro transport evaluation. *Sci. Rep.* 6, 1–9.

Gibhardt, C. S., Cappello, S., Bhardwaj, R., Schober, R., Kirsch, S. A., Bonilla del Rio, Z., Gahbauer, S., Bochicchio, A., Sumanska, M., Ickes, C., et al. (2020). Oxidative Stress-Induced STIM2 Cysteine Modifications Suppress Store-Operated Calcium Entry. *Cell Rep.* 33,.

Giordano, F., Saheki, Y., Idevall-Hagren, O., Colombo, S. F., Pirruccello, M., Milosevic, I., Gracheva, E. O., Bagriantsev, S. N., Borgese, N. and De Camilli, P. (2013). XPI(4,5)P2-Dependent and Ca2+-Regulated ER-PM interactions mediated by the extended synaptotagmins. *Cell* 153, 1494–1509.

Giordano, F., Saheki, Y., Idevall-Hagren, O., Colombo, S. F., Pirruccello, M., Milosevic, I., Gracheva, E. O., Bagriantsev, S. N., Borgese, N. and De Camilli, P. (2013). PI(4,5)P2-Dependent and Ca2+-Regulated ER-PM interactions mediated by the extended synaptotagmins. *Cell* 153, 1494.

Glitsch, M. D., Bakowski, D. and Parekh, A. B. (2002). Store-operated Ca 2 + entry depends on mitochondrial Ca 2 + uptake. 21,.

Gudlur, A., Zeraik, A. E., Hirve, N. and Hogan, P. G. (2020). STIM calcium sensing and conformational change. *J. Physiol.* 598, 1695–1705.

Guido, D., Demaurex, N. and Nunes, P. (2015). Junctate boosts phagocytosis by recruiting endoplasmic reticulum Ca2+ stores near phagosomes. *J. Cell Sci.* 128, 4074–4082.

Gunter, K. K. and Gunter, T. E. (1994). Transport of calcium by mitochondria. *J. Bioenerg. Biomembr.* 26, 471–485.

Hajnóczky, G., Csordás, G., Das, S., Garcia-Perez, C., Saotome, M., Sinha Roy, S. and Yi, M. (2006). Mitochondrial calcium signalling and cell death: Approaches for assessing the role of mitochondrial Ca2+ uptake in apoptosis. *Cell Calcium* 40, 553–560.

Hawkins, B. J., Irrinki, K. M., Mallilankaraman, K., Lien, Y. C., Wang, Y., Bhanumathy, C. D., Subbiah, R., Ritchie, M. F., Soboloff, J., Baba, Y., et al. (2010). S-glutathionylation activates STIM1 and alters mitochondrial homeostasis. *J. Cell Biol.* 190, 391–405.

Hirve, N., Rajanikanth, V., Hogan, P. G. and Gudlur, A. (2018). Coiled-Coil Formation Conveys a STIM1 Signal from ER Lumen to Cytoplasm. *Cell Rep.* 22, 72–83.

Honnappa, S., Gouveia, S. M., Weisbrich, A., Damberger, F. F., Bhavesh, N. S., Jawhari, H., Grigoriev, I., van Rijssel, F. J. A., Buey, R. M., Lawera, A., et al. (2009). An EB1-Binding Motif Acts as a Microtubule Tip Localization Signal. *Cell* 138, 366–376.

Hou, X., Pedi, L., Diver, M. and Long, S. (2012). Crystal structure of the calcium release-activated calcium channel Orai. *Science (80-.).* 23, 1–7.

Hwei, L. O., Liu, X., Tsaneva-Atanasova, K., Singh, B. B., Bandyopadhyay, B. C., Swaim, W. D., Russell, J. T., Hegde, R. S., Sherman, A. and Ambudkar, I. S. (2007). Relocalization of STIM1 for activation of store-operated Ca2+ entry is determined by the depletion of subplasma membrane endoplasmic reticulum Ca2+ store. *J. Biol. Chem.* 282, 12176–12185.

Idevall-Hagren, O., Lü, A., Xie, B. and De Camilli, P. (2015). Triggered Ca 2+ influx is required for extended synaptotagmin 1-induced ER -plasma membrane tethering . *EMBO J.* 34, 2291–2305.

Jardín, I., Albarran, L., Salido, G. M., López, J. J., Sage, S. O. and Rosado, J. A. (2018). Fine-tuning of store-operated calcium entry by fast and slow Ca2+-dependent inactivation: Involvement of SARAF. *Biochim. Biophys. Acta - Mol. Cell Res.* 1865, 463–469.

Jardin, I., Lopez, J. J., Salido, G. M. and Rosado, J. A. (2008). Orai1 mediates the interaction between STIM1 and hTRPC1 and regulates the mode of activation of hTRPC1-forming Ca2+ channels. *J. Biol. Chem.* 283, 25296–25304.

Jouaville, L. S., Pinton, P., Bastianutto, C., Rutter, G. A. and Rizzuto, R. (1999). Regulation of mitochondrial ATP synthesis by calcium: Evidence for a long-term metabolic priming. *Proc. Natl. Acad. Sci. U. S. A.* 96, 13807–13812.

Kang, F., Zhou, M., Huang, X., Fan, J., Wei, L., Boulanger, J., Liu, Z., Salamero, J., Liu, Y. and Chen, L. (2019). E-syt1 Re-arranges STIM1 Clusters to Stabilize Ring-shaped ER-PM Contact Sites and Accelerate Ca 2+ Store Replenishment. *Sci. Rep.* 9, 1–11.

Kawasaki, T., Lange, I. and Feske, S. (2009). A minimal regulatory domain in the C terminus of STIM1 binds to and activates ORAI1 CRAC channels. *Biochem. Biophys. Res. Commun.* 385, 49–54.

Khan, T., Patel, R. and Siddiqui, A. (2021). Furosemide. *StatPearls*.

Kim, S., Kedan, A., Marom, M., Gavert, N., Keinan, O., Selitrennik, M., Laufman, O. and Lev, S. (2013). The phosphatidylinositol-transfer protein Nir2 binds phosphatidic acid and positively regulates phosphoinositide signalling. *EMBO Rep.* 14, 891–899.

Kim, Y. J., Guzman-Hernandez, M. L. and Balla, T. (2011). A highly dynamic ER-derived phosphatidylinositol-synthesizing organelle supplies phosphoinositides to cellular membranes. *Dev. Cell* 21, 813–824.

Kim, Y. J., Guzman-Hernandez, M. L., Wisniewski, E. and Balla, T. (2015). Phosphatidylinositol-Phosphatidic Acid Exchange by Nir2 at ER-PM Contact Sites Maintains Phosphoinositide Signaling Competence. *Dev. Cell* 33, 549–561.

Knapp, M. L., Förderer, K., Alansary, D., Jung, M., Schwarz, Y., Lis, A. and Niemeyer, B. A. (2020). Alternative splicing switches STIM1 targeting to specialized membrane contact sites and modifies SOCE. *bioRxiv* 1–20.

Korzeniowski, M. K., Martín Manjarrés, I., Varnai, P. and Balla, T. (2012). Activation of stim1-orai1 involves an intramolecular switching mechanism. *Sci. Signal.* 3, 1–20.

Korzeniowski, M. K., Popovic, M. A., Szentpetery, Z., Varnai, P., Stojilkovic, S. S. and Balla, T. (2009). Dependence of STIM1/Orai1-mediated calcium entry on plasma membrane phosphoinositides. *J. Biol. Chem.* 284, 21027–21035.

Kyu, P. L., Yuan, J. P., Zeng, W., So, I., Worley, P. F. and Muallem, S. (2009). Molecular determinants of fast Ca2+-dependent inactivation and gating of the Orai channels. *Proc. Natl. Acad. Sci. U. S. A.* 106, 14687–14692.

Lee, B., Palermo, G. and Machaca, K. (2013). Downregulation of store-operated Ca2+ entry during mammalian meiosis is required for the egg-to-embryo transition. *J. Cell Sci.* 126, 1672–1681.

Lemos, F. O., Bultynck, G. and Parys, J. B. (2021). A comprehensive overview of the complex world of the endo- and sarcoplasmic reticulum Ca2+-leak channels. *Biochim. Biophys. Acta - Mol. Cell Res.* 1868, 119020.

Li, C., Qian, T., He, R., Wan, C., Liu, Y. and Yu, H. (2021). Endoplasmic Reticulum–Plasma Membrane Contact Sites: Regulators, Mechanisms, and Physiological Functions. *Front. Cell Dev. Biol.* 9,.

Li, X., Wu, G., Yang, Y., Fu, S., Liu, X., Kang, H., Yang, X., Su, X. C. and Shen, Y. (2017). Calmodulin dissociates the STIM1-Orai1 complex and STIM1 oligomers. *Nat. Commun.* 8,.

Liou, J., Fivaz, M., Inoue, T. and Meyer, T. (2007). Live-cell imaging reveals sequential oligomerization and local plasma membrane targeting of stromal interaction molecule 1 after Ca2+ store depletion. *Proc. Natl. Acad. Sci.* 104, 9301–9306.

Liou, J., Fivaz, M., Inoue, T. and Meyer, T. (2007). Live-cell imaging reveals sequential oligomerization and local plasma membrane targeting of stromal interaction molecule 1 after Ca2+ store depletion. *Proc. Natl. Acad. Sci. U. S. A.* 104, 9301–9306.

Liou, J., Kim, M. L., Won, D. H., Jones, J. T., Myers, J. W., Ferrell, J. E. and Meyer, T. (2005). STIM is a Ca2+ sensor essential for Ca2+-store- depletion-triggered Ca2+ influx. *Curr. Biol.* 15, 1235–1241.

Lis, A., Peinelt, C., Beck, A., Parvez, S., Monteilh-Zoller, M., Fleig, A. and Penner, R. (2007). CRACM1, CRACM2, and CRACM3 Are Store-Operated Ca2+ Channels with Distinct Functional Properties. *Curr. Biol.* 17, 794–800.

Lopez, J. J., Jardin, I., Sanchez-Collado, J., Salido, G. M., Smani, T. and Rosado, J. A. (2020). TRPC Channels in the SOCE Scenario. *Cells* 9, 1–13.

Luik, R. M., Wang, B., Prakriya, M., Wu, M. M. and Lewis, R. S. (2008). Oligomerization of STIM1 couples ER calcium depletion to CRAC channel activation. *Nature* 454, 538–542.

MacLennan, D. H. (1970). Purification and properties of an adenosine triphosphatase from sarcoplasmic reticulum. *J. Biol. Chem.* 245, 4508–4518.

Malli, R., Frieden, M., Hunkova, M., Trenker, M. and Graier, W. F. (2007). Ca2+ refilling of the endoplasmic reticulum is largely preserved albeit reduced Ca2+ entry in endothelial cells. *Cell Calcium* 41, 63–76.

Melzer, W., Herrmann-Frank, A. and Liittgau, Hc. (1995). The role of Ca 2+ ions in excitation-contraction coupling of skeletal muscle fibres. *Biochim. Biophys. Acta* 1241, 59–116.

Miederer, A. M., Alansary, D., Schwär, G., Lee, P. H., Jung, M., Helms, V. and Niemeyer, B. A. (2015). A STIM2 splice variant negatively regulates store-operated calcium entry. *Nat. Commun.* 6,.

Mogami, H., Lloyd Mills, C. and Gallacher, D. V. (1997). Phospholipase C inhibitor, U73122, releases intracellular Ca2+, potentiates Ins(1,4,5)P3-mediated Ca2+ release and directly activates ion channels in mouse pancreatic acinar cells. *Biochem. J.* 324, 645–651.

Moreau, M. (1980). Free Calcium Changes Associated with Hormone Oocytes Action in Amphibian Xenopus laevis , Pleurodeles waltlii , and Preparation of the photoproteins . Microinjection. 214,.

Muik, M., Fahrner, M., Derler, I., Schindl, R., Bergsmann, J., Frischauf, I., Groschner, K. and Romanin, C. (2009). A cytosolic homomerization and a modulatory domain within STIM1 C terminus determine coupling to ORAI1 channels. *J. Biol. Chem.* 284, 8421–8426.

Muik, M., Fahrner, M., Derler, I., Schindl, R., Bergsmann, J., Frischauf, I., Groschner, K. and Romanin, C. (2009). A cytosolic homomerization and a modulatory domain within STIM1 C terminus determine coupling to ORAI1 channels. *J. Biol. Chem.* 284, 8421–8426.

Ng, A. Y. E., Ng, A. Q. E. and Zhang, D. (2018). ER-PM Contacts Restrict Exocytic Sites for Polarized Morphogenesis. *Curr. Biol.* 28, 146-153.e6.

NGAI, C.-Y., KO, W.-H., HE, G.-W., GARLAND, C. and DORA, K. (2006). Depletion of intracellular Ca. *Br. J. Pharmacol.* 147, 506–515.

Orci, L., Ravazzola, M., Le Coadic, M., Shen, W. W., Demaurex, N. and Cosson, P. (2009). STIM1-induced precortical and cortical subdomains of the endoplasmic reticulum. *Proc. Natl. Acad. Sci. U. S. A.* 106, 19358–19362.

Palty, R., Fu, Z. and Isacoff, E. Y. (2017). Sequential Steps of CRAC Channel Activation. *Cell Rep.* 19, 1929–1939.

Parekh, A. B. (1998). Slow feedback inhibition of calcium release-activated calcium current by calcium entry. *J. Biol. Chem.* 273, 14925–14932.

Parekh, A. B. and Putney, J. W. (2005). Store-operated calcium channels. *Physiol. Rev.* 85, 757–810.

Park, C. Y., Hoover, P. J., Mullins, F. M., Bachhawat, P., Covington, E. D., Raunser, S., Walz, T., Garcia, K. C., Dolmetsch, R. E. and Lewis, R. S. (2009). STIM1 Clusters and Activates CRAC Channels via Direct Binding of a Cytosolic Domain to Orai1. *Cell* 136, 876–890.

Payne, R. B. and Walker, B. E. (1979). Serum-Calcium. *Lancet* 313, 1248.

Pelak, K., Shianna, K. V., Ge, D., Maia, J. M., Zhu, M., Smith, J. P., Cirulli, E. T., Fellay, J., Dickson, S. P., Gumbs, C. E., et al. (2010). The characterization of twenty sequenced human genomes. *PLoS Genet.* 6,.

Peng, T. I. and Greenamyre, J. T. (1998). Privileged access to mitochondria of calcium influx through N-methyl-D- aspartate receptors. *Mol. Pharmacol.* 53, 974–980.

Periasamy, M. and Kalyanasundaram, A. (2007). SERCA pump isoforms: Their role in calcium transport and disease. *Muscle and Nerve* 35, 430–442.

Petkovic, M., Jemaiel, A., Daste, F., Specht, C. G., Izeddin, I., Vorkel, D., Verbavatz, J. M., Darzacq, X., Triller, A., Pfenninger, K. H., et al. (2014). The SNARE Sec22b has a non-fusogenic function in plasma membrane expansion. *Nat. Cell Biol.* 16, 434–444.

Petkovic, M., Jemaiel, A., Daste, F., Specht, C. G., Izeddin, I., Vorkel, D., Verbavatz, J. M., Darzacq, X., Triller, A., Pfenninger, K. H., et al. (2014). The SNARE Sec22b has a non-fusogenic function in plasma membrane expansion. *Nat. Cell Biol.* 16, 434–444.

Poteser, M., Leitinger, G., Pritz, E., Platzer, D., Frischauf, I., Romanin, C. and Groschner, K. (2016). Live-cell imaging of ER-PM contact architecture by a novel TIRFM approach reveals extension of junctions in response to store-operated Ca2+-entry. *Sci. Rep.* 6, 1–13.

Poteser, M., Leitinger, G., Pritz, E., Platzer, D., Frischauf, I., Romanin, C. and Groschner, K. (2016). Live-cell imaging of ER-PM contact architecture by a novel TIRFM approach reveals extension of junctions in response to store-operated Ca2+-entry. *Sci. Rep.* 6, 35656.

Pozo-Guisado, E., Casas-Rua, V., Tomas-Martin, P., Lopez-Guerrero, A. M., Martin-Romero, F. J. and Alvarez-Barrientos, A. (2013). Phosphorylation of stim1 at erk1/2 target sites regulates interaction with the microtubule plus-end binding protein eb1. *J. Cell Sci.* 126, 3170–3180.

Prakriya, M. and Lewis, R. S. (2015). Store-operated calcium channels. *Physiol. Rev.* 95, 1383–1436.

Prakriya, M. and Lewis, R. S. (2015). Store-Operated Calcium Channels. *Physiol. Rev.* 95, 1383–1436.

Prasad, V., Okunade, G. W., Miller, M. L. and Shull, G. E. (2004). Phenotypes of SERCA and PMCA knockout mice. *Biochem. Biophys. Res. Commun.* 322, 1192–1203.

Putney, J. W. (1986). A model for receptor-regulated calcium entry. *Cell Calcium* 7, 1–12.

Ramesh, G., Jarzembowski, L., Schwarz, Y., Poth, V., Konrad, M., Knapp, M. L., Schwär, G., Lauer, A. A., Grimm, M. O. W., Alansary, D., et al. (2021). A short isoform of STIM1 confers frequency-dependent synaptic enhancement. *Cell Rep.* 34,.

Rinne, A. and Blatter, L. A. (2010). Activation of NFATc1 is directly mediated by IP 3 in adult cardiac myocytes. *Am. J. Physiol. - Hear. Circ. Physiol.* 299, 1701–1707.

Rizzuto, R., Brini, M., Murgia, M. and Pozzan, T. (2016). Microdomains with High Ca2+ Close to IP 3 - Sensitive Channels That Are Sensed by Neighboring Mitochondria. 262, 744–747.

Rizzuto, R., Pinton, P., Carrington, W., Fay, F. S., Fogarty, K. E., Lifshitz, L. M., Tuft, R. A. and Pozzan, T. (1998). Close contacts with the endoplasmic reticulum as determinants of mitochondrial Ca2+ responses. *Science (80-.).* 280, 1763–1766.

Roos, J., DiGregorio, P. J., Yeromin, A. V., Ohlsen, K., Lioudyno, M., Zhang, S., Safrina, O., Kozak, J. A., Wagner, S. L., Cahalan, M. D., et al. (2005). STIM1, an essential and conserved component of store-operated Ca 2+ channel function. *J. Cell Biol.* 169, 435–445.

Santulli, G., Nakashima, R., Yuan, Q. and Marks, A. R. (2017). Intracellular calcium release channels: an update. *J. Physiol.* 595, 3041–3051.

Saüc, S., Bulla, M., Nunes, P., Orci, L., Marchetti, A., Antigny, F., Bernheim, L., Cosson, P., Frieden, M. and Demaurex, N. (2015). STIM1L traps and gates Orai1 channels without remodeling the cortical ER. *J. Cell Sci.* 128, 1568–1579.

Schauder, C. M., Wu, X., Saheki, Y., Narayanaswamy, P., Torta, F., Wenk, M. R., De Camilli, P. and Reinisch, K. M. (2014). Structure of a lipid-bound extended synaptotagmin indicates a role in lipid transfer. *Nature* 510, 552–555.

Schober, R., Waldherr, L., Schmidt, T., Graziani, A., Stilianu, C., Legat, L., Groschner, K. and Schindl, R. (2019). STIM1 and Orai1 regulate Ca 2+ microdomains for activation of transcription. *Biochim. Biophys. Acta - Mol. Cell Res.* 1866, 1079–1091.

Scorrano, L., De Matteis, M. A., Emr, S., Giordano, F., Hajnóczky, G., Kornmann, B., Lackner, L. L., Levine, T. P., Pellegrini, L., Reinisch, K., et al. (2019). Coming together to define membrane contact sites. *Nat. Commun.* 10, 1–11.

Scrimgeour, N., Litjens, T., Ma, L., Barritt, G. J. and Rychkov, G. Y. (2009). Properties of Orai1 mediated store-operated current depend on the expression levels of STIM1 and Orai1 proteins. *J. Physiol.* 587, 2903–2918.

Scrimgeour, N. R., Wilson, D. P., Barritt, G. J. and Rychkov, G. Y. (2014). Structural and stoichiometric determinants of Ca2 + release-activated Ca2 + (CRAC) channel Ca2 +-dependent inactivation. *Biochim. Biophys. Acta - Biomembr.* 1838, 1281–1287.

Shen, W. W., Frieden, M. and Demaurex, N. (2011). Local cytosolic Ca 2+ elevations are required for stromal interaction molecule 1 (STIM1) de-oligomerization and termination of store-operated Ca 2+ entry. *J. Biol. Chem.* 286, 36448–36459.

Shen, W. W., Frieden, M. and Demaurex, N. (2011). Local cytosolic Ca 2+ elevations are required for stromal interaction molecule 1 (STIM1) de-oligomerization and termination of store-operated Ca 2+ entry. *J. Biol. Chem.* 286, 36448–36459.

Shi, J., Miralles, F., Kinet, J. P., Birnbaumer, L., Large, W. A. and Albert, A. P. (2017). Evidence that Orai1 does not contribute to store-operated TRPC1 channels in vascular smooth muscle cells. *Channels* 11, 329–339.

Shull, G. E. and Greeb, J. (1988). Molecular cloning of two isoforms of the plasma membrane Ca2+-transporting ATPase from rat brain. *J. Biol. Chem.* 263, 8646–8657.

Singh, A. K., McGoldrick, L. L., Twomey, E. C. and Sobolevsky, A. I. (2018). Mechanism of calmodulin inactivation of the calcium-selective TRP channel TRPV6. *Sci. Adv.* 4, 4–10.

Smani, T., Domínguez-rodriguez, A., Callejo-garcía, P., Rosado, J. A. and Avila-medina, J. (2016). Calcium Entry Pathways in Non-excitable Cells. 898, 111–131.

Smani, T., Domínguez-rodriguez, A., Callejo-garcía, P., Rosado, J. A. and Avila-medina, J. (2016). Calcium Entry Pathways in Non-excitable Cells. *Adv. Exp. Med. Biol.* 898, 111–131.

Soboloff, J., Rothberg, B. S., Madesh, M. and Gill, D. L. (2012). STIM proteins: Dynamic calcium signal transducers. *Nat. Rev. Mol. Cell Biol.* 13, 549–565.

Soboloff, J., Rothberg, B. S., Madesh, M. and Gill, D. L. (2012). STIM proteins: dynamic calcium signal transducers. *Nat. Rev. Mol. Cell Biol.* 13, 549–565.

Soboloff, J., Spassova, M. A., Tang, X. D., Hewavitharana, T., Xu, W. and Gill, D. L. (2006). Orai1 and STIM reconstitute store-operated calcium channel function. *J. Biol. Chem.* 281, 20661–20665.

Srikanth, S., Jew, M., Kim, K. Do, Yee, M. K., Abramson, J. and Gwack, Y. (2012). Junctate is a Ca2+-sensing structural component of Orai1 and stromal interaction molecule 1 (STIM1). *Proc. Natl. Acad. Sci. U. S. A.* 109, 8682–8687.

Starkov, A. A., Chinopoulos, C. and Fiskum, G. (2004). Mitochondrial calcium and oxidative stress as mediators of ischemic brain injury. *Cell Calcium* 36, 257–264.

Stathopulos, P. B. and Ikura, M. (2010). Partial unfolding and oligomerization of stromal interaction molecules as an initiation mechanism of store operated calcium entry. *Biochem. Cell Biol.* 88, 175–183.

Stathopulos, P. B., Li, G. Y., Plevin, M. J., Ames, J. B. and Ikura, M. (2006). Stored Ca2+ depletion-induced oligomerization of stromal interaction molecule 1 (STIM1) via the EF-SAM region: An initiation mechanism for capacitive Ca2+ entry. *J. Biol. Chem.* 281, 35855–35862.

Strehler, E. E. and Zacharias, D. A. (2001). Role of alternative splicing in generating isoform diversity among plasma membrane calcium pumps. *Physiol. Rev.* 81, 21–50.

Szabadkai, G., Bianchi, K., Várnai, P., De Stefani, D., Wieckowski, M. R., Cavagna, D., Nagy, A. I., Balla, T. and Rizzuto, R. (2006). Chaperone-mediated coupling of endoplasmic reticulum and mitochondrial Ca2+ channels. *J. Cell Biol.* 175, 901–911.

Thillaiappan, N. B., Chavda, A. P., Tovey, S. C., Prole, D. L. and Taylor, C. W. (2017). Ca2+ signals initiate at immobile IP3 receptors adjacent to ER-plasma membrane junctions. *Nat. Commun.* 8,.

Thomas, J. M., Edwards, P. P. and Kuznetsov, V. L. (2008). Sir Humphry Davy: Boundless chemist, physicist, poet and man of action. *ChemPhysChem* 9, 59–66.

Treves, S., Franzini-Armstrong, C., Moccagatta, L., Arnoult, C., Grasso, C., Schrum, A., Ducreux, S., Zhu, M. X., Mikoshiba, K., Girard, T., et al. (2004). Junctate is a key element in calcium entry induced by activation of InsP3 receptors and/or calcium store depletion. *J. Cell Biol.* 166, 537–548.

Vaeth, M., Maus, M., Klein-Hessling, S., Freinkman, E., Yang, J., Eckstein, M., Cameron, S., Turvey, S. E., Serfling, E., Berberich-Siebelt, F., et al. (2017). Store-Operated Ca2+ Entry Controls Clonal Expansion of T Cells through Metabolic Reprogramming. *Immunity* 47, 664-679.e6.

Vance, J. E. (1990). Phospholipid synthesis in a membrane fraction associated with mitochondria. *J. Biol. Chem.* 265, 7248–7256.

Várnai, P., Tóth, B., Tóth, D. J., Hunyady, L. and Balla, T. (2007). Visualization and manipulation of plasma membrane-endoplasmic reticulum contact sites indicates the presence of additional molecular components within the STIM1-Orai1 complex. *J. Biol. Chem.* 282, 29678–29690.

Vig, M., Peinelt, C., Beck, A., Koomoa, D. L., Rabah, D., Koblan-Huberson, M., Kraft, S., Turner, H., Fleig, A., Penner, R., et al. (2006). CRACM1 is a plasma membrane protein essential for store-operated Ca 2+ entry. *Science (80-.).* 312, 1220–1223.

Villalobos, C., Gutiérrez, L. G., Hernández-Morales, M., del Bosque, D. and Núñez, L. (2018). Mitochondrial control of store-operated Ca 2+ channels in cancer: Pharmacological implications. *Pharmacol. Res.* 135, 136–143.

Walsh, C. M., Chvanov, M., Haynes, L. P., Petersen, O. H., Tepikin, A. V. and Burgoyne, R. D. (2010). Role of phosphoinositides in STIM1 dynamics and store-operated calcium entry. *Biochem. J.* 425, 159–168.

Wasserman, W. J., Pinto, L. H., O'Connor, C. M. and Smith, L. D. (1980). Progesterone induces a rapid increase in [Ca2+](in) of Xenopus laevis oocytes. *Proc. Natl. Acad. Sci. U. S. A.* 77, 1534–1536.

Wei, D., Mei, Y., Xia, J. and Hu, H. (2017). Orai1 and orai3 mediate store-operated calcium entry contributing to neuronal excitability in dorsal root ganglion neurons. *Front. Cell. Neurosci.* 11, 1–15.

Worley, P. F., Baraban, J. M., Colvin, J. S. and Snyder, S. H. (1987). Inositol trisphosphate receptor localization in brain: variable stoichiometry with protein kinase C. *Nature* 325, 159–161.

Wu, M. M., Buchanan, J. A., Luik, R. M. and Lewis, R. S. (2006). Ca2+ store depletion causes STIM1 to accumulate in ER regions closely associated with the plasma membrane. *J. Cell Biol.* 174, 803–813.

Wu, M. M., Buchanan, J., Luik, R. M. and Lewis, R. S. (2006). Ca2+ store depletion causes STIM1 to accumulate in ER regions closely associated with the plasma membrane. *J. Cell Biol.* 174, 803–813.

Wu, Y., Whiteus, C., Xu, C. S., Hayworth, K. J., Weinberg, R. J., Hess, H. F. and De Camilli, P. (2017). Contacts between the endoplasmic reticulum and other membranes in neurons. *Proc. Natl. Acad. Sci. U. S. A.* 114, E4859–E4867.

Yap, K. L., Kim, J., Truong, K., Sherman, M., Yuan, T. and Ikura, M. (2000). Calmodulin target database. *J. Struct. Funct. Genomics* 1, 8–14.

Yen, M., Lokteva, L. A. and Lewis, R. S. (2016). Functional Analysis of Orai1 Concatemers Supports a Hexameric Stoichiometry for the CRAC Channel. *Biophys. J.* 111, 1897–1907.

Yuan, J. P., Zeng, W., Dorwart, M. R., Choi, Y., Paul, F. and Muallem, S. (2009). Orai channels. 11, 337–343.

Zeng, W., Mak, D.-O., Li, Q., Min SHin, D., Foskett, K. and Muallem, S. (2003). A new mode of Ca2+ signaling by G protein-coupled receptors: gating IP3 receptor Ca2+ release cahnnels by Gbetagamma. *Curr. Biol.* 10, 161–168.

Zhang, S. L., Yeromin, A. V., Zhang, X. H. F., Yu, Y., Safrina, O., Penna, A., Roos, J., Stauderman, K. A. and Cahalan, M. D. (2006). Genome-wide RNAi screen of Ca2+ influx identifies genes that regulate Ca2+ release-activated Ca2+ channel activity. *Proc. Natl. Acad. Sci. U. S. A.* 103, 9357–9362.

Zhang, S. L., Yu, Y., Roos, J., Kozak, J. A., Deerinck, T. J., Ellisman, M. H., Stauderman, K. A. and Cahalan, M. D. (2005). STIM1 is a Ca2+ sensor that activates CRAC channels and migrates from the Ca2+ store to the plasma membrane. *Nature* 437, 902–905.

Zhang, S. L., Yu, Y., Roos, J., Kozak, J. A., Deerinck, T. J., Mark, H., Stauderman, K. A. and Cahalan, M. D. (2005). STIM1 is a Ca2+ sensor that activates CRAC channels and migrates from the Ca2+ store to the plasma membrane. *Nature* 437, 902–905.

Zheng, H., Zhou, M. H., Hu, C., Kuo, E., Peng, X., Hu, J., Kuo, L. and Zhang, S. L. (2013). Differential roles of the C and N termini of Orai1 protein in interacting with stromal interaction molecule 1 (STIM1) for Ca2+ release-activated Ca2+ (CRAC) channel activation. *J. Biol. Chem.* 288, 11263–11272.

Zheng, L., Stathopulos, P. B., Li, G. Y. and Ikura, M. (2008). Biophysical characterization of the EF-hand and SAM domain containing Ca2+ sensory region of STIM1 and STIM2. *Biochem. Biophys. Res. Commun.* 369, 240–246.

Zhou, Y., Wang, X., Wang, X., Loktionova, N. A., Cai, X., Nwokonko, R. M., Vrana, E., Wang, Y., Rothberg, B. S. and Gill, D. L. (2015). STIM1 dimers undergo unimolecular coupling to activate Orai1 channels. *Nat. Commun.* 6,.

Zhou, Y., Srinivasan, P., Razavi, S., Seymour, S., Meraner, P., Gudlur, A., Stathopulos, P. B., Ikura, M., Rao, A. and Hogan, P. G. (2013). Initial activation of STIM1, the regulator of store-operated calcium entry. *Nat. Struct. Mol. Biol.* 20, 973–981.

Zhu, W., Cowie, A., Wasfy, G. W., Penn, L. Z., Leber, B. and Andrews, D. W. (1996). Bcl-2 mutants with restricted subcellular location reveal spatially distinct pathways for apoptosis in different cell types. *EMBO J.* 15, 4130–4141.

Zweifach, A. and Lewis, R. S. (1995). Slow calcium-dependent inactivation of depletion-activated calcium current. Store-dependent and -independent mechanisms. *J. Biol. Chem.* 270, 14445–14451.

Zweifach, A. and R. S. L. (1995). Slow Calcium-dependent Inactivation of Depletion-activated Calcium Current. STORE-DEPENDENT AND -INDEPENDENT MECHANISMS. *J. Biol. Chem.*